GA-A12944
UC-77

DEVELOPMENT STATUS OF NEAR-ISOTROPIC GRAPHITES FOR LARGE HTGRs

by
G. B. ENGLE, R. J. PRICE
W. R. JOHNSON, and L. A. BEAVAN

Prepared under
Contract AT(04-3)-167
Project Agreement No. 17
for the
San Francisco Operations Office
U.S. Atomic Energy Commission

GENERAL ATOMIC PROJECT 317

JUNE 1, 1974

GENERAL ATOMIC

GENERAL ATOMIC COMPANY
P.O. BOX 81608
SAN DIEGO, CALIFORNIA 92138

DISCLAIMER

CONTENTS

FIGURES

FIGURES (continued)

TABLES

TABLES (continued)

1. CONCLUSIONS AND SUMMARY

1.1. CONCLUSIONS

Several new near-isotropic graphites have been developed and evaluated for use as core components in large HTGRs. Although the characterization data and design calculations are still continuing, the available information is sufficient to establish a position regarding the use of near-isotropic graphites in large HTGRs.

The information given in this report on the physical, thermal, and mechanical properties and the irradiation behavior of the near-isotropic graphites, as typified by grade H-451, shows that near-isotropic graphites have excellent potential to fulfill all requirements of large HTGR core design. Further testing to full HTGR lifetime exposures is expected to confirm this premise. The current results show grade H-451 to be equal or superior to the current reference needle-coke graphite, grade H-327, in all relevant properties except thermal expansivity. However, the thermal expansivities of near-isotropic graphites are satisfactory to meet the HTGR design requirements.

The stress and differential strain analyses showed the near-isotropic graphites (H-451 used as an example) to be satisfactory in all aspects (Ref. 1). The near-isotropic graphites also appear to be satisfactory with respect to bowing of fuel and reflector elements. All factors considered, the stress calculations indicate near-isotropic graphites will improve the graphite performance and increase structural design margins.

Based on the data presented in this report and the calculations presented in Ref. 1, it is concluded that near-isotropic graphites of the type described above will provide a reference graphite that will be satisfactory for current HTGR core designs and will provide additional margins for increasing core graphite fluences and temperatures if necessary for future designs.

1.2. SUMMARY

1.2.1. Introduction

The data for the near-isotropic graphites are compared herein with those of the anisotropic reference grade H-327. These comparisons show the relative merits of the two different graphite types.

Near-isotropic graphites have been under development during the past 3 years for use as core components in large HTGRs. Two candidate graphite grades, using isotropic petroleum coke as a filler in place of the needle-coke filler used in the current reference grade H-327, have been developed by Great Lakes Carbon Company and Union Carbide Corporation. Full-production-size experimental logs have been evaluated.

The bulk of the data in this report was obtained on Great Lakes Carbon Company grade H-451, or its prototype grade H-429. A lesser amount of data was obtained on Union Carbide Corporation grade TS-1240 because of the late delivery of the latter grade.

When irradiated to high temperatures and fluences the reference needle-coke graphite grade H-327, which is more anisotropic than grades H-451 or TS-1240, exhibits early expansion in the radial (perpendicular) direction and a relatively large axial (parallel) contraction. These characteristics limit the flexibility of design for large HTGRs or

optimization of advanced designs such as process heat or direct cycle gas turbine plants if a needle-coke-based graphite is used.

1.2.2. Experimental Results

Grades H-451 and TS-1240 were characterized by measuring (1) bulk density, (2) thermal expansivity, (3) thermal conductivity, (4) tensile properties including ultimate strength, strain at fracture, Young's modulus of elasticity, and Poisson's ratio, (5) impurity concentrations, and (6) oxidation rate on unirradiated specimens. The irradiation behavior of grade H-451 was assessed by measuring the changes in (1) dimensions, (2) thermal expansivity, (3) thermal conductivity, and (4) tensile properties as a function of temperature and fast fluence. The data for grade H-451 are summarized in Table 1-1 along with comparative data for H-327. Grade H-451 was found to be dimensionally more stable under irradiation than H-327. At 1150°C and 8×10^{21} n/cm^2, grade H-327 shows net expansion in the radial direction whereas H-451 does not. The rate of contraction for H-327 in the axial direction is approximately 2.5 higher than that for H-451. The maximum contraction of H-451 in the radial direction does not exceed about 2%, and net expansion is not anticipated until exposures well beyond the range of large HTGR designs. Increased dimensional stability is desirable because it reduces distortions and stresses within the fuel elements.

The strength and Young's modulus of H-451 increase in both orientations after irradiation. The fractional increase in Young's modulus and axial strength for H-327 is similar to that of H-451, but the radial strength of H-327 showed no increase with irradiation.

The irradiated thermal conductivity values in the radial direction for H-451 (the direction of heat flow) are 10 to 50% higher than those for H-327.

TABLE 1-1
SUMMARY COMPARISON OF PROPERTIES AND IRRADIATION BEHAVIOR OF GRAPHITES H-451 AND H-327

Property	Irradiation Conditions		Property Value			
			Axial		Radial	
	Temperature (°C)	Fast Fluence $\times 10^{-21}$ (n/cm^2) (E>0.18 MeV)	H-451	H-327	H-451	H-327
Mean density, g/cm^3		0	1.74[a]	1.76[a]	-	-
Mean thermal expansivity x 10^6 °C^{-1} (22°-500°C)		0	3.55	1.60	4.55	3.35
Thermal conductivity at irradiation temperature, cal/cm-sec-°C	800	0	0.174	0.194	0.158	0.140
	600-625	2.2-2.9	0.080	0.067	0.079	0.043
	875-920	3.1-5.1	0.094	0.078	0.084	0.063
	1225-1350	3.6-9.9	0.10	0.10	0.09	0.08
Ultimate tensile strength, psi						
End center	-	0	1657	2180	2051	1350
Midlength center	-	0	1564	1630	1671	925
Midlength edge	-	0	2246	2395	1637	1295
Midlength center	860-1020	2.6-3.4	2371	2127	2648	962
Young's modulus, 10^6 psi						
End center	-	0	1.22	1.51	0.96	0.69
Midlength center	-	0	1.14	1.54	1.00	0.58
Midlength edge	-	0	1.28	1.75	0.94	0.65
Midlength center	860-1020	2.6-3.4	2.06	3.02	1.88	1.23
Dimensional change, %	850	4	-0.6	-1.3	-0.3	-0.5
	1150	6.5	-1.8	-4.7	-1.3	-0.1[c]
	1150	8	-2.2[b]	-6.2	-1.5[b]	+1.0
Oxidation rate in 3% steam-helium mixture, %/hr at 5% burnoff at 1000°C	-	0	0.27[a]	0.25[a]	-	-

[a] Orientation heading does not apply.
[b] Extrapolated from 6.5 x 10^{21} n/cm^2.
[c] Specimen expanding.

The resistance to steam oxidation is approximately equal in the two materials.

The thermal expansivity values of H-327 are lower than those for H-451 and show more anisotropy.

2. INTRODUCTION

The design of large HTGRs requires an efficient moderator and reflector material capable of withstanding high temperatures and high fast fluences. Commercial synthetic graphite has been the material choice for the HTGR core graphite because it is an excellent moderator, has refractory properties, can be manufactured and machined in a wide variety of shapes and sizes, and is relatively low in cost.

The hexagonal fuel and reflector blocks for Fort St. Vrain were manufactured by extrusion with petroleum needle coke by conventional manufacturing processes. The core graphite components were extruded as 18.0-in.-diameter by 34-in.-long logs, processed to graphite, and subsequently machined into hexagonal blocks that contain a series of fuel and coolant holes. The anisotropic needle-coke particles are highly aligned during the extrusion process, resulting in a material that exhibits high anisotropy in its properties and irradiation dimensional changes. This anisotropy is responsible for large axial contractions and an initial radial contraction followed by rapid radial expansion in the graphite block when irradiated at high temperatures and to fluences of large HTGRs. The anisotropic behavior of the extruded needle-coke graphites limits their allowable in-core life.

During the 1960s near-isotropic graphites based on Gilsocoke and other raw materials were developed and evaluated in the U.K. for Advanced Gas-Cooled Reactors (AGRs). These materials and the subsequent data resulting from an extensive evaluation program have been extremely helpful in evaluating near-isotropic graphite data for large HTGRs. Unfortunately Gilsocoke has certain disadvantages as a raw material for nuclear graphite production, and other sources were sought by manufacturers in Europe

and the U.S. A more complete review and discussion of Gilsocoke graphites is given in Section 3.

During the past several years, development of nuclear graphites for core components in the U.S. and Europe has been directed toward near-isotropic graphites utilizing raw materials with more assured sources of supply than Gilsocoke. The approach to developing these materials has been to retain conventional manufacturing processes while substituting coke particles with a more isotropic microstructure for needle coke. In Europe cokes derived from coal-tar pitch have been used, whereas in the U.S. near-isotropic cokes derived from petroleum feedstocks were the choice. The development of the near-isotropic materials has progressed to the point where full-production-size logs are available for experimental measurements.

This report describes the status of development of near-isotropic graphites and contains data obtained on several grades plus additional data on the Fort St. Vrain needle-coke graphite H-327. The feasibility of using near-isotropic graphites for large HTGR core components is discussed.

3. REVIEW OF EXPERIENCE WITH NEAR-ISOTROPIC GRAPHITES

3.1. GILSOCOKE-BASED GRAPHITES

3.1.1. Gilsocoke-Based Graphites for AGRs in the U.K.

In the early 1960s the UKAEA was developing AGRs utilizing a fixed graphite moderator structure, CO_2 cooling, and a maximum graphite temperature of 550°C. Compared with the anisotropic PGA graphite previously employed in the U.K. Magnox reactors, this required a graphite with improved dimensional stability (because of the higher total neutron fluences) and better resistance to radiolytic oxidation by CO_2. A specification for the new graphite was written (Ref. 2) which, among other requirements, called for a coefficient of thermal expansion (measured between 20° and 120°C) of at least 5×10^{-6} $°C^{-1}$ in both directions and an open pore volume limit of 6.5 $cm^3/100$ g. The high thermal expansivity was specified because analyses of graphite behavior indicated this would minimize irradiation-induced dimensional change at the temperature of interest. Candidate graphites, extruded using Gilsocoke filler, were submitted by Anglo Great Lakes, Ltd., and British Acheson Electrodes, Ltd., and were eventually qualified.

Irradiation testing of these materials and similar materials made from coal-tar pitch coke and an undisclosed coke type was conducted at temperatures between 370° and 710°C in the Dounreay Fast Reactor (Scotland) and the Belgian BR-2 reactor. The results are summarized in Ref. 3. Examples of the dimensional change versus fluence curves are shown in Figs. 3-1 and 3-2. All the graphites contracted initially in both directions, with

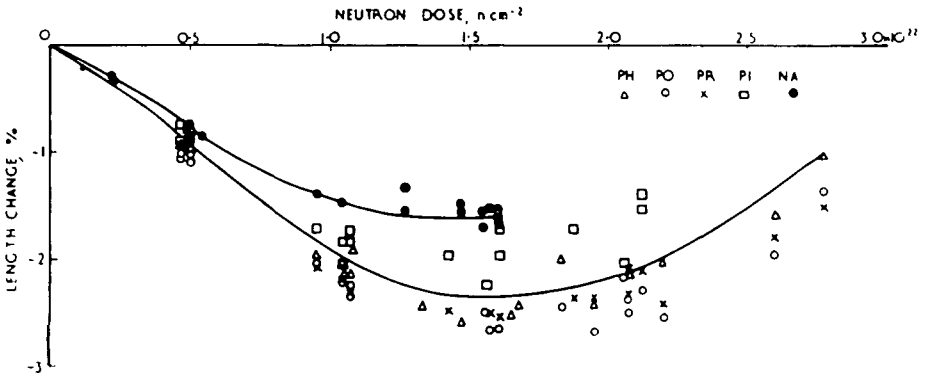

Fig. 3-1. Dimensional changes of U.K. isotropic graphites, perpendicular to extrusion or parallel to molding, at DFR temperatures in the range 370° to 440°C. NA is molded grade; others are extruded. (Neutron dose in NDE units. The conversion factor is NDE units x 1.7 = E > 0.18 MeV units.) (From Ref. 3.)

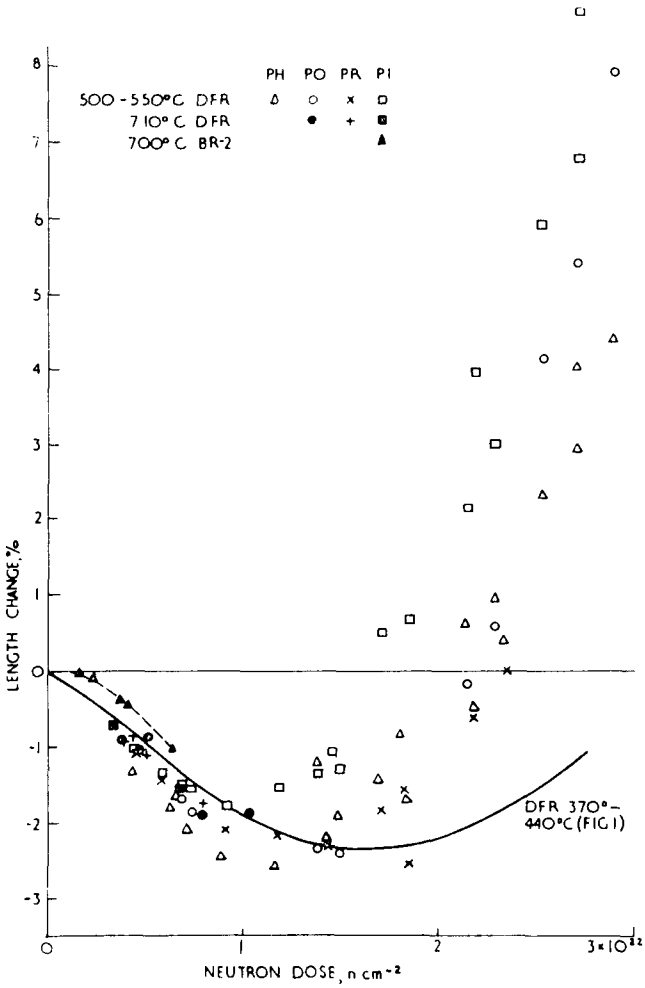

Fig. 3-2. Dimensional changes of U.K. isotropic graphites, perpendicular to extrusion, at temperatures of 500° to 550°C and 710°C in DFR and 700°C in BR-2. (Neutron dose in NDE units. The conversion factor is NDE units x 1.7 = E > 0.18 MeV units.) (From Ref. 3.)

the contraction rates being somewhat lower in molded grades than in the extruded materials. At about 2.5 x 10^{22} n/cm^2 (E > 0.18 MeV) contraction stopped and expansion started. The expansion was more rapid at 500° to 550°C than at 370° to 440°C, and the data points became more scattered after the samples expanded past their original dimensions at 500° to 550°C. Fractional changes in Young's modulus and strength are shown in Fig. 3-3. Young's modulus increased more rapidly with fluence than did the tensile strength. A reduction in strength and thermal conductivity due to radiolytic oxidation by CO_2 was also reported. Monitoring of the dimensions and properties of near-isotropic graphite components in U.K. reactors is carried on continuously (Refs. 4, 5). So far the graphite has performed predictably and its behavior has been consistent with the data from capsule irradiations.

3.1.2. Gilsocoke-Based Graphite for HTGRs in the U.K.

During 1965 through 1968 the successful operation of the Dragon reactor and the AVR pebble-bed reactor caused increased interest in high-temperature gas-cooled reactors in Europe, and design work for commercial HTGRs was undertaken. Because the Gilsocoke-based graphites developed for the AGR program were available as production materials and had demonstrated good dimensional stability and strength at irradiation temperatures up to 700°C, it was decided that the initial reference material for the HTGR moderator and fuel tubes and the pebble-bed reactor reflector blocks should be Gilsocoke-based graphite. An extensive testing program on European-manufactured Gilsocoke-based graphites was started, employing test facilities in the HFR (Petten) and the Dragon reactor and using test temperatures up to 1400°C.

Dragon Project irradiation test data on Gilsocoke graphites are included in Refs. 6 through 10. Figure 3-4 shows an example of the dimensional change behavior of a molded production-quality Gilsocoke graphite (Dragon Reference No. 95). The general behavior pattern resembles that established for lower irradiation temperatures by UKAEA workers, except

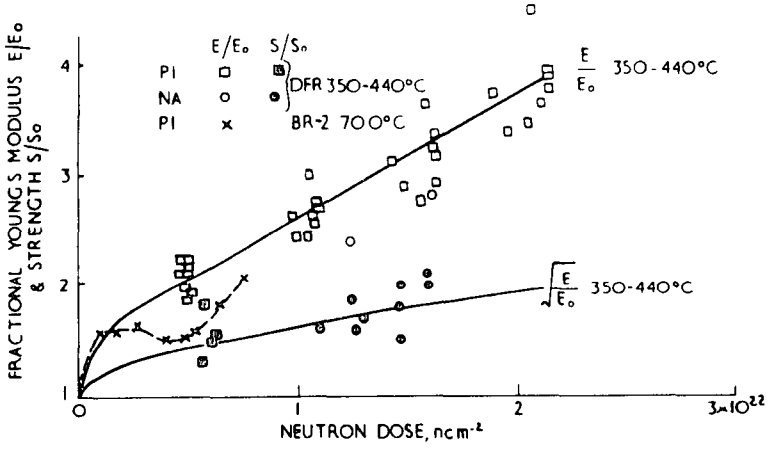

Fig. 3-3. Fractional changes in dynamic Young's modulus E and tensile strength S of U.K. isotropic graphites at temperatures of 350° to 440°C in DFR and 700°C in BR-2. (Neutron dose in NDE units. The conversion factor is NDE units x 1.7 = E > 0.18 MeV units.) (From Ref. 3.)

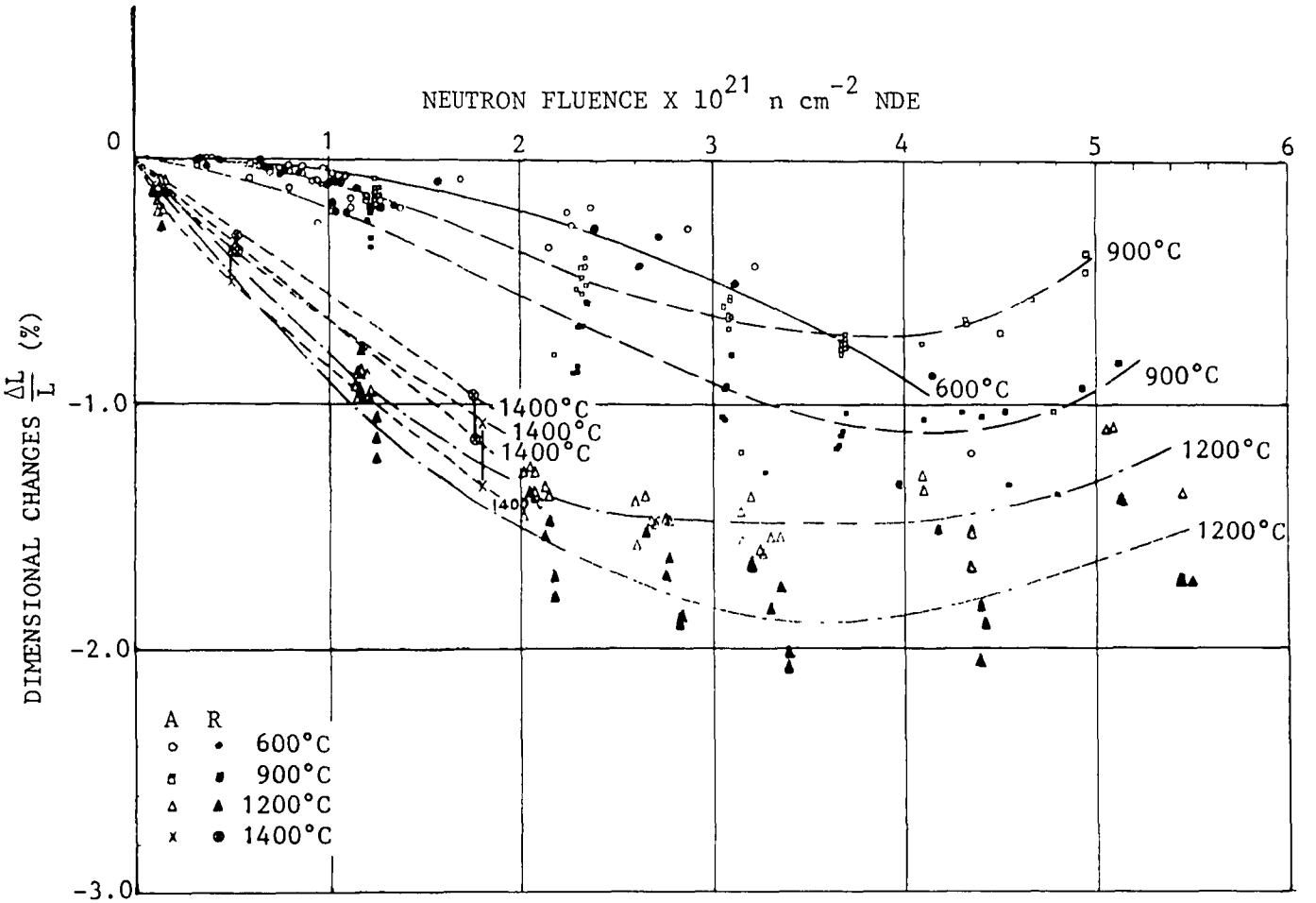

Fig. 3-4. Dragon Project data on dimensional changes of pressed Gilsocoke graphite No. 95. (NDE units x 1.7 = E > 0.18 MeV units.) (From Ref. 8.)

that the change rates are accelerated for irradiation temperatures up to 1200°C. The point of "turnaround" in sample dimensions is 5.0 to 7.0 x 10^{21} n/cm^2 (E > 0.18 MeV) for irradiation temperatures of both 900° and 1200°C, but the maximum linear shrinkage is only about 1% at 900°C compared with 1.5 to 2% at 1200°C. Results for extruded Gilsocoke grades were generally similar except that differences between the parallel and perpendicular directions were more pronounced.

Changes in the thermal expansivity and Young's modulus of the same grade are shown in Figs. 3-5 and 3-6. After a small initial increase in thermal expansivity, further irradiation at 900° and 1200°C reduces the thermal expansivity to less than half its original value. Irradiation first increases Young's modulus by 20 to 60% (depending on the temperature) and then, after a plateau, a second increase during irradiation at 900° or 1200°C carries the Young's modulus to a peak value about 2.5 times its original level.

Irradiation creep measurements, using self-straining tensile assemblies, yielded scattered data (Fig. 3-7). Values for the steady-state creep constant of Gilsocoke grades increased from 1 to 2 x 10^{-27} $(psi)^{-1}$ $(n/cm^2)^{-1}$ at 600°C to 3 to 6 x 10^{-27} $(psi)^{-1}$ $(n/cm^2)^{-1}$ at 1200°C.

A careful postirradiation analysis, including dimensional and residual stress measurements, was made of the inner and outer fuel tube of an experimental Dragon fuel element (FE 923) (Ref. 8). The graphite was an extruded Gilsocoke-grade graphite and the peak fluence was 1.7 x 10^{21} n/cm^2 (E > 0.18 MeV). Operating temperatures fell between 900° and 1100°C. Both the measured shrinkages and the residual stresses agreed well with calculations based on material property data from samples in irradiation capsules.

Strength measurements on near-isotropic graphite samples from this and other Dragon reactor tests (Ref. 11) showed an increase in strength paralleling the increase in dynamic elastic modulus. The relationship is shown in Fig. 3-8.

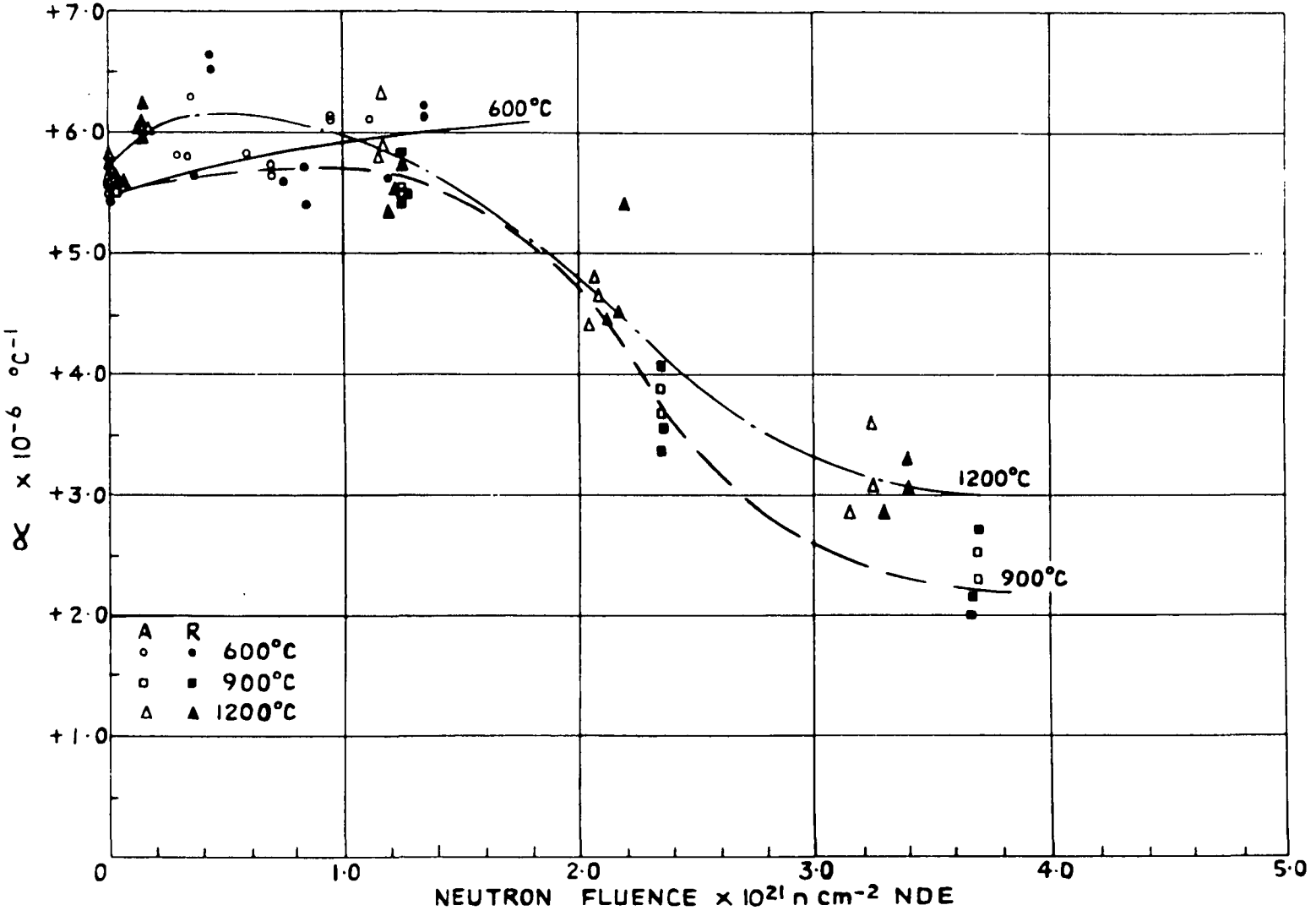

Fig. 3-5. Dragon Project data on the coefficient of thermal expansion (20° to 400°C) of molded Gilsocoke graphite No. 95. (NDE units x 1.7 = E > 0.18 MeV units.) (From Ref. 8.)

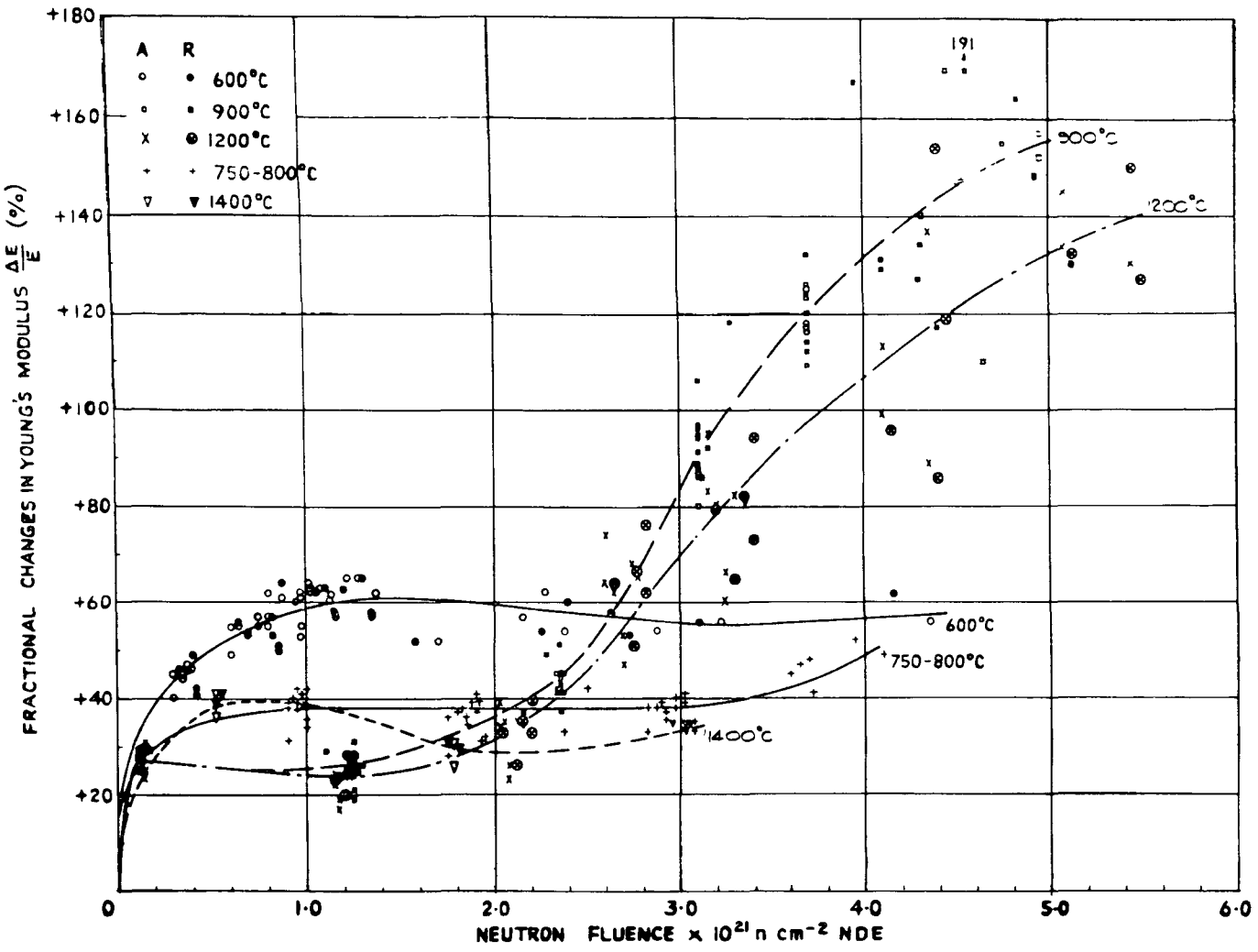

Fig. 3-6. Dragon Project data on the fractional changes in Young's modulus of molded Gilsocoke graphite No. 95. (NDE units x 1.7 = E > 0.18 MeV units.) (From Ref. 8.)

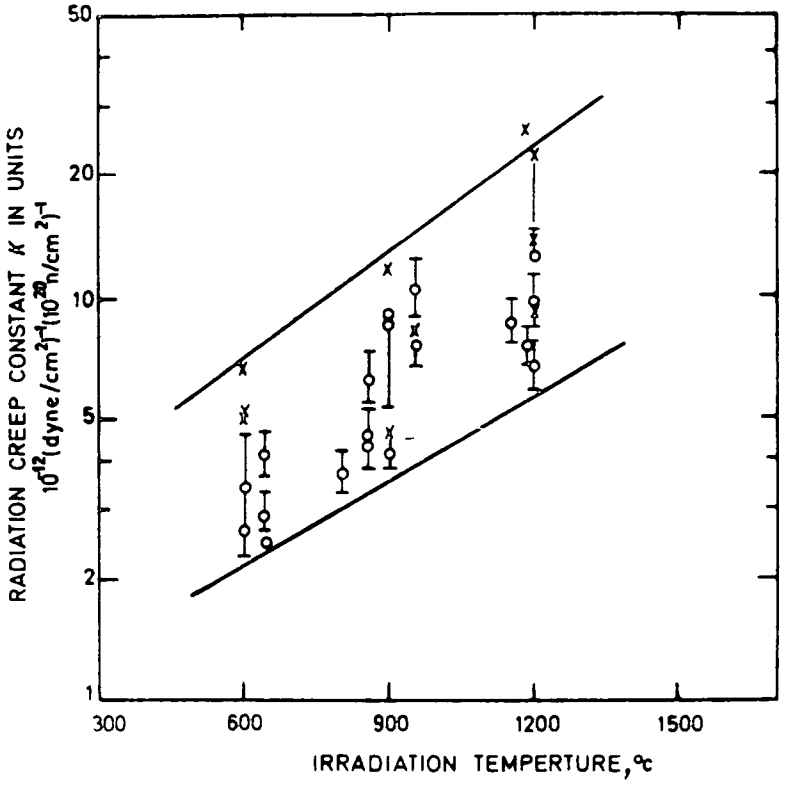

Fig. 3-7. Dragon Project data on the steady-state irradiation creep constant as a function of irradiation temperature. (O - Gilsocoke graphites; X - other reactor graphites.) (From Ref. 7.)

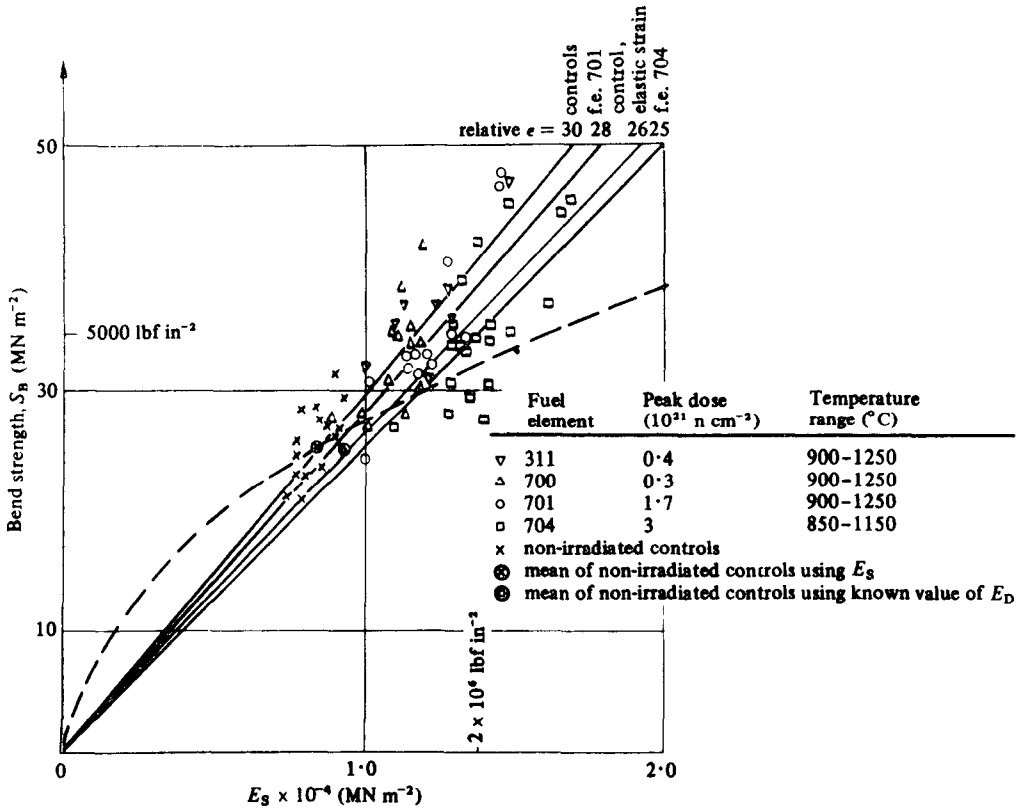

Fig. 3-8. Dragon Project data on the bend strength as a function of the static Young's modulus for irradiated graphite. (From Ref. 11.)

3.1.3. Gilsocoke-Based Graphites in the U.S.

Gilsocoke graphites were never considered as candidate materials for HTGRs in the U.S., but due to the interest shown in the U.K. and their excellent irradiation stability some attention was given to their evaluation. Gilsocoke graphites supplied by the Great Lakes Carbon Company, U.S., were evaluated at General Atomic Company (GAC) and Battelle Northwest Laboratories (BNWL). Dimensional (Ref. 12) and thermal conductivity (Ref. 13) changes as a function of irradiation temperature and fluence are shown in Figs. 3-9 and 3-10. Thermal expansivity (Ref. 14) changes are shown in Fig. 3-11. The U.S. and U.K. data for Gilsocoke graphites were in good agreement.

3.1.4. Assessment of Gilsocoke Graphites

Gilsocoke graphites proved to be more than satisfactory for advanced AGRs and also showed promise for design of U.S. and European HTGRs. However, it was realized their use had several disadvantages, i.e.:

1. High processing costs.

2. A single raw material source (the American Gilsonite Company in the U.S.).

3. A combination of high thermal expansivity and high elastic modulus, which creates relatively high shutdown stresses in components that operate with a steep temperature gradient.

4. Poor machinability especially with respect to cost due to high tool wear.

Thus, while the irradiation stability of the Gilsocoke graphites was superior to the anisotropic materials and desirable, the above mentioned liabilities prevented the acceptance of Gilsocoke graphites for HTGR

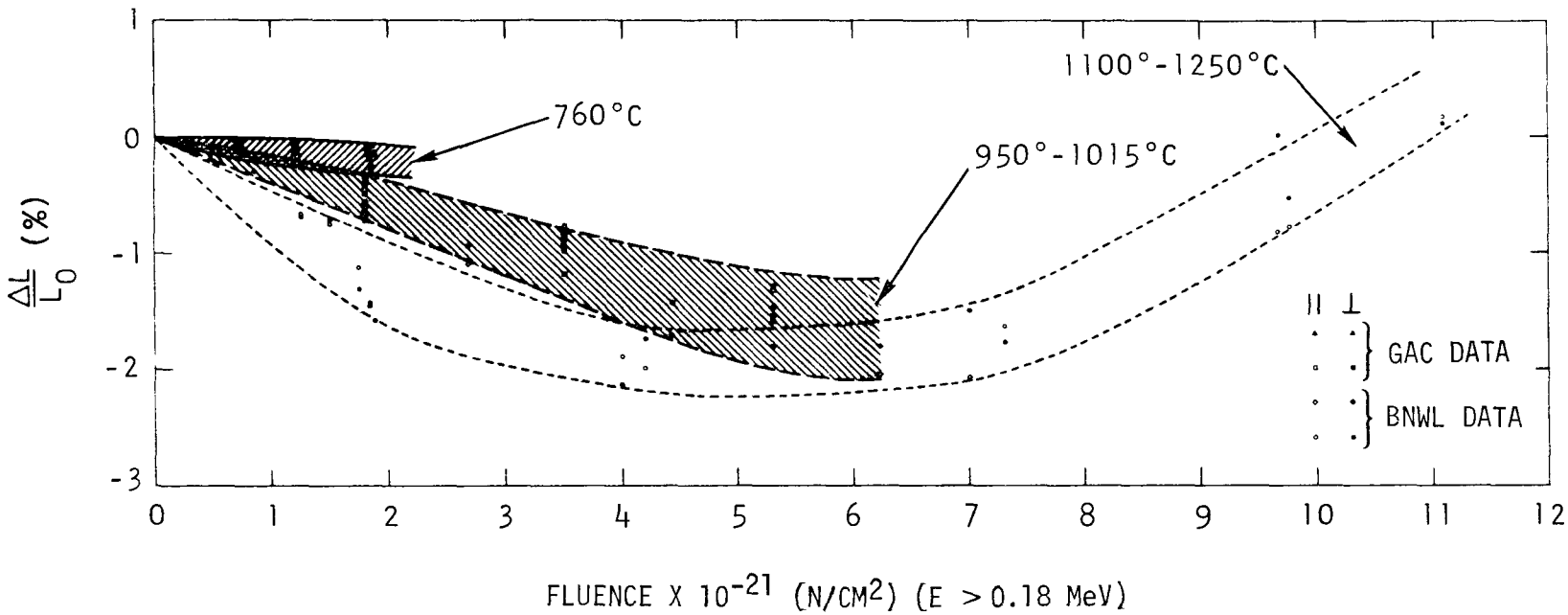

Fig. 3-9. Dimensional changes as a function of fluence for H-328 graphite at 760°, 950° to 1015°C, and 1100° to 1250°C

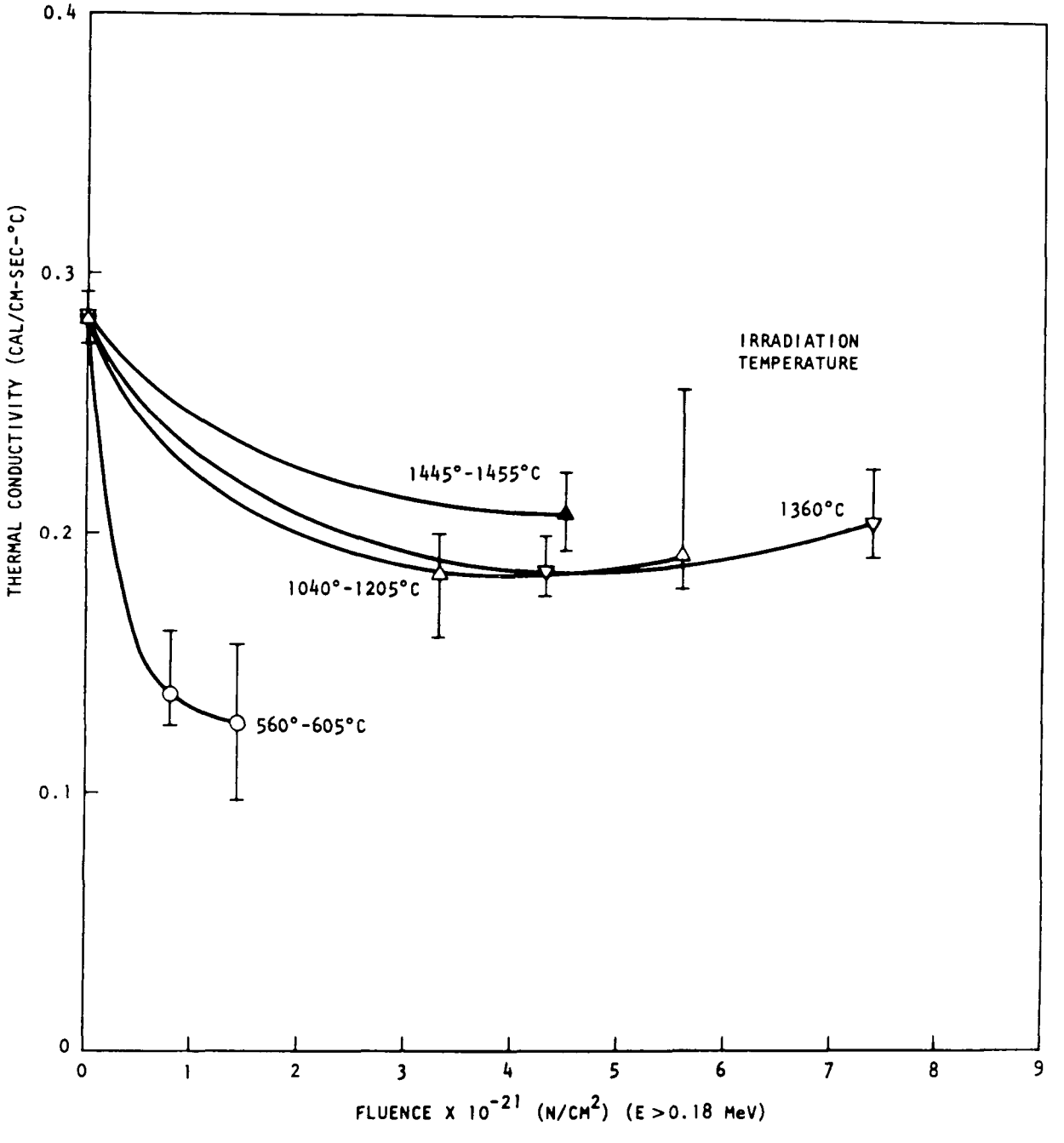

Fig. 3-10. Thermal conductivity versus fluence at 560° to 1455°C for H-328 graphite (perpendicular)

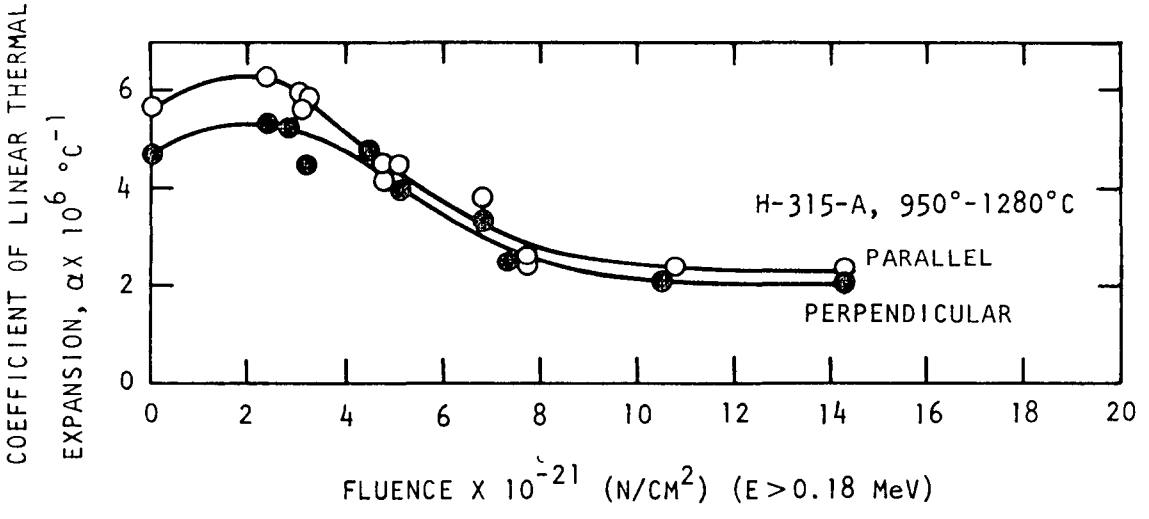

Fig. 3-11. Thermal expansivity changes of Gilsocoke graphite measured at 400°C as a function of neutron fluence

designs in the U.S. HTGR designs in Europe are also being directed away from Gilsocoke graphites as described in the next section.

3.2. NON-GILSOCOKE GRAPHITES FOR HTGRs IN EUROPE

In 1969, technical personnel of the Dragon Project, KFA (Jülich), Euratom, and CEA (Saclay) initiated programs to develop European near-isotropic graphites based on petroleum coke or coal-tar pitch coke. Irradiation testing of several such graphites is under way. Some preliminary data from an extruded pitch-coke graphite are given in Refs. 7 and 15. The dimensional change behavior at low fluences is similar to that of Gilsocoke-based graphite (e.g., Figs. 3-4 and 3-9) except that contraction at 1400°C is more rapid than at 1200°C. Curves showing fractional change in Young's modulus versus neutron fluence closely resemble those of Gilsocoke graphite (e.g., Fig. 3-6), while preliminary thermal expansivity data suggest that changes will be less marked than those of Gilsocoke graphite.

Other physical properties of the European near-isotropic petroleum- and pitch-coke based graphites resemble those of Gilsocoke graphites fabricated similarly, except the initial thermal expansivities are lower. Typical values (measured between 20° and 400°C) are 5 to 6 x 10^{-6} $°C^{-1}$ for Gilsocoke graphites, 4 to 5 x 10^{-6} $°C^{-1}$ for pitch-coke graphites, and 2 to 4 x 10^{-6} $°C^{-1}$ for petroleum-coke graphites. The lower thermal expansivity offers considerable reduction in component shutdown stresses.

Taking into account the lower costs and better raw material supply prospects, the new petroleum-coke-based or pitch-coke-based near-isotropic nuclear graphites appear likely to replace Gilsocoke-based graphites as reference materials for the design of European HTGRs.

4. MATERIALS

Near-isotropic graphites and needle-coke graphites are described in this report. However, of the needle-coke graphites, data are presented for only H-327, which is the fuel and reflector element graphite at Fort St. Vrain. A description of the graphites, along with their mean bulk densities and anisotropy factors, is given in Table 4-1.

4.1. NEAR-ISOTROPIC GRAPHITES

Beginning in 1969, cooperation between GAC and the major U.S. carbon companies under a USAEC research program resulted in the development of near-isotropic graphites made from petroleum-based near-isotropic cokes. The Great Lakes Carbon Company (GLCC) responded in early 1971 with a prototype grade H-429 and late in 1972 with a production-size grade H-451. The Union Carbide Corporation (UCC) responded in 1973 with production-size grade TS-1240. AirCo Speer expects to deliver their version of production-size material in 1974.

The near-isotropic graphites are manufactured with petroleum near-isotropic cokes, which are not currently used extensively for other products. The near-isotropic cokes are characterized by large volume fractions of fine isotropic microstructural constituents (Ref. 16) and the particles are near-isotropic. The manufacturing processes of the near-isotropic graphites are similar to those for the needle-coke graphites.

The grades of near-isotropic graphites described in this section are under study and data for these materials are included later in this report.

TABLE 4-1
DESCRIPTION OF NEAR-ISOTROPIC AND H-327 GRAPHITES

Graphite Grade	Manufacturer	Log Size (in.)		Type	Filler Coke	Binder	Impregnant	Mean Bulk Density (g/cm^3)	Anisotropy Factor $\alpha_\perp/\alpha_\parallel$
		Diameter	Length						
H-429	GLCC	6.0	-	Near-isotropic	Petroleum (near-isotropic)	Coal-tar pitch	Coal-tar pitch	1.73	1.20
H-451	GLCC	18.0	34.0	Near-isotropic	Petroleum (near-isotropic)	Coal-tar pitch	Petroleum pitch	1.76	1.30
TS-1240	UCC	18.0	34.0	Near-isotropic	Petroleum (near-isotropic)	Coal-tar pitch	Coal-tar pitch	1.77	1.20[a]
P_3JHAN	Pechiney	17.0	34.0	Near-isotropic	Coal-tar pitch (near-isotropic)	Coal-tar pitch	Coal-tar pitch	1.72	1.40
H-327	GLCC	18.0	-	Anisotropic	Petroleum (needle)	Coal-tar pitch	Coal-tar pitch	1.77	2.10

[a] Data supplied by UCC.

4.1.1. Great Lakes Carbon Company - Grades H-429 and H-451

4.1.1.1. Grade H-429

Grade H-429 was manufactured by extrusion as a 6-in.-diameter experimental prototype near-isotropic graphite. Grade H-429 was manufactured with a near-isotropic coke and the supplier indicated it was similar in structure to the base graphite used to manufacture the sleeves for Peach Bottom Core 2. Grade H-429 was delivered on January 6, 1971.

4.1.1.2. Grade H-451

Grade H-451 was manufactured by extrusion as an 18-in.-diameter by 34-in.-long experimental preproduction full-production-size near-isotropic graphite. Grade H-451 was first produced as a portion of an experimental furnace that contained other near-isotropic materials. It was manufactured with a proprietary coke and a coal-tar pitch binder and impregnated with petroleum pitch. The first logs of H-451 were delivered August 17, 1972.

A second partial furnace lot of H-451 was manufactured in an effort to improve its properties. These logs were delivered February 7, 1974.

A third partial furance lot of H-451 is in process and will be delivered about May 1974.

4.1.2. Union Carbide Corporation, Carbon Products Division - Grade TS-1240

Grade TS-1240 was manufactured by extrusion as 17-in.-diameter by 34-in.-long logs with a proprietary coke. Grade TS-1240 was produced as a full furnace production lot. The material was received on August 27, 1973.

4.1.3. Pechiney Ugine Kuhlman Group - Grade P_3JHAN

Grade P_3JHAN is an extruded graphite manufactured with coal-tar pitch coke. It is currently being evaluated as an HTGR candidate core graphite by CEA, Saclay, France, for French HTGR designs. A small number of specimens were included in capsule OG-1 for comparative purposes.

4.2. NEEDLE-COKE GRAPHITES

The needle-coke graphites are manufactured with petroleum needle coke of the same type used to manufacture steel furnace electrodes. The needle coke is characterized by a large volume fraction of fine fibrous microstructural constituents (Ref. 16) and the particles are highly anisotropic. The coke is sized, mixed with coal-tar pitch binder, formed into green logs by extrusion, baked slowly to about 800° to 900°C to carbonize the binder, and finally heated to about 2800°C to transform the structure to graphite. Purification of the graphite can be accomplished during the graphitizing process. The resulting material is highly anisotropic in properties and irradiation behavior. Three companies, GLCC, UCC, and AirCo Speer, have supplied needle-coke graphites.

4.2.1. Great Lakes Carbon Company - Grade H-327

An extruded needle-coke graphite (grade H-327) is the current reference material for large HTGRs. Great Lakes Carbon Company grade H-327 was manufactured for replaceable fuel and reflector blocks for the Fort St. Vrain reactor. Great Lakes Carbon Company manufactured three preproduction lots for experimental and qualification purposes prior to the production lots for Fort St. Vrain. The production material exceeded GAC's material specification for density, strength, and purity and was superior to the preproduction material. A large amount of test data obtained during the production and qualification of H-327 for Fort St. Vrain is available on this material.

4.2.2. Union Carbide Corporation, Carbon Products Division - Grade TS-1111

Grade TS-1111 is similar to grade H-327. It is UCC's candidate needle-coke material. No data are presented for this graphite.

4.2.3. AirCo Speer Carbon Company - Grade 9567

Grade 9567 is similar to grade H-327. Based on a low level of preliminary testing, grade 9567 appears to meet GAC's material specification. No data are presented for this graphite.

5. EXPERIMENTAL METHODS

5.1. CAPSULE OG-1

Capsule OG-1 was a fully instrumented graphite irradiation capsule irradiated for 3200 full power hours in the C-3 position of the Oak Ridge Reactor. It contained two cells, each with its own sweep-gas system to facilitate independent temperature control in the upper and lower parts of the capsule. The two cells contained a total of ten graphite crucibles approximately 2.25 in. in diameter by 2 in. high (one crucible was 3 in. high), which were drilled with holes to act as sample holders. The centerline temperature of one crucible in the upper cell and one crucible in the lower cell was maintained at 1000°C during reactor operation by adjustment of the gas mixtures. Centerline temperatures of all crucibles, and peripheral temperatures of eight out of ten crucibles, were monitored with chromel-alumel or tungsten-rhenium thermocouples. The output of the tungsten-rhenium thermocouples was corrected for neutron-induced decalibration using the output from three pairs of adjacent chromel-alumel and tungsten-rhenium thermocouples. Fast neutron fluences ($E > 0.18$ MeV) were derived from the activation of iron and titanium dosimeter wires, using cross sections of 46.5 mb for the $^{54}Fe(n,p)^{54}Mn$ reaction and 6.85 mb for the $^{46}Ti(n,p)^{46}Sc$ reactions. Thermal fluences were measured from cobalt dosimeters assuming a value of 36.8 b for the cross section for the $^{59}Co(n,\alpha)^{60}Co$ reaction. The mean temperatures and fluences in each crucible are listed in Table 5-1.

The sample holes contained three types of graphite samples: 0.2-in.-diameter by 0.45-in.-long cylinders for dimensional and thermal expansivity measurements, 0.25-in.-diameter by 0.9-in.-long cylinders for dimensional and tensile property measurements, and 0.40-in.-diameter by 0.05-in.-thick discs for thermal diffusivity measurements. Some of the small cylinders

TABLE 5-1
MEAN TEMPERATURES AND FLUENCES IN CAPSULE OG-1

Crucible Number	Fast Fluence, x 10^{-21} (n/cm^2) (E > 0.18 MeV)	Thermal Fluence x 10^{-21} (n/cm^2)	Mean Temperature (°C)	
			Centerline	Periphery
1	2.2	1.4	657	558
2	2.9	1.7	754	610
3	3.4	1.9	993	887
4	3.7	2.0	1172	1024
5	3.6	2.0	1395	1327
6	3.4	1.8	1078	938
7	3.1	1.6	992	884
8	2.6	1.4	928	836
9	2.1	1.1	860	753
10	1.6	0.8	650	597

and discs had been previously irradiated in earlier capsules and were included in order to obtain higher fluence data.

5.2. DIMENSIONAL MEASUREMENTS

Dimensions (length) of both unirradiated and irradiated specimens were obtained using a Bausch and Lomb DR-25B optical gage. Measurements were made to the nearest 0.00002 in. according to manufacturer's recommended practices.

5.3. DENSITY

The bulk density was measured according to ASTM Standard Test Method C-559.

5.4. TENSILE PROPERTIES

5.4.1. Stress-Strain Curves

Tensile stress-strain curves were obtained in air at room temperature on unirradiated and irradiated samples using an Instron tensile machine. Tensile tests were conducted on standard (0.505-in.-diameter by 3-in.-long, unirradiated only) and subsize (0.25-in.-diameter by 0.9-in.-long, unirradiated and irradiated) samples using a crosshead speed of 0.005 in./min. Strains were measured for subsize samples using a 0.5-in. gage length nonaveraging clip-on extensometer. A 2.0-in. gage length averaging extensometer was used on standard samples. The samples were fixed to metal end pieces with high-strength epoxy cement, and the load was applied through roller-link chains to maintain uniaxial alignment during testing.

Irradiated samples were tested using a cyclic loading method. Each sample was loaded to 1000 psi (600 psi for H-327 graphite samples of perpendicular orientation) and the crosshead motion reversed. After unloading to ∿100 psi the crosshead was again reversed, and the sample was extended

until it fractured. Some unirradiated subsize samples (controls) were tested in this manner.

Unirradiated standard and subsize specimens (except as noted above) were tested to fracture without crosshead reversal.

Typical stress-strain curves for both methods are shown in Fig. 5-1.

5.4.2. Tensile Strength

The tensile strength of all samples was calculated by dividing the load at fracture (stress corresponding to point q, Fig. 5-1) by the original cross-sectional area of the specimen.

5.4.3. Modulus of Elasticity

5.4.3.1. Young's Modulus

Young's modulus for samples tested by the cyclic loading method (irradiated and subsize control samples) was calculated from the slope of the linear stress-strain curve after load reversal (line o'p, Fig. 5-1a).

Young's modulus for samples tested by the standard method (unirradiated only) was calculated from the stress-strain curve as the initial tangent modulus, the slope of the curve at the origin (tangent line op, Fig. 5-1b).

5.4.3.2. Chord Modulus

The chord modulus for samples tested by the standard method (unirradiated only) was calculated from the stress-strain curve as the slope of the chord drawn between points on the curve for stresses of 250 and 500 psi (chord rs, Fig. 5-1b).

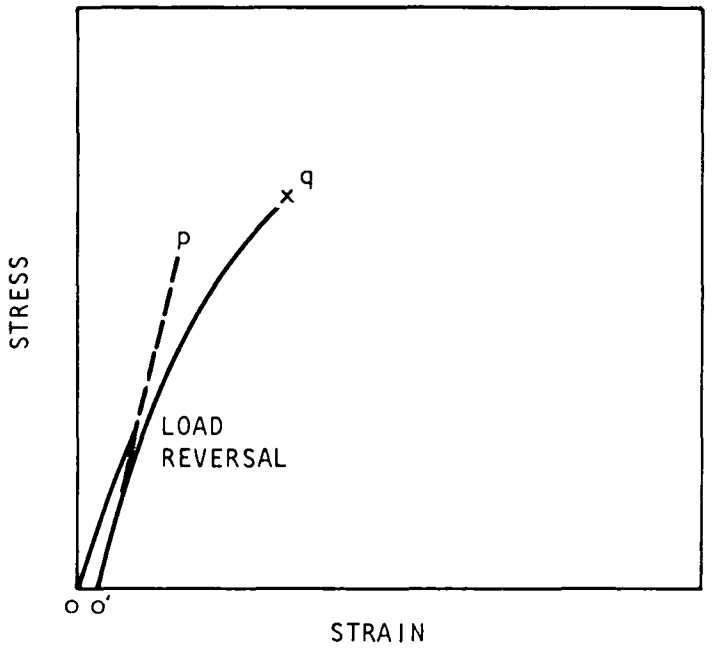

(a)

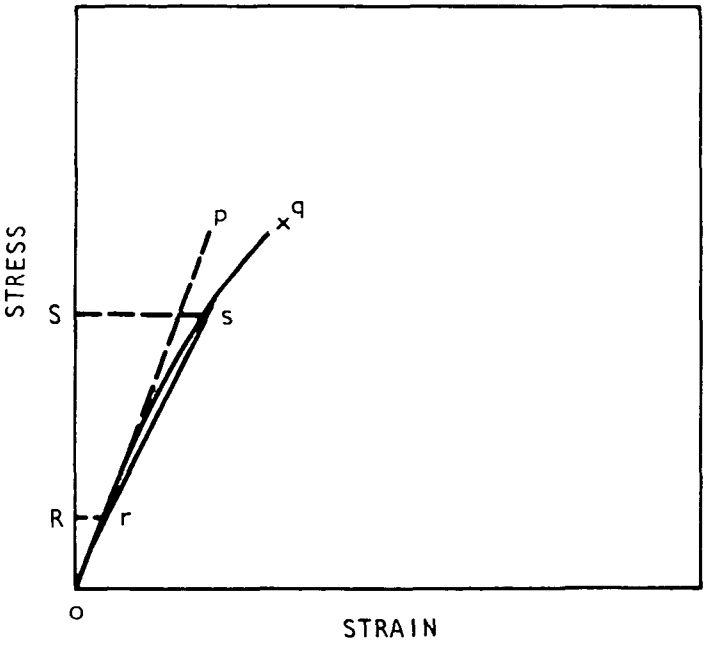

(b)

Fig. 5-1. Stress-strain curves for graphite

5.4.4. Strain at Fracture

The strain at fracture for all samples was taken as the maximum strain as indicated on the stress-strain curve (strain corresponding to point q, Fig. 5-1).

5.4.5. Poisson's Ratio

Poisson's ratio was obtained on unirradiated samples, 0.505 in. in diameter by 5 in. long and 0.5 in. by 0.5 in. by 5 in. long, using a strain gage method. Multiple (two to four) biaxial strain gages, equidistant around the cross section, were aligned with the longitudinal and transverse directions of each specimen and attached in position with an epoxy cement. The samples were fixed to end pieces with a high-strength epoxy cement and were loaded in tension in steps to 1500 psi while recording the strains from each gage. The load was applied through roller-link chains to maintain uniaxial alignment during testing. The transverse and longitudinal strains for each gage were measured at each load using a Vishay, Inc., digital strain indicator. Poisson's ratio was calculated from the ratio of transverse and longitudinal strains for each biaxial gage after first correcting each strain for transverse sensitivity.

5.5. THERMAL CONDUCTIVITY

Thermal diffusivity measurements were made on disc samples, 0.45 in. in diameter by 0.050 in. thick, by the heat pulse method (ASTM Method of Test C-741). The thermal conductivity was calculated from the following equation:

$$k = \alpha C_p \rho \quad ,$$

where α = thermal diffusivity

C_p = heat capacity

ρ = density

Unirradiated specimens were measured at 100°C intervals from room temperature to 800°C. Irradiated specimens were measured at room temperature only or at 100°C intervals from room temperature to 100°C less than the irradiation temperature (up to a maximum of 800°C).

5.6. THERMAL EXPANSIVITY

Thermal expansivity measurements were made on cylindrical samples, 0.20 in. in diameter by 0.45 in. long, using a silica dilatometer. Unirradiated specimens were measured between room temperature and 1000°C. Irradiated specimens were measured between room temperature and 100°C less than the irradiation temperature. ASTM Method of Test E-228 was followed.

5.7. CHEMICAL IMPURITIES

Unirradiated samples were analyzed for B, Fe, V, and Ti by a standard spectrographic method and for ash by burning in a covered crucible in air.

5.8. OXIDATION RATE

Oxidation rates were obtained by measuring the weight loss of samples heated in the quartz envelope of a recording microbalance. Thin slabs, 1/8 in. thick by 1/2 in. by 1 in., were subjected to a flowing 3% steam-helium mixture at temperatures of 700° to 1050°C for several hundred hours. During each test weight losses were continuously recorded on the microbalance. The oxidation rate was calculated as the percent sample weight change per hour.

5.9. CESIUM SORPTION

Cesium sorption measurements were made by annealing the samples with a cesium source for two 8-hr periods in a sealed tantalum container. The source was prepared by loading H-327 graphite of 44 to 74 μm size with cesium nitrate containing a small amount of Cs-137 tracer. The relative

sorptivity of each sample with respect to H-327 graphite was deduced from the weights of the sample and the H-327 graphite source and their cesium concentrations. Appropriate factors were introduced to correct for differences in sample and source forms.

6. EXPERIMENTAL DATA

6.1. PROPERTIES OF UNIRRADIATED GRAPHITES

The candidate near-isotropic graphites are received as logs approximately 18 in. in diameter by 34 in. long. Past experience (Refs. 16, 17) has shown commercial graphites of this size to have variations of microstructure and properties within a single log. Therefore, it is necessary to characterize a log by measuring the properties at the center of the log [midlength center (MLC) and end center (EC)] and at the surface or edge [midlength edge (MLE)].

The following properties were measured on a number of near-isotropic logs: (1) bulk density, (2) thermal expansivity, (3) thermal conductivity, (4) tensile properties including ultimate strength, strain at fracture, modulus of elasticity, and Poisson's ratio, (5) impurity concentrations, and (6) oxidation rates in a mixture of helium and steam.

6.1.1. Bulk Density

The bulk densities of graphites H-451 and TS-1240 are given in the Appendix, Tables A-1 and A-2, respectively. The near-isotropic graphites show low variation in bulk density from the center to the edge of the log. However, variation from log to log was observed.

6.1.2. Thermal Expansivity

Thermal expansivity mean values for near-isotropic graphites H-451, H-429, and P_3JHAN are given in the Appendix, Tables A-3 through A-5, and mean values for H-327 are given in Table A-6. The near-isotropic graphites exhibit higher thermal expansivities in both directions than the needle-

coke H-327 graphite. The small variation in thermal expansivitity values throughout the H-451 log is an indication that the material has a uniform distribution of properties throughout the log. These data illustrate the uniform microstructure and properties of near-isotropic graphites compared with the anisotropic graphites.

6.1.3. Thermal Conductivity

The thermal conductivity values for the near-isotropic graphites are given in the Appendix, Tables A-7 and A-8, and those for H-327 in Table A-9. H-451 and H-327 have comparable thermal conductivity values in the radial direction, while those of TS-1240 were slightly lower.

6.1.4. Mean Values of Thermal Expansivity and Thermal Conductivity of Graphites

The mean values for thermal expansivity and thermal conductivity of the candidate graphites can be compared in Table 6-1.

6.1.5. Tensile Properties

6.1.5.1. Ultimate Tensile Strength, Modulus of Elasticity, and Strain at Fracture

The tensile property data are given in the Appendix, Tables A-10 through A-12. These data were measured on 0.505-in.-diameter by 3.0- or 4.0-in.-long and 0.250-in.-diameter by 0.90-in.-long specimens. The mean tensile properties of H-451 and H-327 graphite are compared in Table 6-2. In the axial direction, the ultimate tensile strength (UTS) of the two graphites is about the same, but H-327 is noticeably stiffer as evidenced by higher chord modulus values between 250 and 500 psi [E_{chord} (250-500)] and the lower values of strain to failure (ε_f). Graphite H-451 is noticeably stronger in the radial direction. The near-isotropic graphite is also stiffer than H-327 in the radial direction.

TABLE 6-1
MEAN VALUES OF THERMAL PROPERTIES OF CANDIDATE GRAPHITES

Type	Grade	Orientation	Location in Log	Mean Thermal Expansivity, $\alpha \times 10^6$ °C^{-1} (22°-500°C)	Thermal Conductivity (cal/cm-sec-°C)			
					22°C	200°C	500°C	800°C
Near-isotropic	H-451	Perpendicular	MLC MLE	4.41 4.49	0.294	0.262	0.204	0.158
		Parallel	MLC MLE	3.45 3.45	0.347	0.302	0.226	0.174
	TS-1240	Perpendicular	MLC	3.82[a]	0.235	0.213	0.171	0.134
		Parallel	MLC	3.30[a]	0.245	0.222	0.173	0.136
	P_3JHAN	Perpendicular	---	4.33	--	--	--	--
		Parallel	---	3.16	--	--	--	--
	H-429	Perpendicular	---	5.0	--	--	--	--
		Parallel	---	4.25	--	--	--	--
Anisotropic	H-327	Perpendicular	---	3.35	0.331	0.262	0.183	0.140
		Parallel	---	1.60	0.450	0.332	0.267	0.194

[a] Data supplied by manufacturer.

TABLE 6-2
AVERAGE TENSILE PROPERTIES OF H-451 AND H-327 GRAPHITE SAMPLES
(SAMPLES 0.505 IN. IN DIAMETER AND 4 IN. LONG)

Grade	Orientation	Location in Log: End Center UTS (psi)	End Center $E_{chord} \times 10^{-6}$ (250-500) (psi)	End Center $\varepsilon_f \times 10^2$ (in./in.)	Midlength Center UTS (psi)	Midlength Center $E_{chord} \times 10^{-6}$ (250-500) (psi)	Midlength Center $\varepsilon_f \times 10^2$ (in./in.)	Midlength Edge UTS (psi)	Midlength Edge $E_{chord} \times 10^{-6}$ (250-500) (psi)	Midlength Edge $\varepsilon_f \times 10^2$ (in./in.)
H-451	Parallel	1889	1.22	0.196	1776	1.23	0.188	2215	1.28	0.237
H-327	Parallel	2180	1.51	0.193	1629	1.54	0.148	2394	1.75	0.211
H-451	Perpendicular	1396	0.96	0.173	1262	0.93	0.158	1465	0.94	0.181
H-327	Perpendicular	1349	0.69	0.287	924	0.58	0.208	1293	0.65	0.274

Experience with GLCC indicates that production-scale nuclear graphites exhibit higher UTS values than preproduction samples, which implies that H-451 has a high probability of being stronger than H-327 without the severe strength gradient evident in the needle-coke graphite.

6.1.5.2. Poisson's Ratio

Poisson's ratio for H-451 graphite has been measured as a function of orientation and location in a log at stresses up to 1500 psi. The longitudinal and transverse strains for the measurements were obtained with biaxial strain gages attached to one or more surfaces of each specimen.

Poisson's ratio was found to decrease slightly with increasing stress during initial loading and reached a constant value for all stresses after three or four loadings. The values obtained for each specimen after several loadings are shown in Table 6-3. The Poisson's ratios for each location and orientation differ by approximately ±10% and their average is 0.123.

6.1.6. Impurity Concentrations

The chemical impurities found in H-451, TS-1240, and P_3JHAN graphite are given in the Appendix, Tables A-13 through A-15. With a few exceptions, the impurities are uniformly distributed throughout the graphite logs.

6.1.7. Effects of Steam-Graphite Oxidation - H-451 and H-327

Graphite will undergo measurable chemical oxidation by steam at temperatures in excess of 700°C according to the equation:

$$H_2O + C \rightarrow CO + H_2 + \Delta H \quad ,$$

where the endothermic heat of reaction, ΔH, is +31.14 kcal/mole. The steam-graphite reaction has been extensively investigated by numerous research groups in an effort to elucidate the kinetics of the reaction

TABLE 6-3
POISSON'S RATIO FOR GRADE H-451 GRAPHITE
(Log Number 5651-28)

Specimen No.	Specimen Size (in.)	No. of Biaxial Gages	Location and Orientation (Stress Axis)	Poisson's Ratio			
				∥ to Extrusion	⊥ to Extrusion	∥ to Radius	⊥ to Radius
5947-102-1	0.5 x 0.5 x 6 long	2 (90° apart)	MLC (⊥)	0.120	0.136		
5947-102-2	0.5 x 0.5 x 6 long	4 (90° apart)	MLC (⊥)	0.116[a]	0.128[a]		
5947-102-4	0.5 x 0.5 x 6 long	2 (90° apart)	MLC (∥)			0.134	0.118
5947-102-5	0.505 diam. x 6 long	3 (120° apart)	MLC (∥)			0.130[b]	
5651-28-133	0.5 x 0.5 x 6 long	4 (90° apart)	MLE (∥)			0.123[a]	0.110[a]
Average	---	---	MLC (⊥)	0.125 ± 0.010			
Average	---	---	MLC (∥)			0.127 ± 0.008	
Average	---	---	MLE (∥)			0.117 ± 0.007	

[a] Average of values obtained from two gages on opposite faces.

[b] Average of values obtained from all gages.

(Refs. 18, 19). The expression most commonly formulated for the rate of reaction follows the generalized Langmuir-Hinshelwood form, in which the rate is dependent on steam and hydrogen partial pressures and temperature-dependent Arrhenius coefficients:

$$R = \frac{K_1 P_{H_2O} F_b F_c}{1 + K_2 P_{H_2}^n + K_3 P_{H_2O}} .$$

In this expression, R is the local graphite mass fraction or percent reacting per unit time, P_{H_2O} and P_{H_2} are local partial pressures of steam and hydrogen, F_b and F_c are modifiers for the effects of prior reaction (burnoff) and catalysts, and the terms K_1, K_2, and K_3 are reaction rate and sorption constants.

Computer codes have been developed for analysis of the steam-graphite reaction in the HTGR core. These codes are OXIDE (Ref. 20), which was developed at GAC, and GOP (Ref. 21), which was developed at BNWL. Both codes utilize forms of the Langmuir-Hinshelwood equation but also include mass transport to and through the porous graphite substrate, core temperature profiles, and proper coolant flow geometry.

Much experimental work on the steam-graphite reaction has been documented. Results were reported for H-327 and AGOT graphites oxidized via high partial pressures of steam (2.8%) in helium at temperatures ranging from 750° to 1050°C (Ref. 22). An Arrhenius plot of the data in Fig. 6-1 verifies that H-327 has an overall activation energy (28.8 kcal/mole) and reaction rate similar to other typical nuclear graphites (i.e., AGOT graphite).

Preliminary oxidation rate data on small samples of preproduction H-451 are shown in Fig. 6-2. These results show the oxidation rate behavior and activation energy (25.2 kcal/mole) of H-451 are quite similar

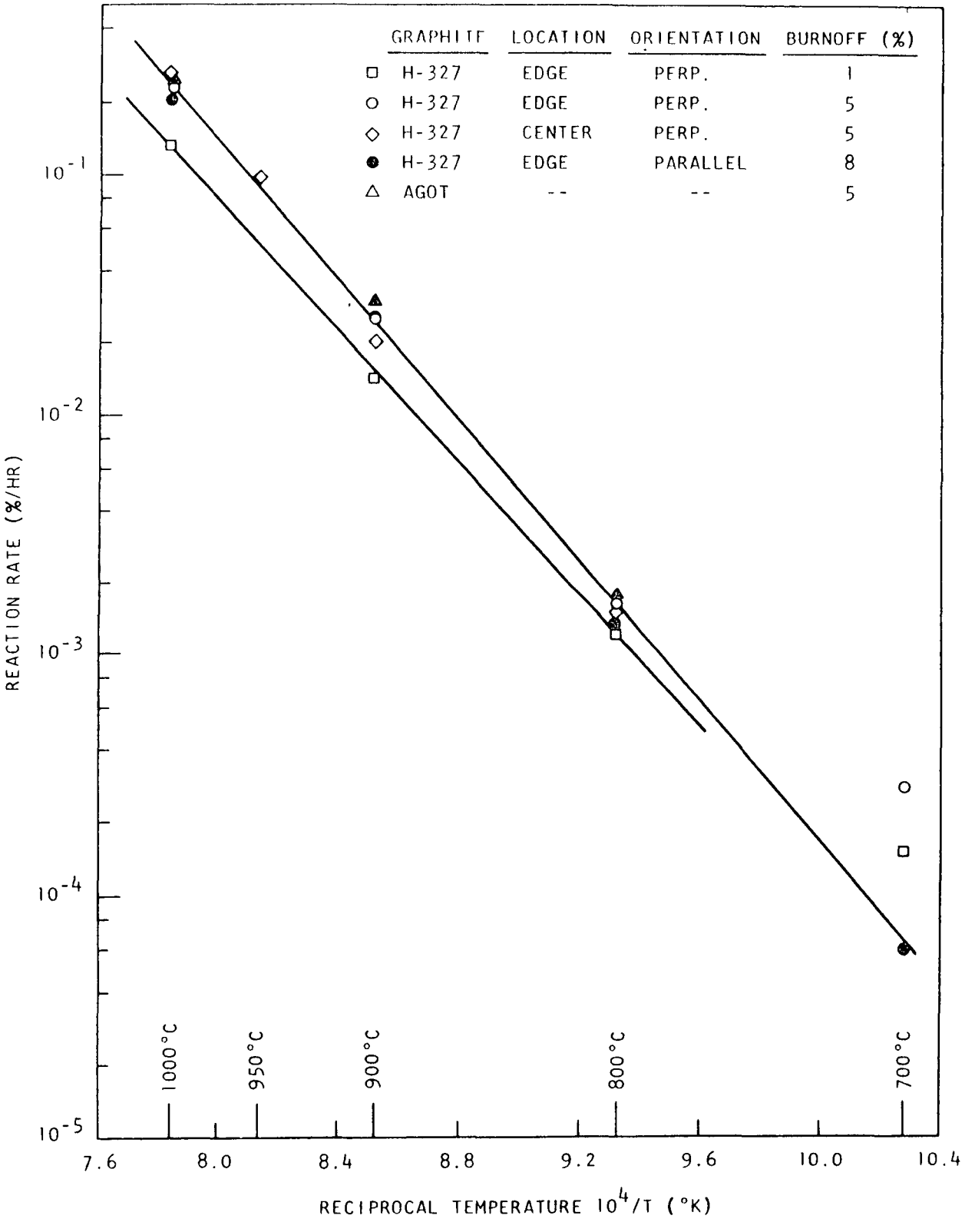

Fig. 6-1. Temperature dependence of steam-graphite reaction rate data measured at conditions of 2.8% H_2O in helium with a helium flow rate of about 150 cm^3/min

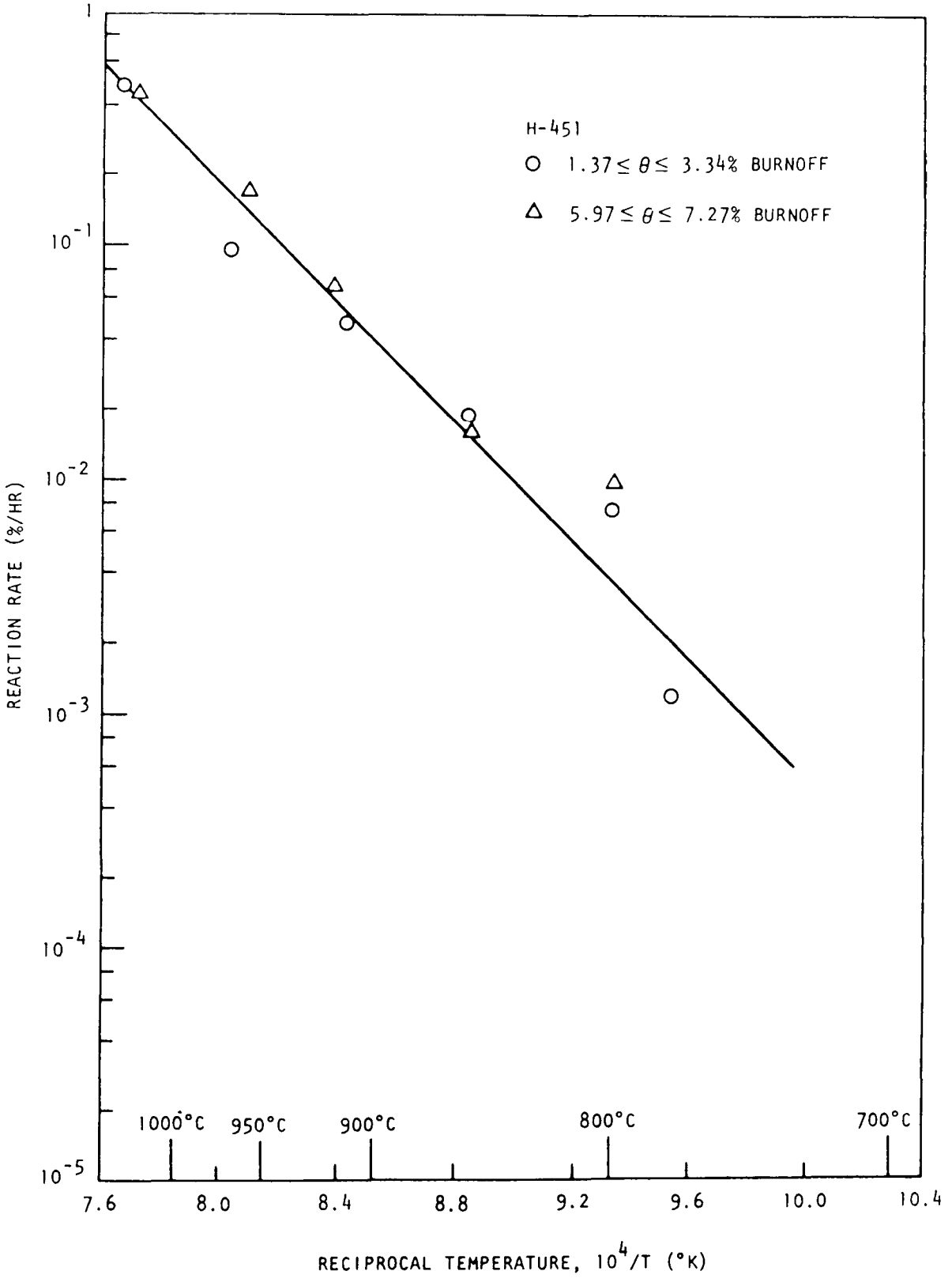

Fig. 6-2. Temperature dependence of steam-graphite reaction rate data measured at conditions of 2.8% H_2O in helium with a helium flow rate of about 100 cm^3/min

to H-327 and AGOT graphites. Thus, H-451 is expected to behave very much like previously approved nuclear graphites.

6.2. IRRADIATION BEHAVIOR

The results of recent irradiation tests at GAC on near-isotropic graphites are presented in this section. The bulk of the data was obtained on grades H-451 and H-429. New data are also available on grade H-327, along with a small amount of data on grade P_3JHAN which was irradiated for comparative purposes. The H-451/H-429 data are compared to the H-327 data where possible. The irradiation data, in most cases, parallel the data obtained on unirradiated material.

6.2.1. Dimensional Changes

The irradiation-induced dimensional changes of the candidate graphites have been measured in a series of irradiation experiments, the most recent one being capsule OG-1. There were 346 parallel and 261 perpendicular H-451 specimens, 35 parallel and 35 perpendicular H-429 specimens, 195 parallel and 123 perpendicular H-327 specimens, and 45 parallel and 45 perpendicular P_3JHAN specimens in capsule OG-1. All of the H-451 and 252 of the H-327 specimens were irradiated for the first time in OG-1. All of the H-429 specimens along with the remainder of the H-327 specimens had been previously irradiated in capsules at BNWL.

The new dimensional change data on H-451 and H-429 are plotted as a function of neutron fluence in Figs. 6-3 and 6-4. The data for H-451 and H-429 were combined (H-451/H-429) to provide data to fluences of about 6×10^{21} n/cm^2. The new H-327 data from capsule OG-1 are given in the Appendix, Tables A-16 and A-17. Comparative dimensional change curves of H-327 versus H-451/H-429 are shown in Fig. 6-5. These curves were computer calculated from a least-squares fit of the data. The H-451/H-429 data were extrapolated to 8×10^{21} n/cm^2. The mean dimensional change observed in virgin H-451 and H-327 specimens irradiated side by side in capsule OG-1 are given in Table 6-4.

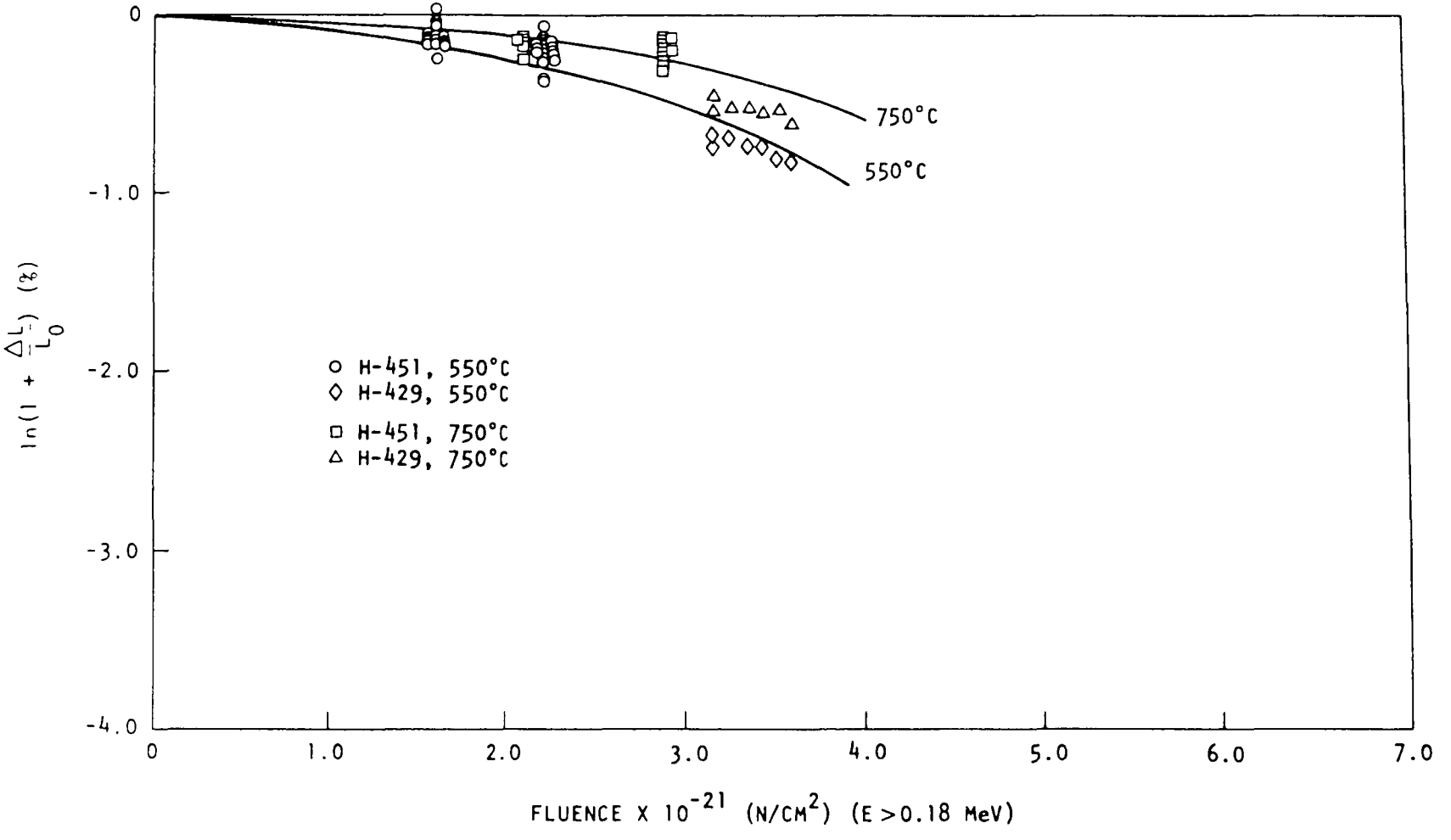

Fig. 6-3. Dimensional changes of near-isotropic graphites H-451/H-429 in the parallel direction: (a) 550° and 750°C

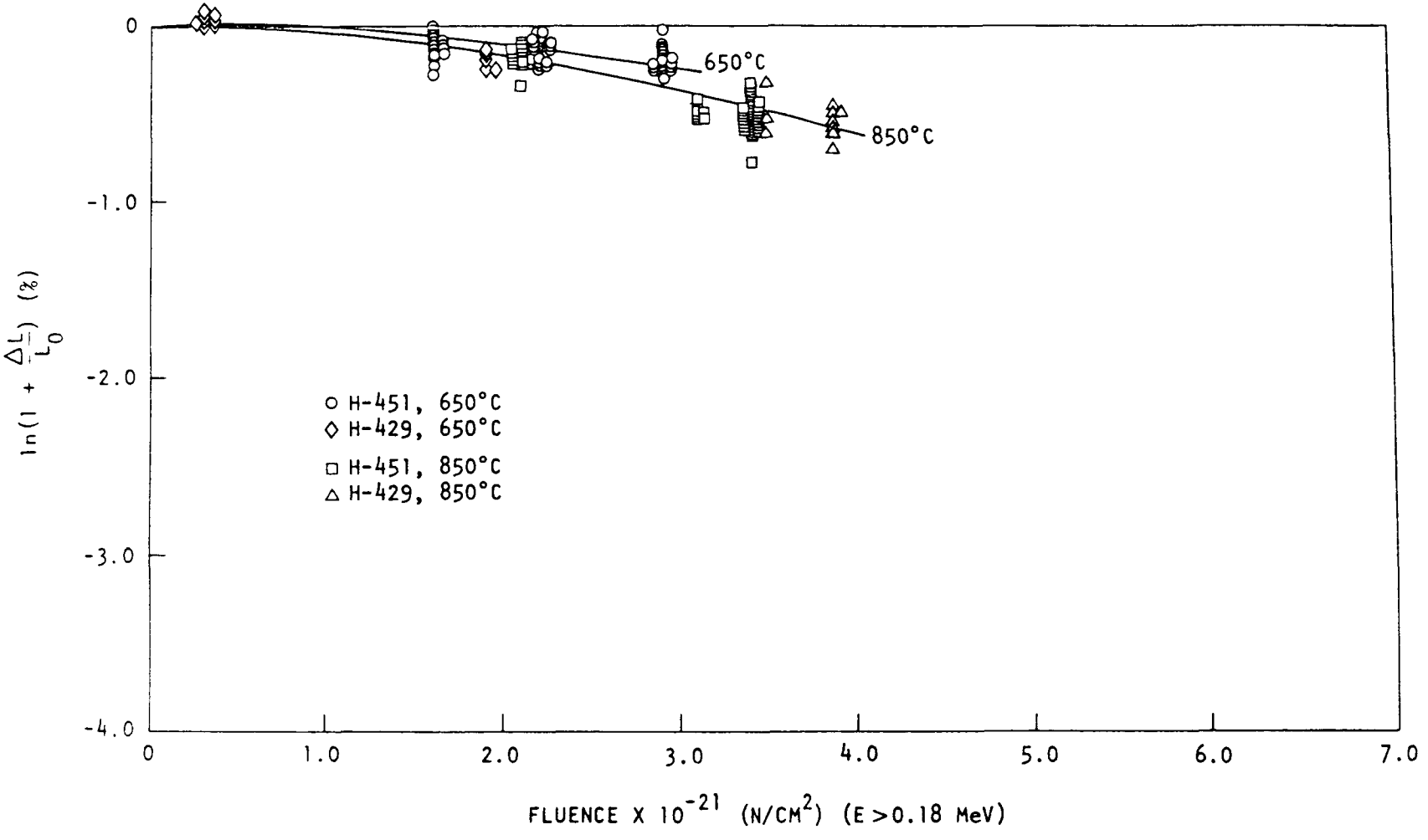

Fig. 6-3. Dimensional changes of near-isotropic graphites H-451/H-429 in the parallel direction: (b) 650° and 850°C

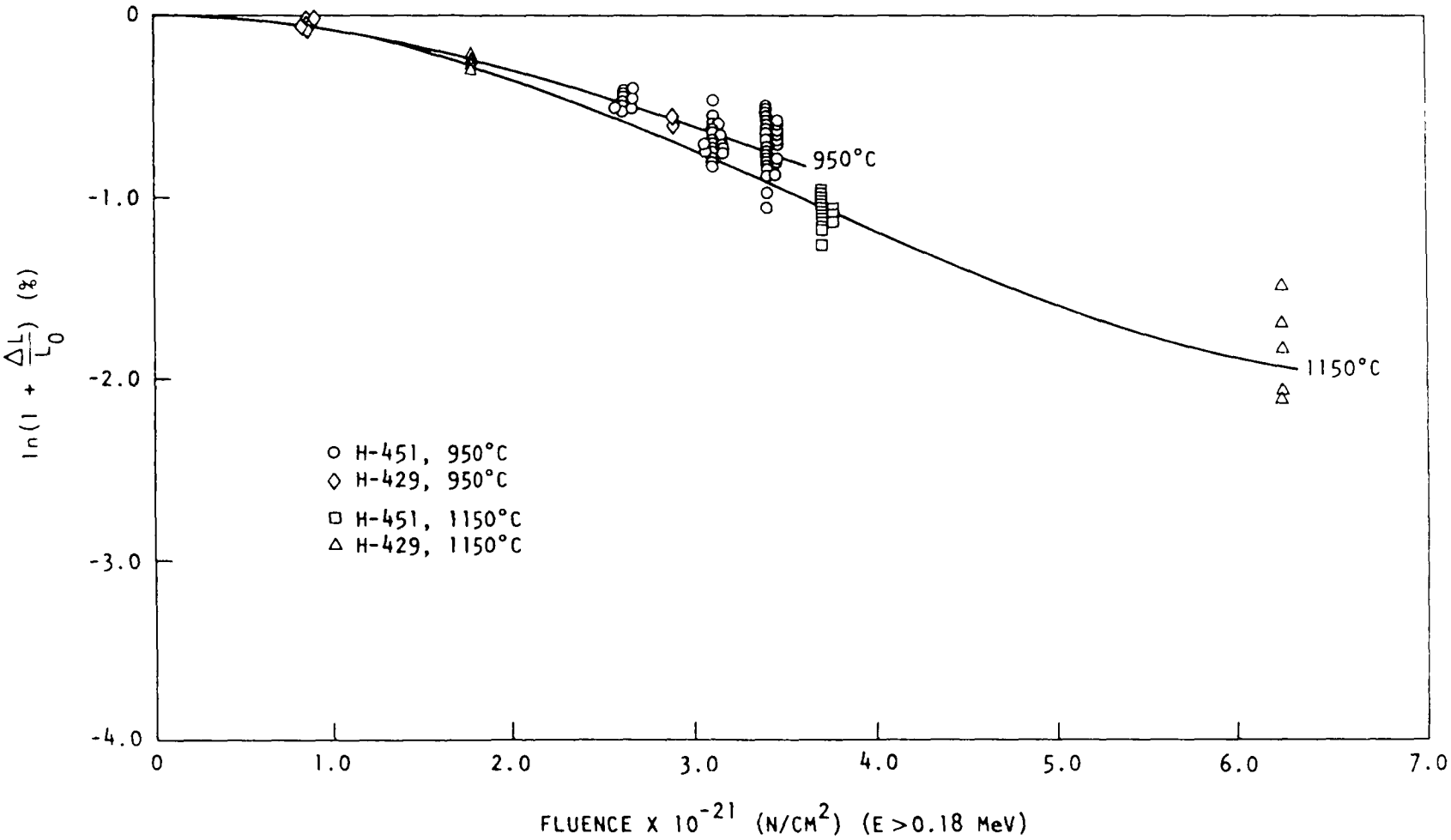

Fig. 6-3. Dimensional changes of near-isotropic graphites H-451/H-429 in the parallel direction: (c) 950° and 1150°C

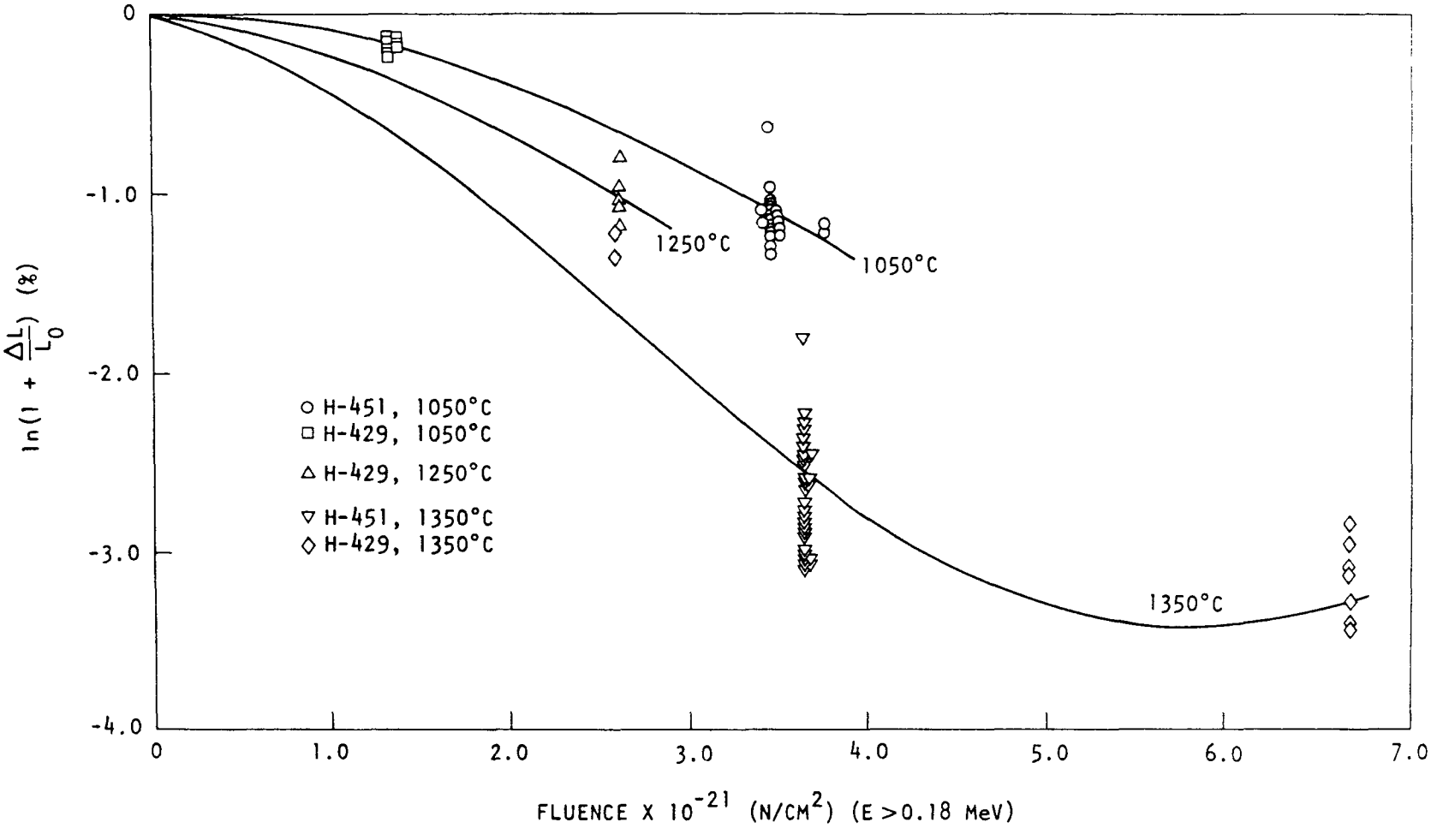

Fig. 6-3. Dimensional changes of near-isotropic graphites H-451/H-429 in the parallel direction: (d) 1050°, 1250°, and 1350°C

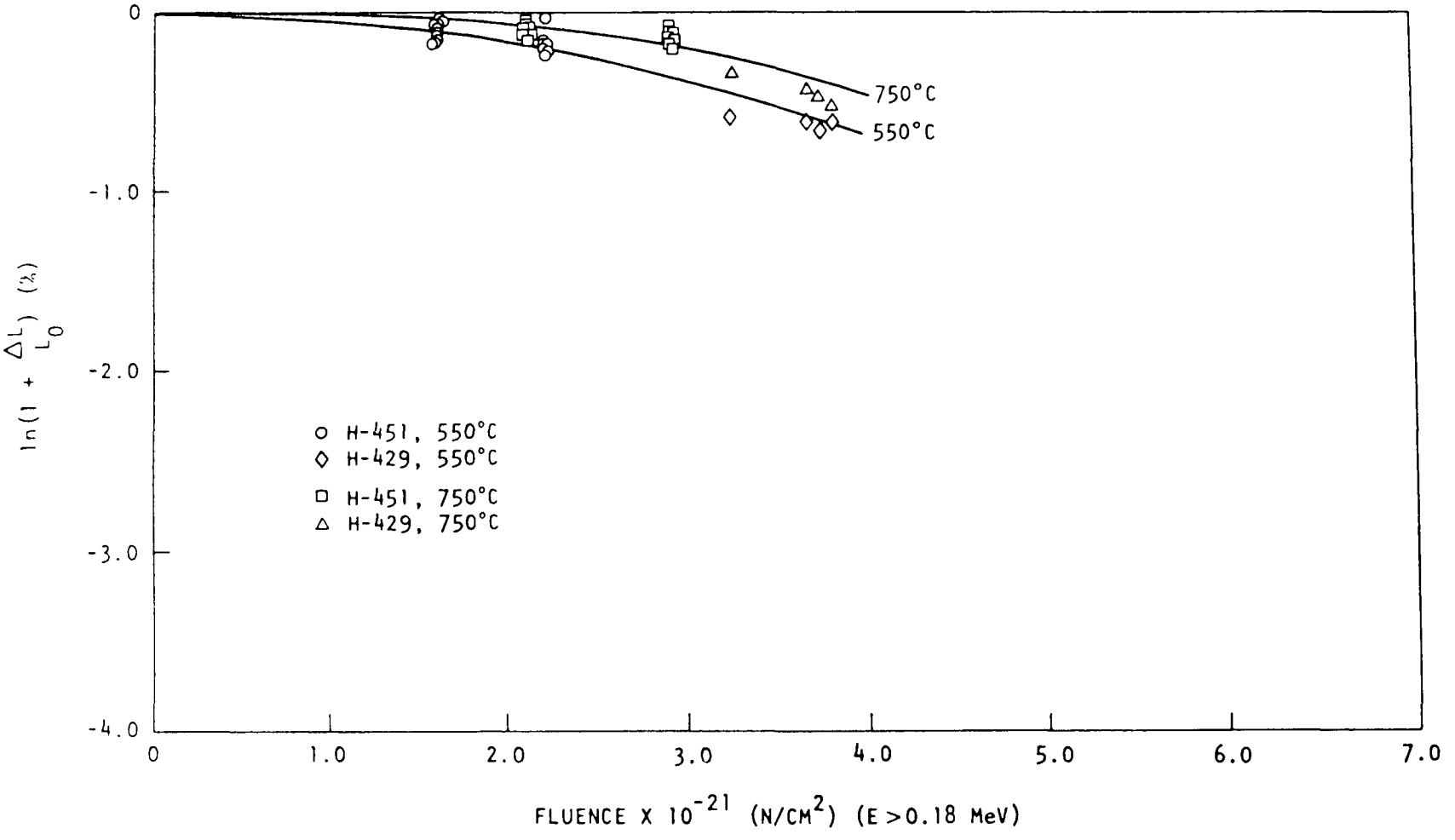

Fig. 6-4. Dimensional changes of near-isotropic graphites H-451/H-429 in the perpendicular direction: (a) 550° and 750°C

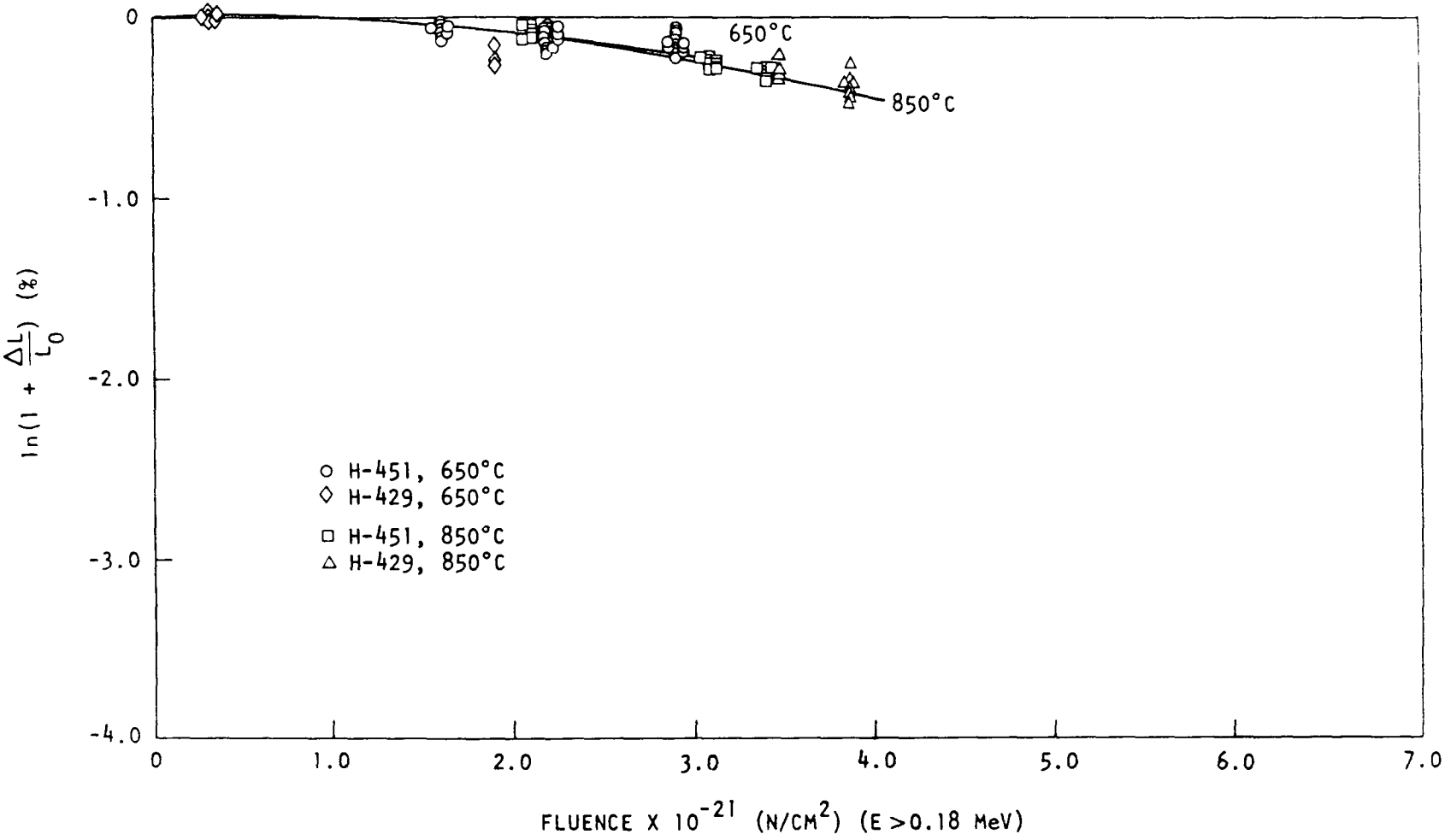

Fig. 6-4. Dimensional changes of near-isotropic graphites H-451/H-429 in the perpendicular direction: (b) 650° and 850°C

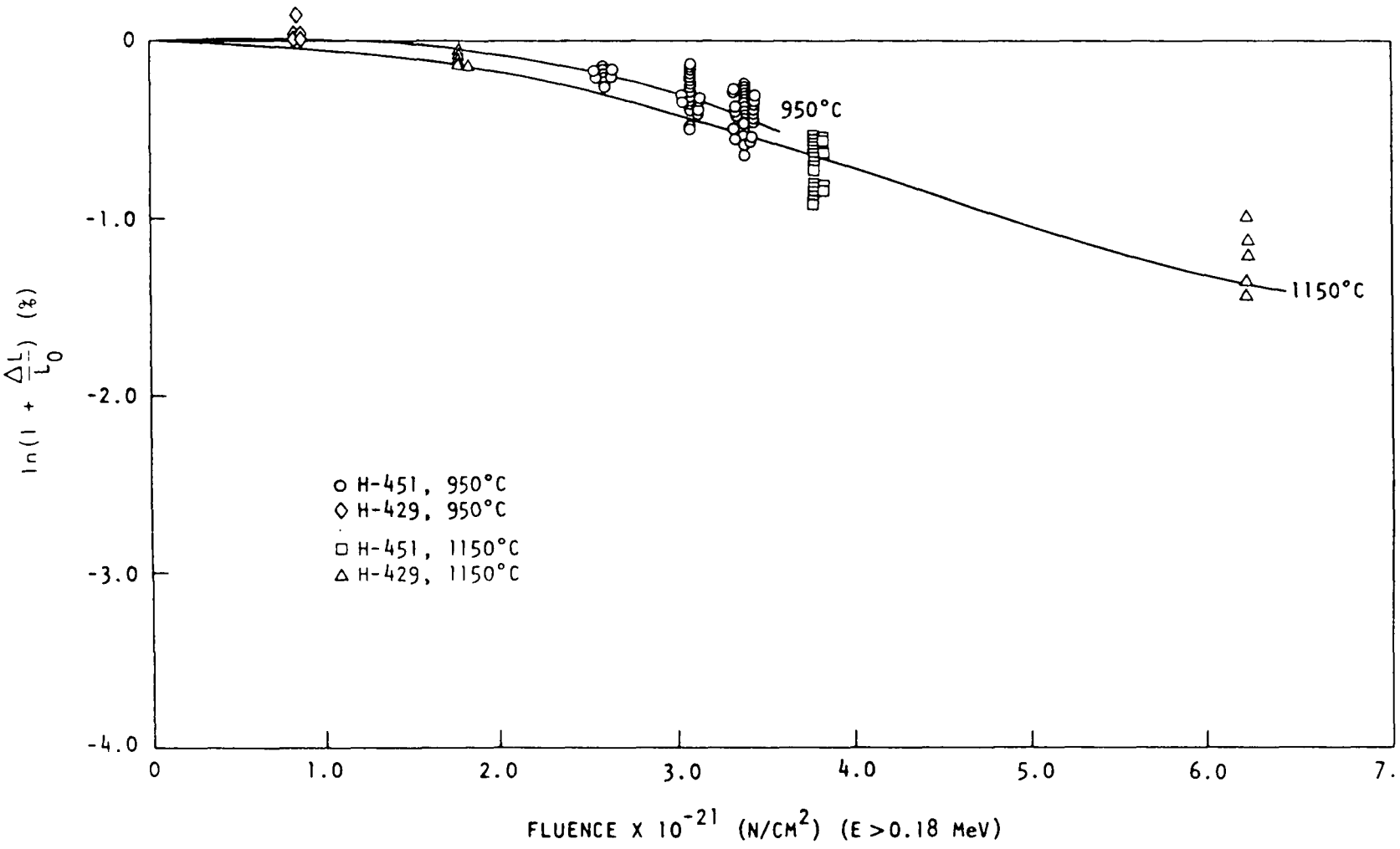

Fig. 6-4. Dimensional changes of near-isotropic graphites H-451/H-429 in the perpendicular direction: (c) 950° and 1150°C

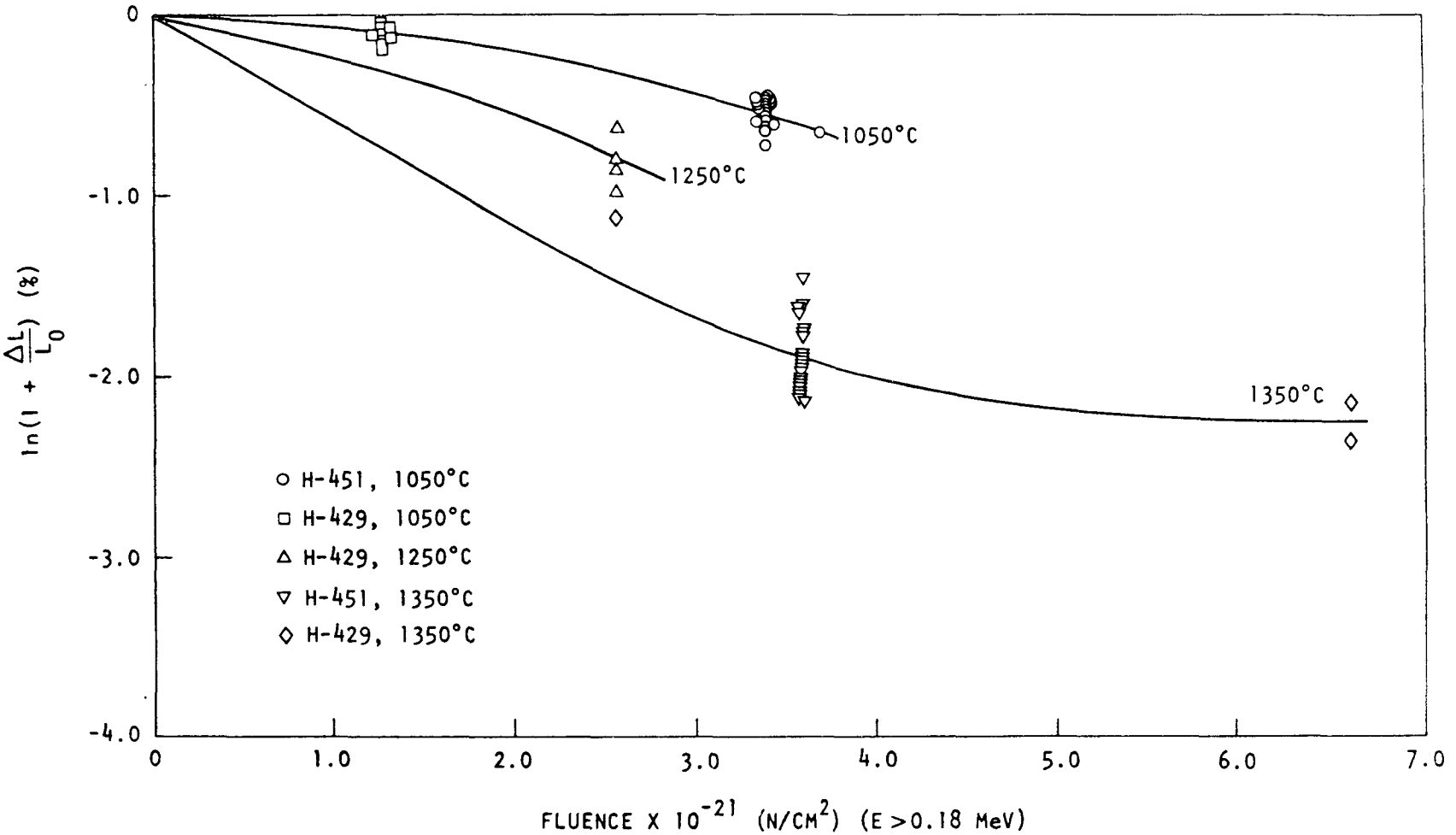

Fig. 6-4. Dimensional changes of near-isotropic graphites H-451/H-429 in the perpendicular direction: (d) 1050°, 1250°, and 1350°C

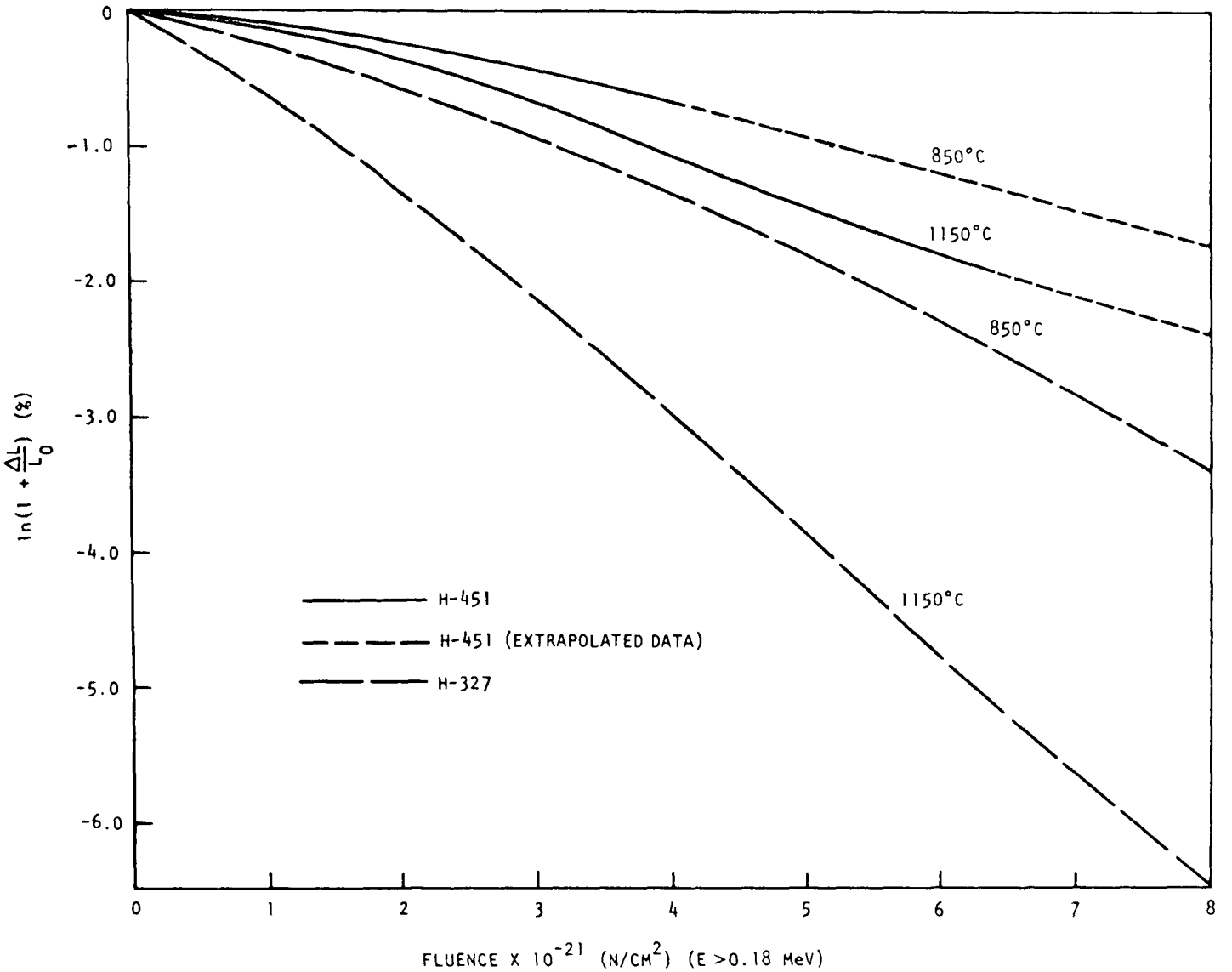

Fig. 6-5. Comparison of dimensional changes of H-327 and H-451/H-429: (a) parallel

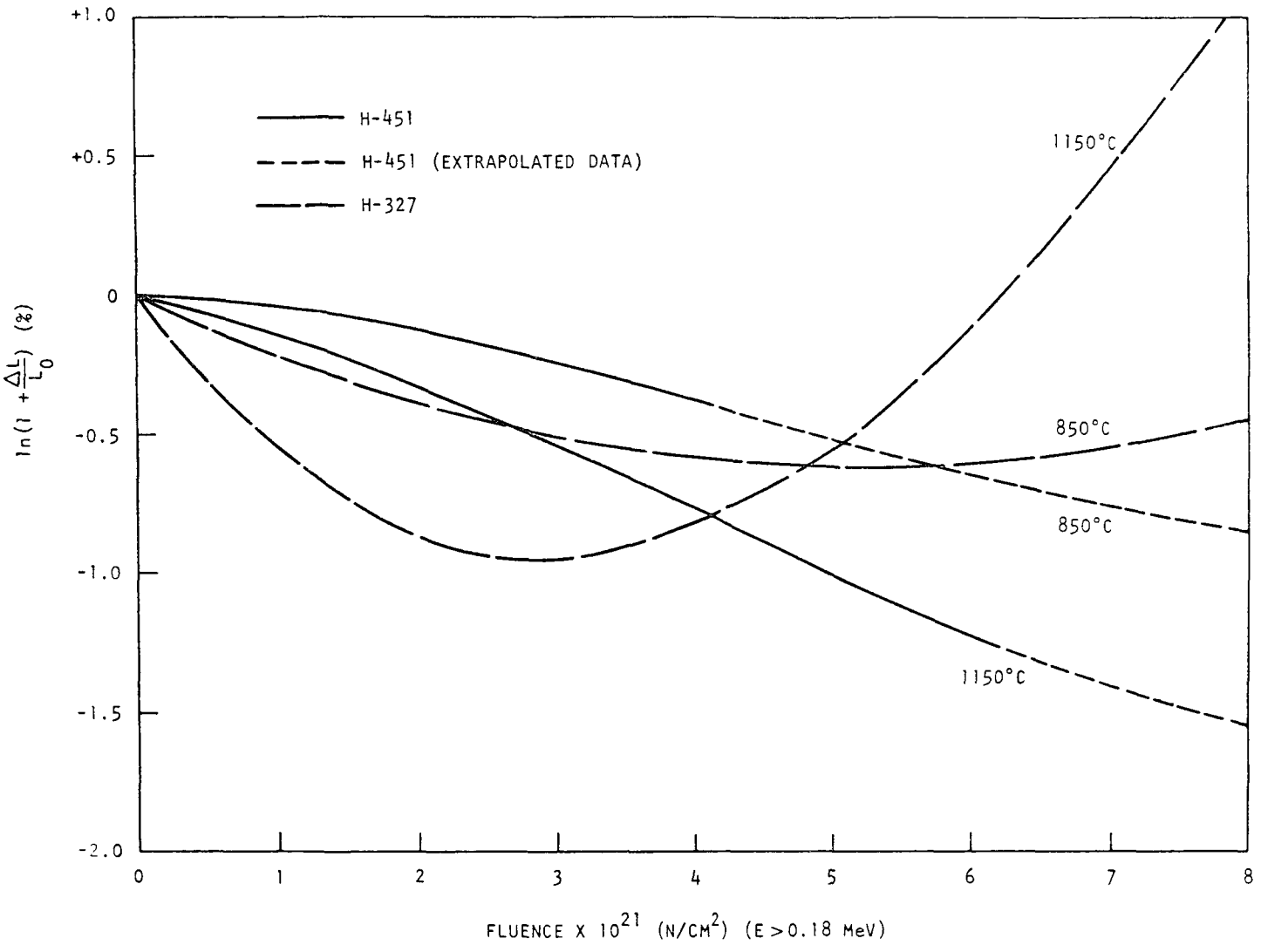

Fig. 6-5. Comparison of dimensional changes of H-327 and H-451/H-429: (b) perpendicular

TABLE 6-4
COMPARISON OF MEAN IRRADIATION-INDUCED DIMENSIONAL CHANGES
IN H-327 AND H-451 GRAPHITES IRRADIATED IN OG-1

Crucible	Fluence x 10^{-21} (n/cm^2) (E > 0.18 MeV)	Irradiation Temperature (°C)	Dimensional Change $\ln(1 + \frac{\Delta L}{L_0})$			
			Parallel		Perpendicular	
			H-327	H-451	H-327	H-451
1	2.2	645	-0.14	-0.10	-0.10	-0.08
		615	-0.19	-0.16	-0.15	-0.13
		560	-0.17	-0.20	-0.19	-0.16
2	2.9	740	-0.22	-0.17	-0.13	-0.11
		690	-0.21	-0.20	-0.22	-0.15
		610	-0.28	-0.22	-0.23	-0.15
3	3.4	945	--	--	-0.46	-0.37
		890	-0.59	-0.49	--	--
4	3.7	1110	-1.82	-0.71	--	--
		1040	-1.36	-0.80	--	--
6	3.4	1020	-1.22	-0.90	-0.46	-0.49
		940	-0.79	-0.62	-0.38	-0.32
7	3.1	990	-1.09	-0.81	-0.30	-0.41
		980	-0.99	-0.47	-0.28	-0.20
		885	-0.74	-0.50	-0.34	-0.26
8	2.6	930	-0.60	-0.54	-0.25	-0.18
		920	-0.53	-0.47	-0.15	-0.20
		835	-0.32	-0.33	-0.11	-0.13
9	2.1	810	-0.12	-0.18	--	--
		750	-0.13	-0.15	--	--
10	1.6	650	-0.06	-0.06	-0.06	-0.06
		645	-0.13	-0.09	-0.07	-0.06
		595	-0.15	-0.12	-0.06	-0.09

In the perpendicular direction the needle-coke graphite undergoes initial contraction followed by expansion which can lead to a total net expansion at high fluences and temperatures. The near-isotropic graphite contracts more slowly initially than the needle-coke graphite and the shrinkage passes through its minimum at neutron fluences where the needle-coke graphite has already expanded past its original dimensions. The data in Table 6-4 show H-327 contracts at a higher rate in the parallel direction than H-451. This effect is particularly evident at higher fluences and temperatures. The difference in behavior between the two graphites in the perpendicular direction is less marked because H-327 is nearing turnaround at the higher temperatures.

These data indicate the H-451 graphite is behaving dimensionally much like the Gilsocoke graphites shown in Figs. 3-4 and 3-9. It is concluded that near-isotropic graphites will provide much improved dimensional stability compared to needle-coke graphites at high temperatures and fluences and its use for core components will permit longer residence time in large HTGRs.

6.2.2. Thermal Expansivity

Thermal expansivity measurements were made on 72 samples of irradiated graphite from capsule OG-1. Measurements were made between room temperature and 100°C less than the irradiation temperature. The samples were cylinders measuring 0.2 in. in diameter by 0.45 in. long. Graphites included H-327 (production-grade needle coke), H-451 (preproduction near-isotropic petroleum coke), and H-429 (prototype of H-451). The H-429 samples and some of the H-327 samples had been previously irradiated in capsule GEH-13-422 (Ref. 23), thus providing high-fluence data on a near-isotropic petroleum-coke-based material.

The mean expansivities between room temperature and 500°C are listed in the Appendix in Tables A-18 and A-19. The expansivity of H-327 graphite is plotted as a function of fast neutron fluence in Fig. 6-6, and that of

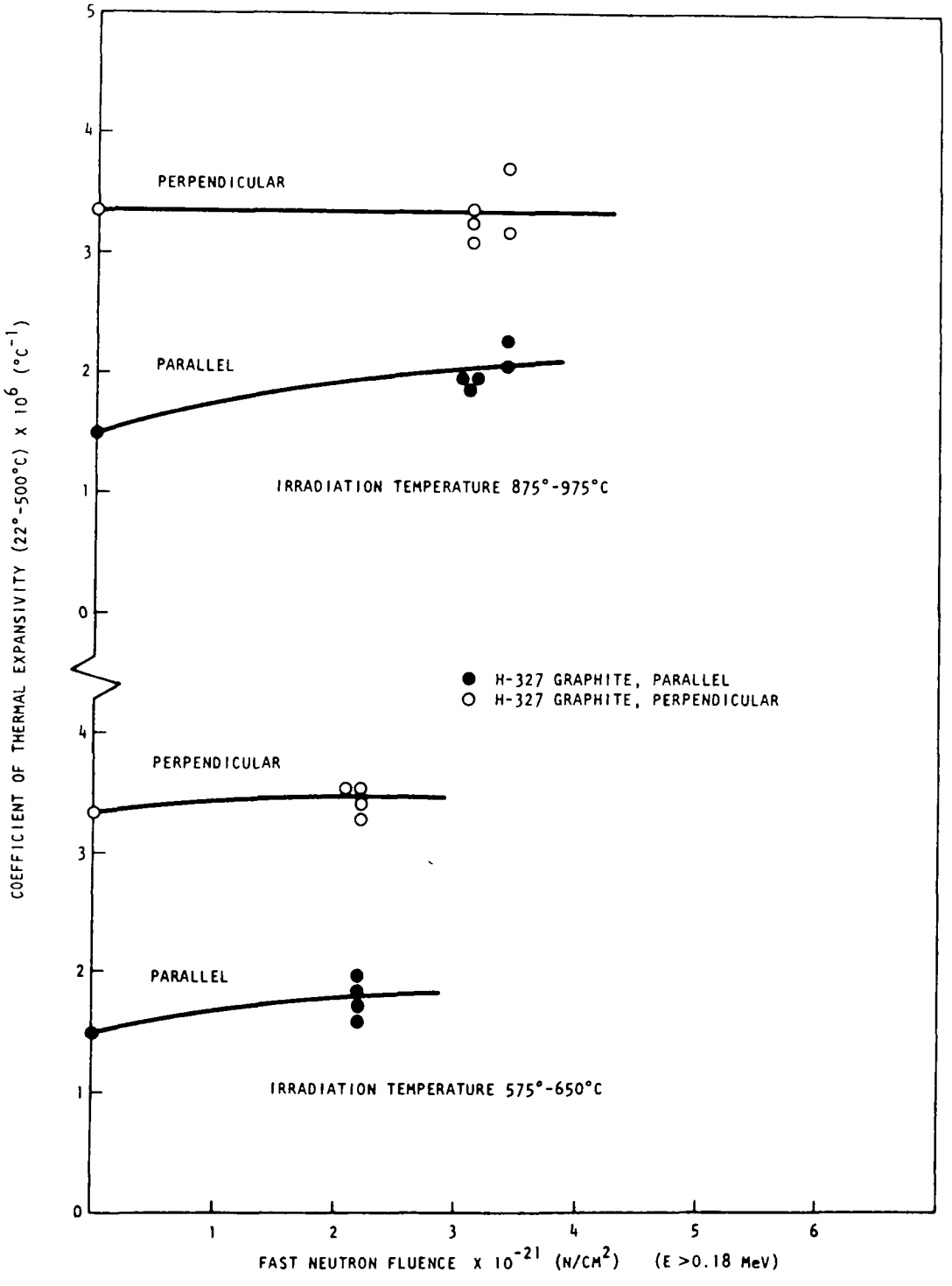

Fig. 6-6. Thermal expansivity of H-327 graphite as a function of fast neutron fluence at 875° to 975°C and 575° to 650°C.

H-429/H-451 is shown in Figs. 6-7 and 6-8. The thermal expansivity of H-327 graphite increased by about 0.5 x 10^{-6} $°C^{-1}$ in the parallel direction after a fluence of 2 to 3 x 10^{21} n/cm^2 (E > 0.18 MeV) at 575° to 650°C and 875° to 975°C, but remained unchanged in the perpendicular direction. The irradiation-induced changes in the thermal expansivity of H-429/H-451 (Figs. 6-7 and 6-8) were quite small. At 650°C and 850°C the expansivity increased by about 0.5 x 10^{-6} $°C^{-1}$ in both the parallel and perpendicular directions for a fluence of $\sim$2 x 10^{21} n/cm^2 (E > 0.18 MeV). At higher temperatures the changes were smaller; there was some indication of a net decrease in expansivity after irradiation to 6.6 x 10^{21} n/cm^2 at 1370° to 1500°C (Fig. 6-7). These changes are much less than those occurring in Gilsocoke-based graphites, whose thermal expansivities first increase and later decrease to about half their preirradiation value at around 5 x 10^{21} n/cm^2 (E > 0.18 MeV) for temperatures in the vicinity of 1000°C.

6.2.3. Thermal Conductivity

Thermal diffusivity measurements were made on 51 discs (0.45 in. in diameter by 0.05 in. thick) of H-327 and H-451 graphites after irradiation in the OG-1 capsule. The H-327 discs had previously been irradiated in capsule GEH-13-422 (Ref. 13). Thermal diffusivity measurements were made by the heat-pulse method (ASTM Method of Test C-741) and the thermal diffusivity values were converted to thermal conductivities by multiplying by density and literature values for the heat capacity of graphite. About half the samples were tested at room temperature only, and half were measured with the temperature increasing in 100°C steps to 100°C less than the irradiation temperature or to 800°C, whichever was lower.

The results are listed in the Appendix, Tables A-20 and A-21. The conductivity at the irradiation temperature was estimated by extrapolating the data points, assuming a temperature dependence curve appropriate for irradiated graphite (Ref. 24). The mean values for the conductivity at the irradiation temperature are summarized in Table A-22. Because of its high degree of orientation, the H-327 graphite had a higher conductivity

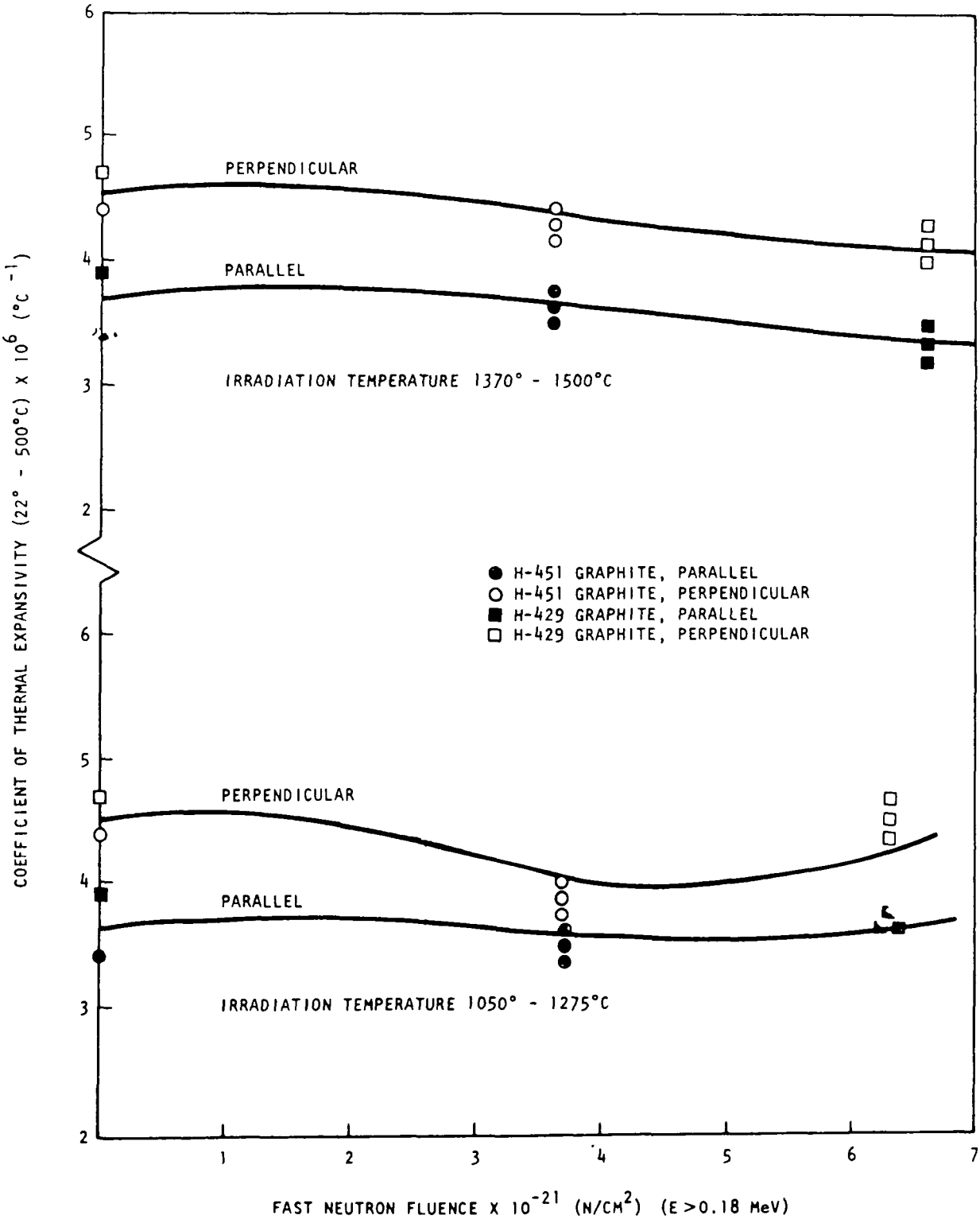

Fig. 6-7. Thermal expansivity of H-451/H-429 graphites as a function of fast neutron fluence at 1370° to 1500°C and 1050° to 1275°C

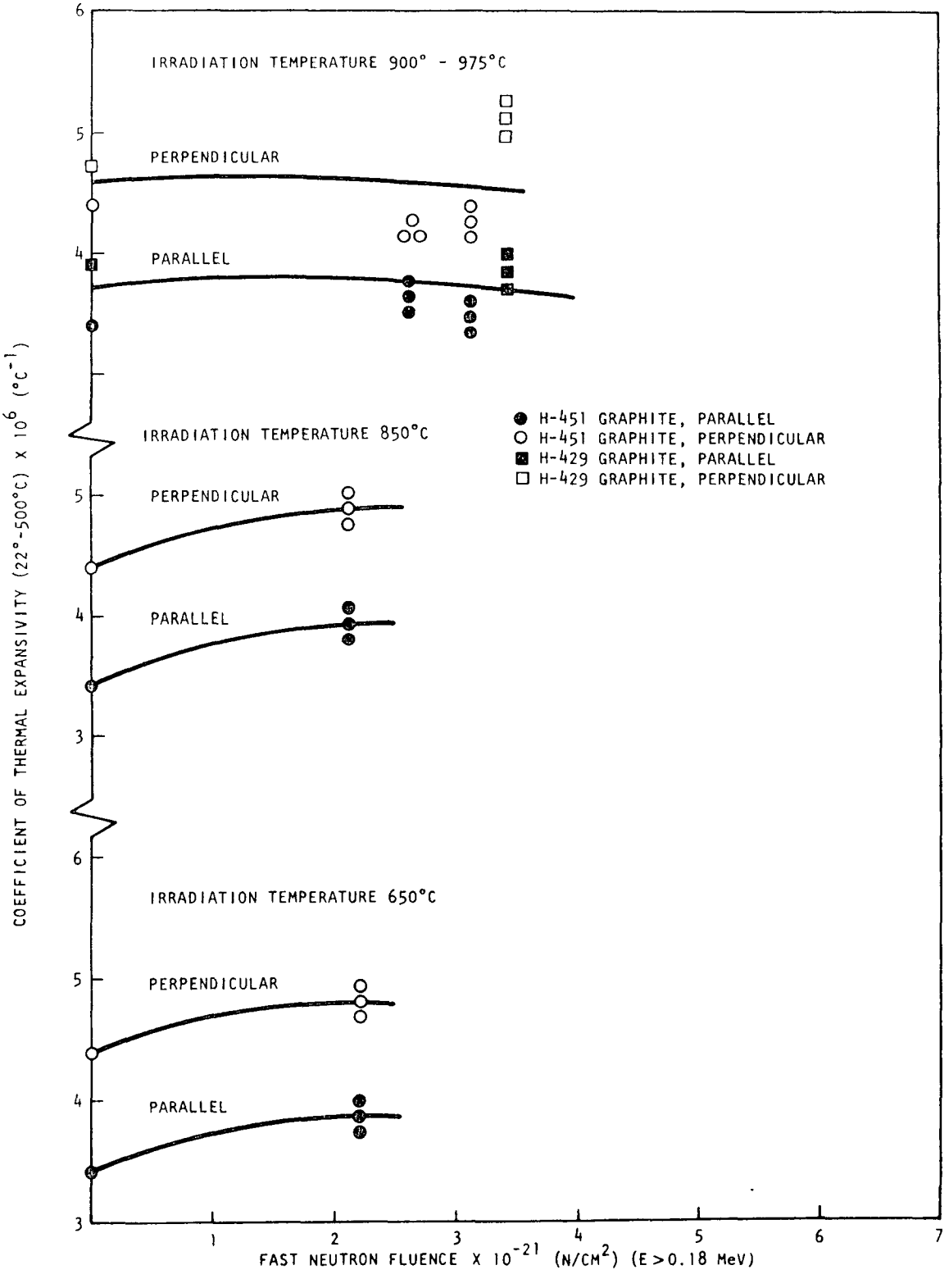

Fig. 6-8. Thermal expansivity of H-451/H-429 graphites as a function of fast neutron fluence at 900° to 975°C, 850°C, and 650°C

parallel to extrusion than perpendicular to extrusion. For H-451 graphite the difference was much less marked. At 600° and 900°C the perpendicular conductivity of irradiated H-451 graphite was considerably greater than that of irradiated H-327 graphite; the H-451 perpendicular conductivity also was slightly higher than H-327 graphite in the parallel direction. The thermal conductivity of irradiated H-451 graphite was in good agreement with curves calculated from the irradiation behavior of Gilsocoke-based graphites (Ref. 24). The comparison is shown in Fig. 6-9.

6.2.4. Tensile Properties

Tensile tests were conducted in air at room temperature on 0.25-in.-diameter by 0.9-in.-long cylinders of H-327 and H-451 graphite irradiated in capsule OG-1. Typical stress-strain curves for unirradiated and irradiated H-451 graphite are shown in Fig. 6-10. Because of the inelastic component in the deformation of graphite, the unloading curve does not retrace the initial loading curve but reaches zero load with a positive "permanent set." The second loading curve superimposes on the unloading curve, and beyond the first strain reversal point it forms a continuation of the initial loading curve. Irradiation greatly reduces the inelastic strain component and the stress-strain curve loses much of its curvature, particularly for irradiation at lower temperature (see Fig. 6-10). In the present tests Young's modulus was measured from the 100 to 1000 psi reloading portion of the curve because this represents the effective modulus of a graphite component after its first stress excursion and because its slope is more accurately measured than that of a tangent to the curve at the origin.

The results of the tensile tests are listed in the Appendix, Tables A-23 and A-24. The tensile data for unirradiated material were obtained from companion samples from the same log locations as the irradiated samples, except in the case of H-327 from the center of the log where earlier results on 0.5-in.-diameter samples were used (see Table A-23). The changes in strength and Young's modulus with neutron exposure are

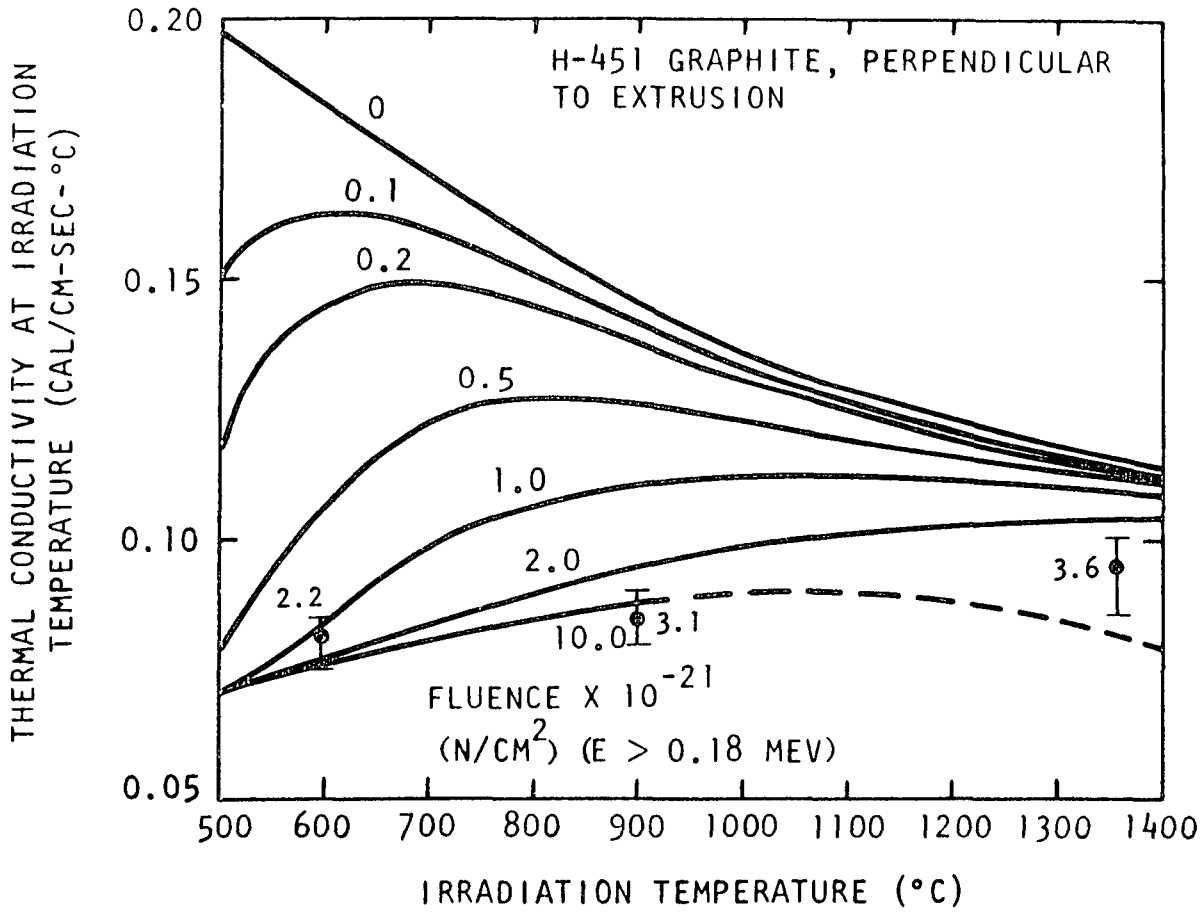

Fig. 6-9. Calculated curves of the thermal conductivity of H-451 graphite at the irradiation temperature as a function of irradiation temperature; based on the bahavior of Gilsocoke-based graphites (Ref. 24). Data points are experimental measurements from OG-1 capsule.

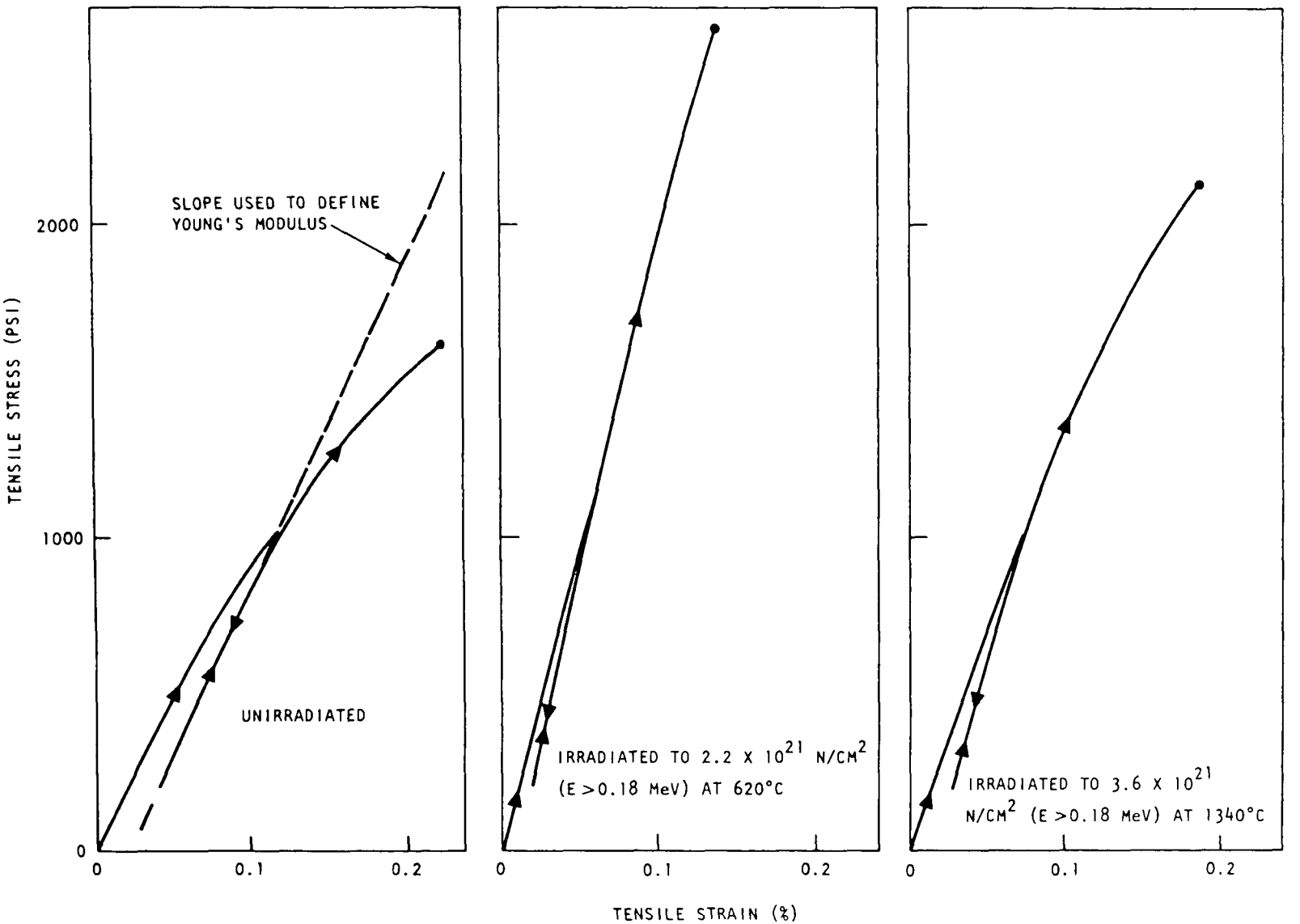

Fig. 6-10. Typical stress-strain curves for unirradiated and irradiated H-451 graphite

illustrated in Figs. 6-11 through 6-13. The strength and Young's modulus of the parallel-cut samples of H-327 graphite and both parallel and perpendicular samples of H-451 graphite increased, with a greater increase for lower temperature irradiation than for higher temperature irradiation. The percentage increases in strength were in the range 30 to 60%, while increases in elastic modulus ranged from 60 to 130%. The single group of perpendicular samples of H-327 graphite from the center of the log showed no change in strength after irradiation, while their elastic modulus doubled. With the possible exception of the perpendicular samples of H-327 graphite, there was no significant change in the scatter of the strength data following irradiation, with the coefficient of variation remaining at about 10%. Average strength values (plus or minus one standard deviation) for material from the center of the log (the weakest portion) irradiated to 2.6 to 3.4 x 10^{21} n/cm^2 at 860° to 1080°C were:

H-327 parallel	2127 ± 281 psi
H-327 perpendicular	962 ± 198 psi
H-451 parallel	2371 ± 271 psi
H-451 perpendicular	2648 ± 270 psi

6.2.5. Cesium Sorption

Cesium sorptivity and cesium vapor pressure measurements have been made on H-451 and H-327 graphites. No differences were found in either cesium sorption or cesium vapor pressure properties between unirradiated H-327 and H-451 graphites.

Preliminary results from capsule OG-1 at 700° to 1150°C and 2.9 to 3.7 x 10^{21} n/cm^2 on irradiated H-327 and H-451 graphites showed that irradiation caused an average increase of a factor of 7 in their cesium sorptivity.

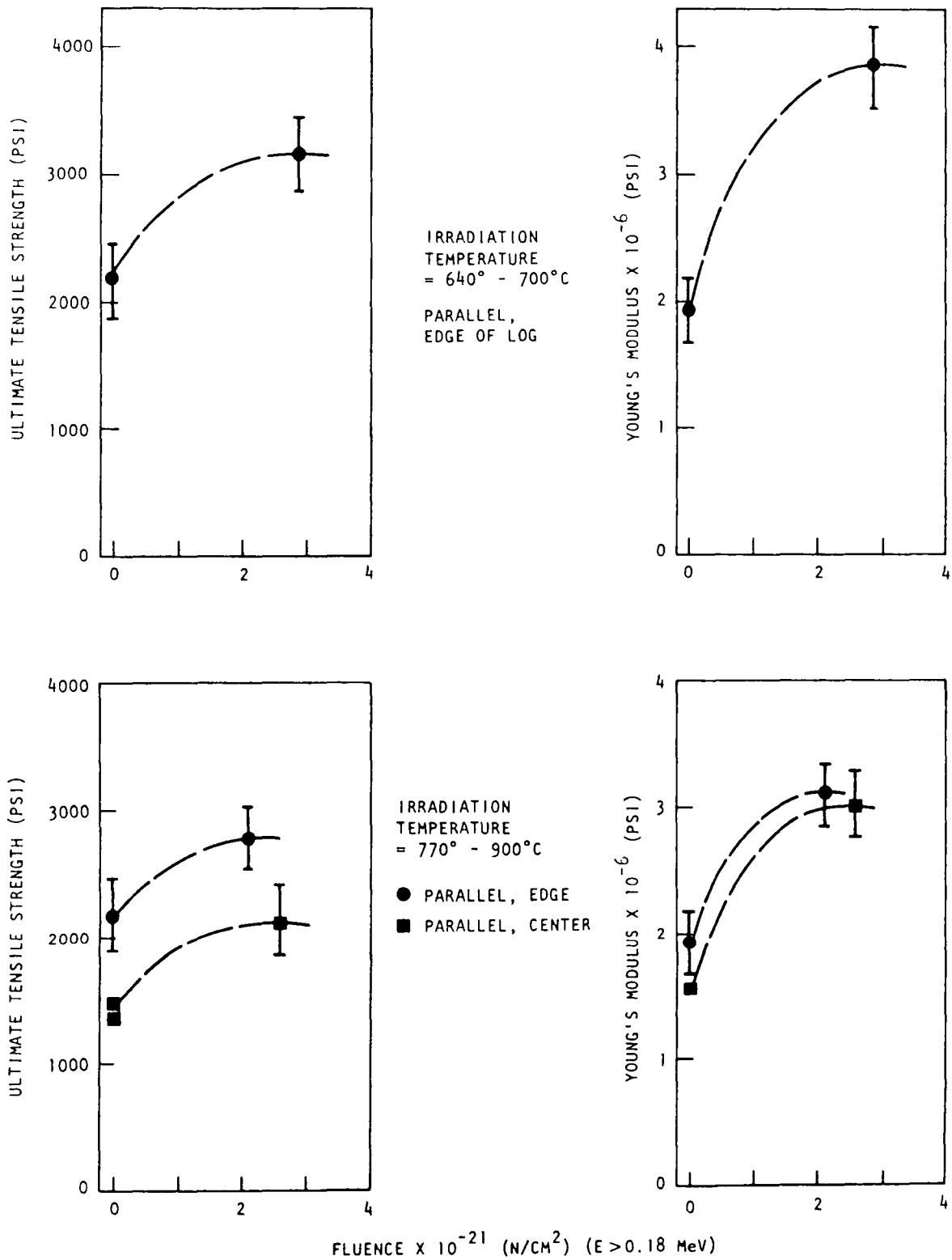

Fig. 6-11. Change in ultimate tensile strength and Young's modulus as a function of fluence, H-327 graphite, 640° to 700°C and 770° to 900°C

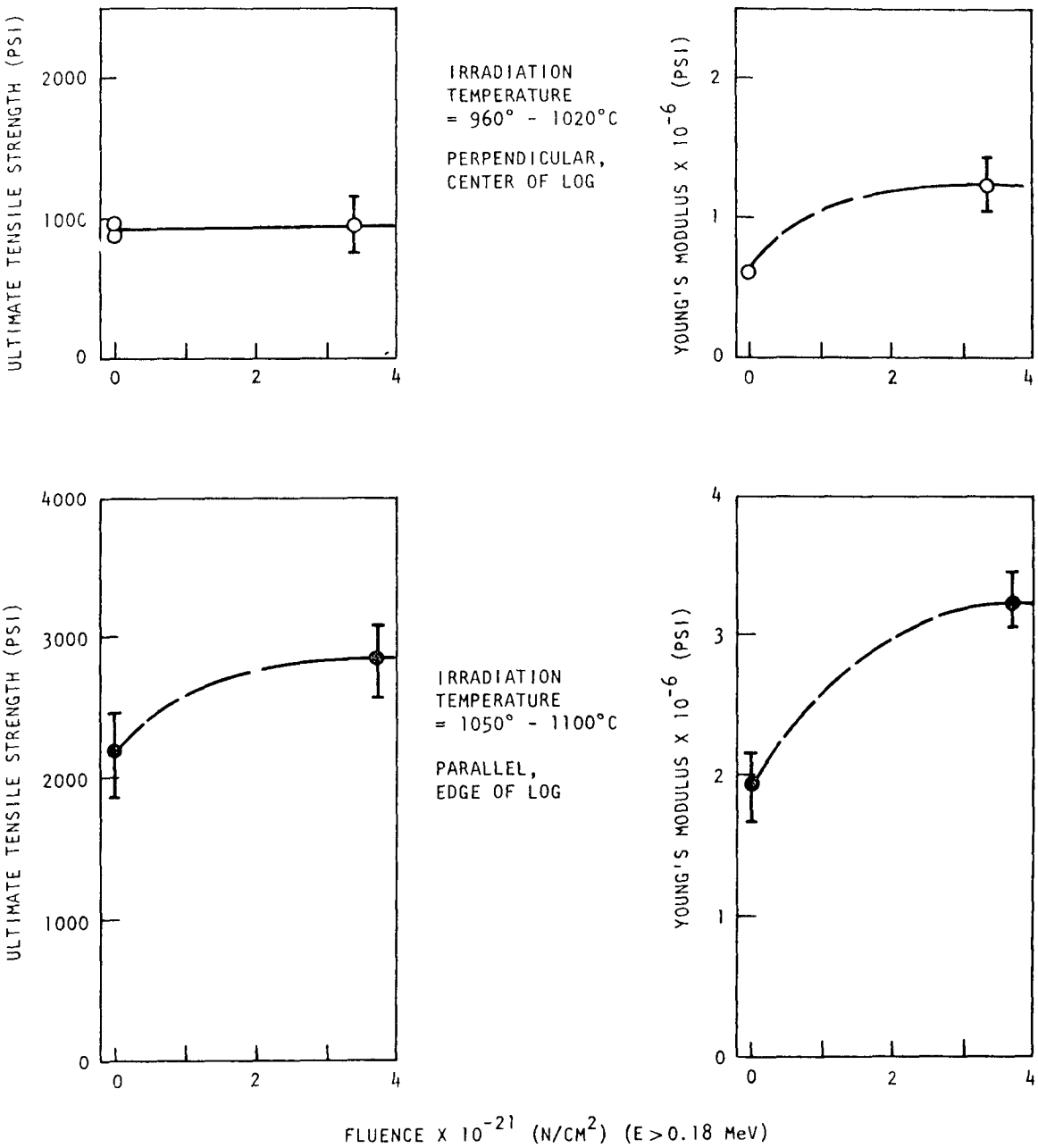

Fig. 6-12. Change in ultimate tensile strength and Young's modulus as a function of fluence, H-327 graphite, 960° to 1020°C and 1050° to 1100°C

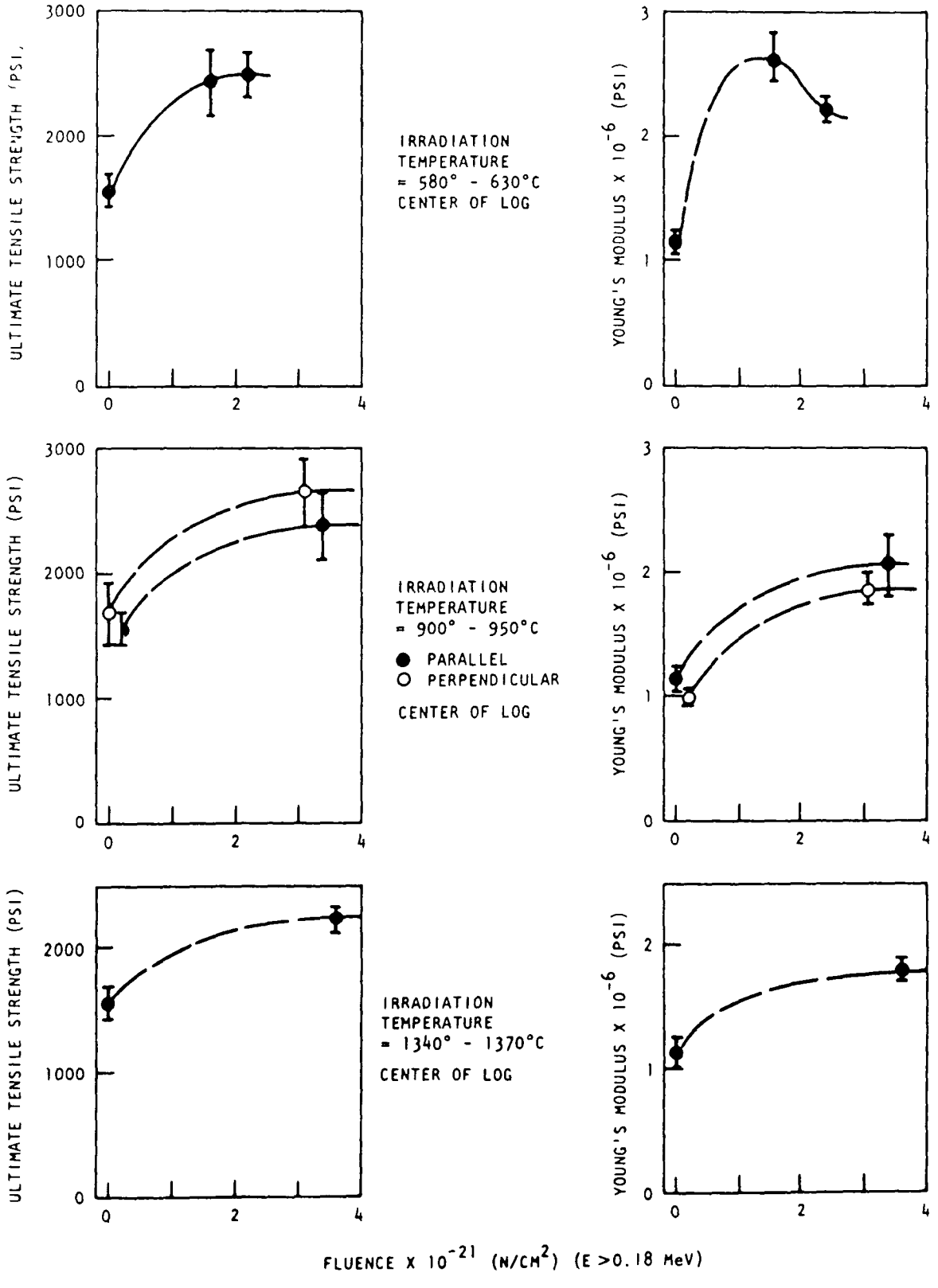

Fig. 6-13. Change in ultimate tensile strength and Young's modulus as a function of fluence, H-451 graphite, 580° to 630°C, 900° to 950°C, and 1340° to 1370°C

7. ACKNOWLEDGMENTS

The authors wish to express their thanks to L. Bailey, C. H. Richards, Jr., J. R. Whaley, and H. H. Evans who performed the laboratory work. Grateful acknowledgments are given to J. S. Steibel and the GAC Capsule Irradiation Branch who designed and fabricated capsule OG-1. Thanks are also extended to D. W. Stevens for his help with thermal property measurements. Thanks are extended to R. D. Burnette and D. D. Jensen for the oxidation data and to L. Yang and to H. G. Staley for the Ce sorption data.

REFERENCES

1. Homeyer, W. G., and R. M. Sullivan, General Atomic Company unpublished data, 1974.
2. Hutcheon, J. M., and R. P. Thorne, in Proceedings of Second Conference on Industrial Carbons and Graphites, Society of Chemical Industry, London, 1966, p. 441.
3. Nettley, P. T., et al., in Proceedings of Symposium on Advanced and High-Temperature Gas-Cooled Reactors, IAEA, Vienna, 1969, p. 603.
4. Prince, N., et al., in Proceedings of Conference on Graphite Structures for Nuclear Reactors, Institute of Mechanical Engineers, London, 1972, p. 87.
5. Welch, E. E., et al., in Proceedings of Conference on Graphite Structures for Nuclear Reactors, Institute of Mechanical Engineers, London, 1972, p. 367.
6. Blackstone, R., et al., in Proceedings of Symposium on Radiation Damage to Reactor Materials, Vol. II, IAEA, Vienna, 1969, p. 543.
7. Everett, M. R., in Proceedings of Third Conference on Industrial Carbons and Graphites, Society of Chemical Industry, London, 1971, p. 373.
8. Everett, M. R., et al., in Proceedings of Conference on Graphite Structures for Nuclear Reactors, Institute of Mechanical Engineers, London, 1972, p. 321.
9. Blackstone, R., et al., paper presented at the 11th Conference on Carbon, Gatlinburg, Tennessee, June 1973.
10. Everett, M. R., et al., Carbon 9, 417 (1971).
11. Everett, M. R., and F. Ridealgh, High Temperatures - High Pressures 4, 329 (1972).
12. Engle, G. B., and A. L. Pitner, "High-Temperature Irradiation Behavior of Production-Grade Nuclear Graphites, USAEC Report GA-9973, Gulf General Atomic, July 10, 1972.

13. Engle, G. B., and K. Koyama, "Thermal Conductivity Changes in Nuclear Graphites at High Temperatures and High Fluences," USAEC Report Gulf-GA-A12137, Gulf General Atomic, June 30, 1972.
14. Engle, G. B., "Irradiation Behavior of Nuclear Graphites at Elevated Temperatures," Carbon 9, 539 (1971).
15. Motett, P., et al., "Physical and Mechanical Properties of Nuclear Graphites, Their Application in High Temperature Reactors," "Carbon 72," International Carbon Conference, Baden-Baden, West Germany, June 1972.
16. White, J. L., and R. J. Price, "The Formation of Mesophase Microstructure During the Pyrolysis of Selected Coker Feedstocks," Gulf General Atomic Report Gulf-GA-A12722, August 20, 1973.
17. Cobb, H. R. W., G. B. Engle, and S. J. S. Parry, "Characterization of Production-Grade H-327 Graphite for HTGR Design," in Proceedings of Conference on Continuum Aspects of Graphite Design, Gatlinburg, Tennessee, November 9-12, 1970, USAEC Report CONF-701105, p. 98.
18. Walker, P. L., et al., Adv. in Catalysis 11, 133, (1959).
19. "HTGR Base Program Quarterly Progress Report for the Period Ending November 30, 1971," USAEC Report Gulf-GA-A10930, Gulf General Atomic, December 31, 1971.
20. Peroomian, M. B., A. W. Barsell, and J. C. Saeger, "Oxide-3: A Computer Code for Analysis of HTGR Steam or Air Ingress Accidents," General Atomic Company Report GA-A12493, (GA-LTR-7) January 15, 1972.
21. Giberson, R. C., and G. L. Tingey, "Reaction of Gaseous Impurities in a High-Temperature Gas-Cooled Reactor," USAEC Report BNWL-974, Battelle Northwest Laboratories, December 1968.
22. "Public Service Company of Colorado 330-MW(e) High-Temperature Gas-Cooled Reactor Research and Development Program, Quarterly Progress Report for the Period Ending March 31, 1970," USAEC Report GA-10010, Gulf General Atomic, April 30, 1970.
23. Engle, G. B., "Relationship Between Crystal Structure and Properties and Irradiation Behavior of Reactor Graphites," Gulf General Atomic Report Gulf-GA-A12124, June 30, 1972.

24. Price, R. J., "Review of Thermal Conductivity of Nuclear Graphite under HTGR Conditions," Gulf General Atomic Report Gulf-GA-A12615 (GA-LTR-3), September 1973.

25. Price, R. J., "Calculation of the Thermal Conductivity of Irradiated Graphite for a Changing Irradiation Temperature," October 16, 1973, General Atomic Company unpublished data.

APPENDIX

TABLE A-1
BULK DENSITIES OF H-451 GRAPHITE

Specimen No.	Location in Log	Bulk Density (g/cm^3)	Specimen No.	Location in Log	Bulk Density (g/cm^3)
Log Number 5651-28					
5651-28-201	Midlength	1.70	5651-28-224	Midlength	1.72
202	center	1.74	225	edge	1.75
203		1.74	229		1.74
204		1.75	230		1.75
205		1.75	234		1.74
206		1.74	235		1.74
207		1.74	239		1.74
208		1.73	240		1.76
209		1.73	244		1.75
210		1.75	245		1.75
211		1.74	249		1.73
212		1.74	250		1.75
221		1.75	254		1.74
222		1.75	255		1.72
223		1.74			
226		1.69			1.74 ±0.01
227		1.75			
228		1.73			
231		1.75			
232		1.75			
233		1.74			
236		1.65			
237		1.75			
238		1.74			
241		1.77			
242		1.74			
243		1.72			
246		1.75			
247		1.75			
248		1.75			
251		1.72			
252		1.74			
253		1.75			
256		1.73			
		1.74 ±0.02			

TABLE A-1 (continued)

Specimen No.	Location in Log	Bulk Density (g/cm^3)	Specimen No.	Location in Log	Bulk Density (g/cm^3)
		Log Number 5651-58			
5651-58- 1	Midlength	1.73	5651-58-21	Midlength	1.73
2	center	1.73	22	edge	1.73
3		1.73	23		1.73
4		1.72	24		1.73
5		1.72	25		1.73
6		1.72	26		1.73
7		1.73	27		1.73
8		1.73	28		1.73
9		1.74	29		1.73
10		1.73			
11		1.73			1.73 ±0.00
12		1.74			
13		1.73			
14		1.73			
15		1.73			
16		1.73			
17		1.73			
18		1.73			
19		1.73			
		1.73 ±0.01			

TABLE A-2
BULK DENSITIES OF TS-1240 GRAPHITE

Specimen No.	Location in Log	Bulk Density (g/cm^3)	Specimen No.	Location in Log	Bulk Density (g/cm^3)
		Log Number	5651-72		
5651-72-3A-151	Midlength	1.73	5651-72-3A-50	Midlength	1.72
153	edge	1.76	53	center	1.72
155		1.77	54		1.72
157		1.77	58		1.74
-3B-161		1.77	-3B-61		1.74
162		1.73	64		1.73
164		1.75	65		1.72
166		1.74	69		1.73
-3A-175		1.76			
176		1.76	-3A-76		1.74
179		1.75	77		1.73
180		1.75	80		1.73
-3B-193		1.73	-3B-87		1.72
194		1.73	88		1.73
197		1.75	89		1.73
198		1.75	92		1.73
		1.75 ±0.02			1.73 ±0.01
5651-72-1A-101	End edge	1.74	5651 -1A- 1	End center	1.74
103		1.75	4		1.72
105		1.74	5		1.70
107		1.77	9		1.73
-1B-111		1.75	-1B-11		1.73
112		1.75	14		1.72
114		1.73	15		1.71
116		1.71	19		1.73
-1A-125		1.74	-1A-25		1.75
126		1.75	26		1.74
129		1.75	27		1.72
130		1.75	28		1.72
-1B-142		1.74	-1B-37		1.73
143		1.74	38		1.72
146		1.74	39		1.73
147		1.73	42		1.72
		1.74 ±0.01			1.73 ±0.01

TABLE A-2 (continued)

Specimen No.	Location in Log	Bulk Density (g/cm^3)	Specimen No.	Location in Log	Bulk Density (g/cm^3)
		Log Number 5651-75			
5651-75-3A-50	Midlength center	1.81			
53		1.81			
54		1.81			
58		1.81			
-3B-61		1.81			
64		1.81			
65		1.81			
69		1.81			
-3A-75		1.81			
76		1.80			
77		1.81			
80		1.81			
-3B-87		1.81			
89		1.81			
92		1.81			
		1.81 ±0.00			
5651-75-1A- 1	End center	1.82	5651-75-1A-101	End edge	1.78
4		1.81	103		1.79
5		1.81	105		1.78
9		1.82	107		1.78
-1B-11		1.82	-1B-111		1.78
14		1.82	112		1.79
15		1.82	114		1.79
19		1.82	116		1.79
-1A-25		1.81	-1A-125		1.81
26		1.81	126		1.80
27		1.81	129		1.81
30		1.81	130		1.81
37		1.82	-1B-142		1.82
38		1.82	143		1.81
39		1.81	146		1.81
42		1.81	147		1.81
		1.82 ±0.01			1.80 ±0.01

TABLE A-3
THERMAL EXPANSIVITY OF H-451 GRAPHITE
(Log Number 5651-28)

Specimen No.	Location in Log	Mean Coefficient of Thermal Expansion, $\alpha \times 10^6$ °C^{-1} (22° -500°C)	
		Perpendicular	Parallel
KO 341	Midlength	4.43	
2	center	4.36	
3		4.40	
4		4.20	
5		4.60	
6		4.45	
		4.41 ±0.13	
KO 347	Midlength	4.34	
8	edge	4.58	
9		4.61	
50		4.63	
51		4.53	
2		4.25	
		4.49 ±0.16	
KO 353	Midlength		3.44
4	center		3.44
5			3.49
6			3.42
7			3.46
			3.45 ±0.03
KO 359	Midlength		3.36
60	edge		3.52
61			3.51
2			3.43
3			3.48
4			3.41
			3.45 ±0.06

TABLE A-4
THERMAL EXPANSIVITY OF H-429 GRAPHITE
(Log Number 5651-38)

Specimen No.	Location in Log	Mean Coefficient of Thermal Expansion, $\alpha \times 10^6$ °C^{-1} (22° -500°C)	
		Perpendicular	Parallel
J0 277	Not available		4.27
278			4.29
279			4.46
280			4.24
281			4.01
			4.25 ±0.16
J0 282		4.86	
3		5.13	
4		5.02	
5		4.98	
6		5.03	
		5.00 ±0.10	

TABLE A-5
THERMAL EXPANSIVITY OF P_3JHAN GRAPHITE
(Log Number 5651-53)

Specimen No.	Location in Log	Mean Coefficient of Thermal Expansion, $\alpha \times 10^6$ °C^{-1} (22° -500°C)	
		Perpendicular	Parallel
LO 018	Not available		3.41
19			3.14
20			3.18
21			3.13
22			2.96
			3.16 ±0.16
LO 023		4.30	
24		4.40	
25		4.38	
26		4.34	
27		4.22	
		4.33 ±0.07	

TABLE A-6
THERMAL EXPANSIVITY OF H-327 GRAPHITE

Specimen No.	Location in Log	Mean Coefficient of Thermal Expansion, $\alpha \times 10^6$ °C^{-1} (22° -500°C)	
		Perpendicular	Parallel
HO 238	Not available	2.51	
239		3.75	
254		3.62	
255		3.65	
IO 296		3.77	
298		3.67	
300		3.54	
302		3.53	
304		3.83	
306		3.81	
308		3.75	
310		3.87	
312		3.81	
314		3.63	
JO 422		4.06	
424		3.95	
426		3.82	
428		4.02	
		3.70 ±0.33	
HO 240			1.80
241			1.63
256			1.59
257			1.98
IO 297			1.91
299			2.03
301			1.98
303			1.87
305			2.09
307			2.06
309			2.06
311			2.07
313			1.98
315			1.87
JO 421			2.12
423			2.01
425			2.09
427			1.96 ±0.16

TABLE A-7
THERMAL CONDUCTIVITY OF H-451 GRAPHITE
(Log Number 5651-28)

Specimen No.	Orientation	Location in Log	Thermal Conductivity (cal/cm-sec-°C)				
			22°C	200°C	400°C	500°C	800°C
L-0011	Perpendicular	Midlength center	0.302	0.249	0.210	0.188	0.147
0012			0.324	0.273	0.235	0.216	0.163
0013			0.315	0.277	0.225	0.210	0.160
0014			0.317	0.275	0.223	0.202	0.145
0015			0.310	0.270	0.235	0.214	0.175
0017			0.287	0.245	0.204	0.190	0.150
0028			0.283	0.265	0.225	0.212	0.155
0029			0.278	0.265	0.226	0.215	0.165
0030			0.274	0.245	0.212	0.200	0.155
0031			0.270	0.261	0.223	0.203	0.162
0033			0.295	0.264	0.224	0.207	0.162
0034			0.285	0.260	0.222	0.191	0.154
			0.295 ±0.018	0.262 ±0.011	0.222 ±0.009	0.204 ±0.010	0.158 ±0.008
L-0137	Parallel	Midlength center	0.355	0.308	0.220	0.214	0.166
0138			0.346	0.309	0.252	0.234	0.179
0139			0.344	0.306	0.250	0.237	0.188
0140			0.345	0.307	0.257	0.230	0.174
0141			0.347	0.300	0.253	0.231	0.175
0142			0.346	0.305	0.264	0.234	0.173
0143			0.351	0.303	0.244	0.224	0.168
0144			0.343	0.297	0.257	0.225	0.173
0145			0.345	0.298	0.251	0.221	0.174
0146			0.345	0.291	0.232	0.213	0.172
0147			0.346	0.300	0.241	0.222	0.173
0148			0.348	0.301	0.232	0.226	0.171
			0.347 ±0.003	0.302 ±0.005	0.246 ±0.013	0.226 ±0.008	0.174 ±0.006

TABLE A-8
THERMAL CONDUCTIVITY OF TS-1240 GRAPHITE
(Log Number 5651-72)

Specimen No.	Orientation	Location in Log	Thermal Conductivity (cal/cm-sec-°C)				
			22°C	200°C	400°C	500°C	800°C
5651-72-3A-	Perpendicular	Midlength					
78A		center	0.219	0.208	0.183	0.163	0.123
78B			0.243	0.230	0.193	0.185	0.146
81A			0.229	0.216	0.181	0.175	0.141
81B			0.247	0.219	0.186	0.167	0.130
5651-72-3B-							
90A			0.242	0.198	0.178	0.166	0.127
90B			0.248	0.216	0.184	0.177	0.139
93A			0.231	0.215	0.187	0.183	0.142
93B			0.222	0.201	0.170	0.155	0.125
			0.235	0.213	0.183	0.171	0.134
			±0.011	±0.010	±0.007	±0.010	±0.009
5651-72-3A-	Parallel	Midlength					
51A		center	0.234	0.222	0.196	0.169	0.130
51B			0.242	0.236	0.190	0.177	0.139
55A			0.265	0.237	0.193	0.179	0.139
55B			0.256	0.220	0.193	0.162	0.134
5651-72-3B-							
62A			0.224	0.207	0.183	0.162	0.133
62B			0.231	0.205	0.182	0.166	0.129
66A			0.266	0.232	0.213	0.193	0.151
			0.245	0.222	0.193	0.173	0.136
			±0.017	±0.013	±0.010	±0.011	±0.007

TABLE A-9
THERMAL CONDUCTIVITY OF H-327 GRAPHITE

Specimen No.	Orientation	Location in Log	Thermal Conductivity (cal/cm-sec-°C)				
			22°C	200°C	400°C	500°C	800°C
L-0094	Perpendicular	1/2 radius	0.338	0.270	0.197	0.184	0.140
0095			0.330	0.264	0.204	0.181	0.143
0096			0.337	0.269	0.202	0.180	0.142
0097			0.336	0.274	0.209	0.197	0.141
0098			0.325	0.248	0.197	0.182	0.138
0099			0.321	0.245	0.195	0.175	0.136
			0.331	0.262	0.201	0.183	0.140
			±0.007	±0.012	±0.005	±0.007	±0.003
L-0101	Parallel	1/2 radius	0.451	0.384	0.299	0.269	0.193
0102			0.443	0.352	0.267	0.242	0.186
0103			0.444	0.377	0.311	0.276	0.187
0104			0.470	0.375	0.300	0.276	0.191
0105			0.417	0.353	0.284	0.264	0.203
0100			0.472	0.363	0.295	0.275	0.202
			0.450	0.367	0.293	0.267	0.194
			±0.020	±0.013	±0.015	±0.013	±0.007

TABLE A-10
TENSILE PROPERTIES OF H-451 GRAPHITE
(0.505-in.-diameter x 4-in.-long samples)

Specimen No.	Orientation	Location in Log	Strain at Failure (%)	Stress at Failure (psi)	Chord Modulus (250-500 psi) E x 10^{-6} (psi)
Log Number 5651-28					
5651-28-10005	Parallel	End	0.198	1910	1.25
5 10006		center	0.158	1706	1.32
10007			0.216	2012	1.25
10008			0.182	1910	1.32
10009			0.195	1920	1.19
10010			0.229	1874	1.00
			0.196	1889	1.22
			±0.025	±101	±0.12
5651-28-10014	Parallel	Midlength	0.214	1910	1.32
10015		center	0.206	1874	1.19
10016			0.173	1849	1.39
10017			0.194	1900	1.25
10018			0.204	1935	1.19
10019			0.200	1976	1.32
10020			0.216	1951	1.14
			0.201	1914	1.26
			±0.015	±44	±0.09
5651-28-10024	Parallel	Midlength	0.256	2251	1.19
10025		edge	0.237	2190	1.19
10026			0.216	2215	1.47
10027			0.193	1920	1.25
10028			0.240	2231	1.25
10029			0.244	2256	1.32
10030			0.271	2445	1.32
			0.237	2215	1.28
			±0.026	±155	±0.10
5651-28-10001	Perpendicular	End	0.210	1564	0.96
10002		center	0.176	1411	0.93
10003			0.132	1212	1.00
			0.173	1396	0.96
			±0.039	±177	±0.04
5651-28-10011	Perpendicular	Midlength	0.180	1324	1.00
10012		center	0.120	952	0.86
10013			0.093	983	0.96
			0.131	1086	0.94
			±0.045	±206	±0.07
5651-28-10021	Perpendicular	Midlength	0.147	1243	0.93
10022		edge	0.165	1334	0.93
10023			0.092	876	0.93
			0.135	1151	0.93
			±0.038	±242	±0.00

TABLE A-10 (Continued)

Specimen No.	Orientation	Location in Log	Strain at Failure (%)	Stress at Failure (psi)	Chord Modulus (250-500 psi) $E \times 10^{-6}$ (psi)
			Log Number 5651-58		
5651-58-10061	Parallel	Midlength center	0.191	1681	1.14
10062			0.168	1477	1.09
10063			0.174	1630	1.25
10064			0.166	1630	1.19
10065			0.172	1620	1.09
10066			0.130	1263	1.14
10067			0.204	1859	1.25
10068			0.200	2088	1.47
			0.176	1656	1.20
			±0.024	±244	±0.13
5651-58-10069	Perpendicular	Midlength center	0.171	1289	0.96
10070			0.155	1273	0.96
10071			0.120	1146	1.04
10072			0.137	1070	0.64
10073			0.185	1462	0.93
10074			0.205	1589	1.04
10075			0.220	1538	0.93
			0.170	1338	0.93
			±0.036	±197	±0.14
5651-58-10076	Perpendicular	Midlength edge	0.221	1716	0.93
10077			0.150	1304	0.96
10078			0.160	1401	0.93
10079			0.190	1492	0.93
10080			0.250	1905	1.00
10081			0.225	1716	0.96
10082			0.210	1665	0.96
			0.210	1600	0.95
			±0.036	±209	±0.03

TABLE A-11
TENSILE PROPERTIES OF H-451 GRAPHITE
(0.25-in.-diameter x 0.9-in.-long samples)

Specimen No.	Orientation	Location in Log	Strain at Failure (%)	Stress at Failure (psi)	Chord Modulus (250-500 psi) E x 10^{-6} (psi)
Log Number 5651-28					
5651-28-10034	Parallel	End	0.233	1691	1.00
10035		center	0.231	1670	1.00
10036			0.179	1732	1.25
10037			0.163	1548	1.00
10038			0.257	1966	1.00
10059			0.171	1283	N.A.
10060			0.212	1711	N.A.
			0.207	1657	1.05
			±0.036	±207	±0.11
5651-28-10042	Parallel	Midlength	0.202	1681	1.00
10043		center	0.225	1752	1.11
10044			0.206	1803	1.18
10045			0.238	1966	1.00
10046			0.225	1772	1.05
10047			0.220	1874	1.33
10048			0.154	1721	1.18
			0.210	1796	1.12
			±0.028	±97	±0.12
5651-28-10052	Parallel	Midlength	0.294	2322	1.11
10053		edge	0.253	2118	1.05
10054			0.272	2220	1.18
10055			0.280	2220	1.11
10056			0.272	2200	1.00
10057			0.276	2241	1.18
10058			0.303	2404	1.11
			0.279	2246	1.11
			±0.016	±92	±0.07
5651-28-10031	Perpendicular	End	0.348	2384	1.00
10032		center	0.225	2078	1.25
10033			0.235	1691	0.87
			0.269	2051	1.05
			±0.068	±347	±0.19
5651-28-10039	Perpendicular	Midlength	0.206	1487	0.83
10040		center	0.240	1548	0.83
10041			0.245	1640	0.95
			0.230	1558	0.87
			±0.021	±77	±0.07
5651-28-10049	Perpendicular	Midlength	0.312	2037	0.91
10050		edge	0.125	1141	0.95
10051			0.247	1732	1.00
			0.228	1637	0.95
			±0.095	±456	±0.05

TABLE A-12
TENSILE PROPERTIES OF FORT ST. VRAIN PRODUCTION LOGS OF
H-327 GRAPHITE

Log Position and Property	Mean	Std. Dev.	Max.	Min.	Range
End edge, parallel					
Ultimate tensile strength, 10^3 psi	2304	177	2566	1995	571
Strain at fracture, 10^{-3} in.	1.94	0.462	2.5	1.2	1.3
Secant modulus, 10^6 psi	1.263	0.269	1.81	0.98	0.82
Chord modulus, 10^6 psi	1.712	0.702	3.5	1.25	2.25
Midlength edge, parallel					
Ultimate tensile strength, 10^3 psi	2394	220	2667	2130	537
Strain at fracture, 10^{-3} in.	2.107	0.566	2.98	1.6	1.38
Secant modulus, 10^6 psi	1.232	0.270	1.58	0.9	0.6
Chord modulus, 10^6 psi	1.744	0.63	2.7	0.926	1.7
Midlength center, parallel					
Ultimate tensile strength, 10^3 psi	1629	194	1920	1340	580
Strain at fracture, 10^{-3} in.	1.48	0.225	1.73	1.1	0.6
Secant modulus, 10^6 psi	1.062	0.134	1.22	0.89	0.6
Chord modulus, 10^6 psi	1.539	0.429	2.080	1.0	1.080
End center, parallel					
Ultimate tensile strength, 10^3 psi	2180	257	2540	1716	820
Strain at fracture, 10^{-3} in.	1.927	0.253	2.34	1.6	0.74
Secant modulus, 10^6 psi	0.979	0.324	1.27	0.425	0.845
Chord modulus, 10^6 psi	1.514	0.308	2.08	1.25	0.83
End edge, perpendicular					
Ultimate tensile strength, 10^3 psi	1408	152	1678	1210	468
Strain at fracture, 10^{-3} in.	2.96	0.72	3.8	1.3	2.5
Secant modulus, 10^6 psi	0.54	0.18	0.93	0.57	0.56
Chord modulus, 10^6 psi	0.66	0.24	1.25	0.45	0.8
Midlength edge, perpendicular					
Ultimate tensile strength, 10^3 psi	1293	131	1374	1060	314
Strain at fracture, 10^{-3} in.	2.74	0.44	3.3	2.13	1.17
Secant modulus, 10^6 psi	0.480	0.058	0.57	0.42	0.15
Chord modulus, 10^6 psi	0.65	0.27	1.25	0.5	0.75
Midlength center, perpendicular					
Ultimate tensile strength, 10^3 psi	924	112	1010	686	324
Strain at fracture, 10^{-3} in.	2.08	0.47	2.63	1.3	1.3
Secant modulus, 10^6 psi	0.46	0.03	0.56	0.34	0.22
Chord modulus, 10^6 psi	0.58	0.19	0.96	0.41	0.55
End center, perpendicular					
Ultimate tensile strength, 10^3 psi	1349	253	1760	1067	693
Strain at fracture, 10^{-3} in.	2.87	0.82	3.94	1.5	2.4
Secant modulus, 10^6 psi	0.48	0.09	0.67	0.359	0.31
Chord modulus, 10^6 psi	0.688	0.282	1.38	0.38	1.0

TABLE A-13
CHEMICAL IMPURITIES IN H-451 GRAPHITE

Specimen No.	Location in Log	Spectrographic Analysis (ppm)				
		B	Fe	V	Ti	Ash
30434-1	Midlength center	1	4	20	8	530
30434-2		2	10	80	10	270
	Average	1.5	7	50	9	400
30434-3	Midlength edge	4	2	<4	4	440
30434-4		5	4	<4	2	490
	Average	4.5	3	<4	3	465
30434-5	End edge	3	4	<4	4	230
30434-6		2	4	<4	1	360
	Average	2.5	4	<4	2.5	295
	Average for whole log	3	5	18	5	385

TABLE A-14
CHEMICAL IMPURITIES IN TS-1240 GRAPHITE

Specimen No.	Location in Log	Spectrographic Analysis (ppm)				
		B	Fe	V	Ti	Ash
5651-75-3A-82	Midlength center	<0.5	<10	10	20	95
5651-75-3B-94		<0.5	<10	10	20	81
5651-72-3A-82		1	<10	20	20	94
5651-72-3B-94		1	<10	10	20	120
	Average	<1	<10	12.5	20	98
5651-75-3B-165	Midlength edge	<0.5	<10	10	20	47
5651-75-3A-156		<0.5	<10	20	20	74
5651-72-3A-156		1	<10	10	10	140
5651-72-3B-165		1	<10	10	10	92
	Average	<1	<10	12.5	15	88
5651-75-1B-115	End edge	<0.5	<10	20	20	39
5651-75-1A-106		<0.5	<10	10	10	58
5651-72-1B-115		<0.5	<10	10	10	120
5651-72-1A-106		<0.5	<10	10	10	110
	Average	<0.5	<10	12.5	12.5	82
5651-75-1B-43	End center	<0.5	<10	20	20	89
5651-75-1A-31		<0.5	<10	10	20	55
5651-72-1B-43		1	<10	10	10	69
5651-72-1A-31		1	<10	20	20	68
	Average	<1	<10	15	17.5	70

TABLE A-15
CHEMICAL IMPURITIES IN P_3JHAN GRAPHITE

Specimen No.	Location in Log	Spectrographic Analysis (ppm)				
		B	Fe	V	Ti	Ash
31281-1	Not available	0.5	4	4	<1	100
31282-2		0.5	4	2	<1	30
	Average	0.5	4	3	<1	65

TABLE A-16
DIMENSIONAL CHANGES OF NEEDLE-COKE H-327 GRAPHITE
FROM CAPSULE OG-1
AXIAL (PARALLEL) ORIENTATION

Record No.	Dimensional Change $\ln\left(1+\frac{\Delta L}{L_0}\right)$ (%)	Total Fluence x 10^{-21} (n/cm^2)(E > 0.18 MeV)	Average Irradiation Temperature (°C)	Previous Record No.
5005	-0.15	2.2	645	
5009	-0.16			
5013	-0.17			
5017	-0.14			
5021	-0.11			
5025	-0.13			
5029	-0.11			
5033	-0.15			
5037	-0.20		615	
5041	-0.18		615	
5114	-0.14		560	
5115	-0.16			
5118	-0.16			
5119	-0.20			
5124	-0.15			
5125	-0.21			
5128	-0.14			
5129	-0.18			
5134	-0.14			
5135	-0.20			
5147	-0.25	2.9	740	
5151	-0.24			
5155	-0.17			
5159	-0.24			
5163	-0.26			
5167	-0.20			
5171	-0.23			
5175	-0.17			
5179	-0.24		690	
5182	-0.28			
5185	-0.24			
5186	-0.17			
5195	-0.25			
5196	-0.10			
5205	-0.25			
5215	-0.22			
5216	-0.23			
5241	-0.28		610	
5242	-0.33			
5251	-0.28			

TABLE A-16 (Continued)

Record No.	Dimensional Change $\ln\left(1+\frac{\Delta L}{L_0}\right)$ (%)	Total Fluence x 10^{-21} (n/cm^2) (E > 0.18 MeV)	Average Irradiation Temperature (°C)	Previous Record No.
5252	-0.31	2.9	610	
5257	-0.24	↓	↓	
5258	-0.34			
5261	-0.32			
5262	-0.27			
5263	-0.34			
5264	-0.33			
5267	-0.25			
5268	-0.21			
5271	-0.29			
5272	-0.27			
5273	-0.21			
5274	-0.33			
5277	-0.31			
5278	-0.28			
5281	-0.20			
5282	-0.28			
5291	-0.33			
5292	-0.28			
5466	-0.62	3.4	890	
5467	-0.50	↓	↓	
5473	-0.65			
5474	-0.54			
5477	-0.69			
5478	-0.53			
5509	-8.96	14.9	1255	2914
5510	-9.74	↓	↓	2920
5511	-9.61			2906
5513	-1.70	3.7	1110	
5514	-1.83	↓	↓	
5523	-1.79			
5524	-1.96			
5533	-1.19		1040	
5534	-1.48		↓	
5543	-1.75			
5544	-1.03			
5546	-1.40			
5547	-1.57			
5550	-5.28	9.9	1220	2433
5551	-5.37	↓	1220	2447
5555	-3.98		1185	2774
5556	-1.19	3.7	1040	
5557	-1.37	3.7	1040	

TABLE A-16 (Continued)

Record No.	Dimensional Change $\ln\left(1+\frac{\Delta L}{L_0}\right)$ (%)	Total Fluence x 10^{-21} (n/cm^2)(E > 0.18 MeV)	Average Irradiation Temperature (°C)	Previous Record No.
5560	-4.60	9.9	1185	2450
5561	-4.01	9.9	1185	2407
5566	-1.22	3.7	1040	
5567	-1.32	↓	↓	
5568	-1.29			
5569	-1.47			
5629	-7.73	11.3	1510	2842
5738	-1.31	3.4	1020	
5748	-1.18	↓	↓	
5758	-1.11			
5766	-1.30		940	
5771	-0.83		↓	
5775	-0.88			
5779	-0.83			
5784	-0.77			
5791	-0.71			
5797	-0.71	↓	↓	
5804	-1.09	3.1	990	
5811	-0.91		980	
5815	-1.07		↓	
5819	-1.00			
5823	-1.00			
5856	-0.79		945	
5857	-0.78		↓	
5860	-0.72			
5861	-0.72			
5864	-0.75			
5865	-0.70	↓	↓	
5907	-0.60	2.6	930	
5911	-0.49		920	
5915	-0.52		↓	
5919	-0.56			
5923	-0.52			
5927	-0.51			
5954	-0.42		885	
5955	-0.34	↓	885	
5958	-1.31	4.6	890	2585
5959	-1.30	4.6	890	2616
5965	-0.30	2.6	885	
5974	-0.43	↓	885	
5975	-0.43		885	
5996	-0.33		835	
5997	-0.25	↓	835	

TABLE A-16 (Continued)

Record No.	Dimensional Change $\ln\left(1+\frac{\Delta L}{L_0}\right)$ (%)	Total Fluence x 10^{-21} (n/cm^2) (E > 0.18 MeV)	Average Irradiation Temperature (°C)	Previous Record No.
6006	-0.29	2.6	835	
6007	-0.20	↓	↓	
6008	-0.31			
6009	-0.20			
6018	-0.27			
6019	-0.16			
6024	-0.32			
6025	-0.27			
6028	-0.29			
6029	-0.20			
6030	-0.26			
6031	-0.28			
6034	-0.27			
6035	-0.30			
6038	-0.64			
6039	-0.20			
6092	-0.17	2.1	810	
6093	-0.11	↓	↓	
6102	-0.15			
6103	-0.11			
6112	-0.15			
6113	-0.12			
6122	-0.05			
6123	-0.11			
6148	-0.15		750	
6149	-0.18		↓	
6158	-0.11			
6159	-0.07			
6168	-0.18			
6169	-0.09			
6178	-0.12			
6179	-0.15			
6188	-0.13			
6189	-0.13			
6198	-0.15			
6199	-0.08			
6209	-0.06	1.6	650	
6213	-0.09	↓	645	
6217	-0.12		↓	
6221	-0.11			
6225	-0.24			
6229	-0.10			
6233	-0.16			

TABLE A-16 (Continued)

Record No.	Dimensional Change $\ln\left(1+\frac{\Delta L}{L_0}\right)$ (%)	Total Fluence x 10^{-21} (n/cm^2) (E > 0.18 MeV)	Average Irradiation Temperature (°C)	Previous Record No.
6237	-0.15	1.6	645	
6241	-0.10	1.6	645	
6246	-0.41	2.4	625	2465
6250	-0.34	↓	↓	2458
6251	-0.20			2410
6254	-0.37			2472
6255	-0.25			2457
6260	-0.40			2493
6261	-0.19			2435
6264	-0.43			2474
6265	-0.34			2698
6301	-0.15	1.6	595	

TABLE A-17
DIMENSIONAL CHANGES OF NEEDLE-COKE H-327 GRAPHITE
FROM CAPSULE OG-1
RADIAL (PERPENDICULAR) ORIENTATION

Record No.	Dimensional Change $\ln\left(1+\frac{\Delta L}{L_0}\right)$ (%)	Total Fluence x 10^{-21} (n/cm^2) (E > 0.18 MeV)	Average Irradiation Temperature (°C)	Previous Record No.
5007	-0.12	2.2	645	
5011	-0.12	↓	↓	
5015	-0.11			
5019	-0.10			
5023	-0.06			
5027	-0.08			
5031	-0.08			
5035	-0.16			
5039	-0.14		615	
5043	-0.16		615	
5116	-0.16		560	
5117	-0.08		↓	
5120	-0.14			
5121	-0.35			
5126	-0.19			
5127	-0.19			
5130	-0.19			
5131	-0.14			
5136	-0.26	↓	↓	
5137	-0.17			
5149	-0.13	2.9	740	
5153	-0.16	↓	↓	
5157	-0.17			
5161	09.14			
5165	-0.10			
5169	-0.11			
5173	-0.16			
5177	-0.04		↓	
5181	-0.24		690	
5184	-0.19		↓	
5206	-0.21			
5259	-0.26		610	
5260	-0.28		↓	
5265	-0.16			
5266	-0.19			
5269	-0.22			
5270	-0.23			
5275	-0.20			
5276	-0.21			
5279	-0.26	↓	↓	

TABLE A-17 (Continued)

Record No.	Dimensional Change $\ln\left(1+\frac{\Delta L}{L_0}\right)$ (%)	Total Fluence x 10^{-21} (n/cm^2) (E > 0.18 MeV)	Irradiation Temperature (°C)	Previous Record No.
5280	-0.26	2.9	610	
5357	-0.43	3.4	945	
5358	-0.36	↓	↓	
5362	-0.48			
5363	-0.42			
5369	-0.65			
5370	-0.40			
5506	9.43	14.9	1255	2910
5507	8.70	14.9	1255	2909
5548	-0.06	9.9	1220	2443
5549	0.91	↓	1220	2455
5552	-0.25		1190	2772
5553	0.90		↓	2760
5558	-0.04			2451
5559	0.35	↓	↓	2429
5630	2.39	11.3	1510	2839
5739	-0.32	3.4	1020	
5749	-0.51	↓		
5759	-0.50			
5767	-0.52		940	
5772	-0.36		↓	
5776	-0.40			
5780	-0.42			
5785	-0.41			
5792	-0.32			
5798	-0.40	↓	↓	
5809	-0.30	3.1	990	
5813	-0.16	↓	980	
5817	-0.26		↓	
5821	-0.35			
5825	-0.37			
5858	-0.43		945	
5859	-0.12		↓	
5862	-0.39			
5863	-0.37			
5866	-0.37			
5867	-0.35	↓	↓	
5909	-0.25	2.6	930	
5913	-0.12	↓	920	
5917	-0.08		↓	
5921	-0.02			
5925	-0.24			
5929	-0.22	↓	↓	

TABLE A-17 (Continued)

Record No.	Dimensional Change $\ln\left(1+\frac{\Delta L}{L_0}\right)$ (%)	Total Fluence x 10^{-21} (n/cm^2) (E > 0.18 MeV)	Average Irradiation Temperature (°C)	Previous Record No.
5956	-0.79	4.6	890	2638
5957	-0.59	4.6	890	2552
6026	-0.19	2.6	835	
6027	-0.12	↓	↓	
6032	-0.23			
6033	-0.02			
6036	-0.14			
6037	-0.08			
6211	-0.06	1.6	650	
6215	-0.12	↓	645 ↓	
6219	-0.07			
6223	-0.04			
6227	-0.06			
6231	-0.04			
6235	-0.09			
6239	-0.05			
6243	-0.06			
6244	-0.54	2.4	625	
6245	-0.31	↓	↓	
6248	-0.39			
6249	-0.33			
6252	-0.46			
6253	-0.33			
6258	-0.46			
6259	-0.25			
6262	-0.43			
6263	-0.29			
6303	-0.06	↓	595	

TABLE A-18
THERMAL EXPANSIVITY OF H-327 GRAPHITE SPECIMENS
IRRADIATED IN CAPSULE OG-1

Specimen No.	Orientation and Location[a]	Crucible No.	Hole No.	Mean Irradiation Temperature (°C)	Fluence x 10^{-21} (n/cm^2) (E > 0.18 MeV)	Coefficient of Thermal Expansivity, $\alpha \times 10^6 °C^{-1}$ (22°-500°C)
1	C para	1	2	640	2.2	1.84
2	C para	↓	3	640	↓	1.87
201	E para	↓	40	580	↓	1.72
202	E para	↓	40	580	↓	1.65
101	C perp	↓	2	640	↓	3.47
102	C perp	↓	3	640	↓	3.25
251	E perp	↓	40	580	↓	3.55
252	E perp	↓	40	580	↓	3.54
222	E para	7	2	980	3.1	1.97
223	E para	↓	3	↓	↓	1.96
224	E para	↓	4	↓	↓	1.93
272	E perp	↓	2	↓	↓	3.10
273	E perp	↓	3	↓	↓	3.38
274	E perp	↓	4	↓	↓	3.27
176	C para	8	19	875-890	3.4	2.03
177	E para	↓	19	↓	↓	2.27
174	C perp	↓	19	↓	↓	3.18
175	E perp	↓	19	↓	↓	3.70

[a] C = center, E = edge; para = parallel, perp = perpendicular.

TABLE A-19
THERMAL EXPANSIVITY OF H-429 AND H-451 GRAPHITE SPECIMENS
IRRADIATED IN CAPSULE OG-1

Graphite Grade	Specimen No.	Log Location and Orientation[a]	Crucible No.	Hole No.	Mean Irradiation Temperature (°C)	Fluence x 10^{-21} (n/cm^2) (E > 0.18 MeV)	Coefficient of Thermal Expansivity, $\alpha \times 10^6 °C^{-1}$ (22°-500°C)
H-451	303	C para	1	2	640	2.2	3.98
	304	C para		3			3.80
	305	C para		4			3.72
	428	C perp		2			4.82
	429	C perp		3			4.89
	430	C perp		4			4.73
	613	E para	9	2	850	2.1	3.92
	614	E para		3			3.83
	615	E para		4			4.09
	713	E perp		2			5.04
	714	E perp		3			4.85
	715	E perp		4			4.78
	371	C para	8	7	920	2.6	3.52
	372	C para		7			3.75
	373	C para		8			3.61
	496	C perp		7			4.39
	497	C perp		7			4.15
	498	C perp		8			4.16
H-429	389	Para	8	16	890	3.4	3.70
	390	Para		16			3.90
	391	Para		16			4.06
	419	Perp		15			4.93
	420	Perp		15			5.19
	421	Perp		15			5.16
H-451	596	E para	7	2	980	3.1	3.33
	597	E para		3			3.38
	598	E para		4			3.58
	696	E perp		2			4.11
	697	E perp		3			4.25
	698	E perp		4			4.44
	583	E para	4	2	1150	3.7	3.49
	584	E para		2			3.55
	585	E para		3			3.64
	683	E perp		2			3.70
	684	E perp		2			4.01
	685	E perp		3			3.78
H-429	404	Para	4	30	1050-1275	6.3	3.77
	405	Para		30			3.67
	406	Para		30			3.66
	434	Perp		30			4.70
	435	Perp		30			4.52
	436	Perp		40			4.37
H-451	341	C para	5	6	1390	3.6	3.49
	342	C para		6			3.73
	343	C para		7			3.69
	466	C perp		6			4.30
	467	C perp		6			4.37
	468	C perp		7			4.16
H-429	141	Para	5	16	1370-1500	6.6	3.58
	142	Para		16			3.38
	143	Para		17			3.05
	161	Perp		16			4.16
	162	Perp		16			4.07
	163	Perp		17			4.29

[a] C = center, E = edge; para = parallel, perp = perpendicular.

TABLE A-20
THERMAL CONDUCTIVITY OF H-327 GRAPHITE SPECIMENS IRRADIATED IN CAPSULE OG-1

Specimen No.	Log Location and Orientation[a]	Crucible No.	Mean Irradiation Temperature (°C)	Fluence x 10^{-21} (n/cm^2) (E > 0.18 MeV)	Thermal Conductivity (cal/cm-sec-°C)					
					22°C	200°C	400°C	600°C	800°C	Irradiated Temperature (extrapolated)
1	E perp	1	600-625	2.9	0.038	0.044	0.044			0.044
2	E perp	1	600-625	2.9	0.038	0.044	0.043			0.041
13	E perp	1	600-625	2.9	0.040	-	-			-
81	E para	1	600-625	2.9	0.059	0.066	0.070			0.063
82	E para	1	600-625	2.9	0.064	0.081	0.080			0.071
43	E perp	5	1225-1350	9.9	0.133	0.159	0.143	0.127	0.112	0.085
44	E perp	5	1225-1350	9.9	0.131	0.136	0.118	0.105	0.093	0.078
45	E perp	5	1225-1350	9.9	0.149	-	-	-	-	-
86	E para	5	1225-1350	9.9	0.212	0.222	0.195	0.176	0.139	0.10
87	E para	5	1225-1350	9.9	0.198	0.219	0.203	0.170	0.144	0.10
3	E perp	7	875-920	5.1	0.0794	0.097	0.083	0.078	0.072	0.070
4	E perp	7	875-920	5.1	0.072	0.076	0.071	0.066	0.058	0.055
32	E perp	7	875-920	5.1	0.085	-	-	-	-	-
83	E para	7	875-920	5.1	0.095	0.094	0.083	0.081	0.077	0.075
84	E para	7	875-920	5.1	0.094	0.110	0.100	0.094	0.085	0.080

[a] E = edge; para = parallel, perp = perpendicular.

TABLE A-21
THERMAL CONDUCTIVITY OF H-451 GRAPHITE SPECIMENS IRRADIATED IN CAPSULE OG-1

Specimen No.	Orientation[a]	Crucible No.	Mean Irradiation Temperature (°C)	Fluence x 10^{-21} (n/cm^2) (E > 0.18 MeV)	Thermal Conductivity (cal/cm-sec-°C)					
					22°C	200°C	400°C	600°C	800°C	Irradiated Temperature (extrapolated)
221	Perp	1	600	2.2	0.085	0.081	0.082			0.080
222	Perp				0.078	0.083	0.080			0.077
223	Perp				0.078	0.082	0.082			0.081
224	Perp				0.077	-	-			-
225	Perp				0.068	-	-			-
226	Perp				0.074	-	-			-
227	Perp				0.076	-	-			-
228	Perp				0.073	-	-			-
201	Para				0.079	0.083	0.080			0.075
202	Para				0.087	0.095	0.097			0.084
203	Para				0.083	-	-			-
204	Para				0.083	-	-			-
242	Perp	5	1340	3.6	0.195	0.175	0.164	0.143	0.123	0.09
243	Perp				0.202	0.213	0.190	0.161	0.127	0.085
244	Perp				0.216	0.203	0.185	0.162	0.129	0.09
245	Perp				0.205	-	-	-	-	-
246	Perp				0.214	-	-	-	-	-
247	Perp				0.202	-	-	-	-	-
248	Perp				0.205	-	-	-	-	-
249	Perp				0.215	-	-	-	-	-
210	Para				0.193	0.216	0.188	0.158	0.142	0.10
211	Para				0.195	0.209	0.182	0.159	0.143	0.10
212	Para				0.195	-	-	-	-	-
213	Para				0.198	-	-	-	-	-
231	Perp	7	920	3.1	0.104	0.131	0.112	0.101	0.092	0.090
232	Perp				0.097	0.111	0.105	0.092	0.085	0.082
233	Perp				0.109	0.113	0.100	0.092	0.082	0.080
234	Perp				0.110	-	-	-	-	-
235	Perp				0.114	-	-	-	-	-
236	Perp				0.099	-	-	-	-	-
237	Perp				0.104	-	-	-	-	-
238	Perp				0.085	-	-	-	-	-
205	Para				0.117	0.132	0.123	0.110	0.100	0.095
206	Para				0.118	0.130	0.117	0.107	0.096	0.092
207	Para				0.112	-	-	-	-	-
208	Para				0.113	-	-	-	-	-

[a] Perp = perpendicular, Para = parallel.

TABLE A-22
MEAN THERMAL CONDUCTIVITY OF GRAPHITE SPECIMENS IRRADIATED IN CAPSULE OG-1

Crucible No.	Mean Irradiation Temperature (°C)	Fluence x 10^{-21} (n/cm^2) (E >0.18 MeV)	Graphite Grade	Orientation[a]	Thermal Conductivity (cal/cm-sec-°C)	
					22°C	At Irradiation Temperature (extrapolated)
1	600-625	2.9	H-327	Perp	0.039	0.043
1	600-625	2.9	H-327	Para	0.062	0.067
1	600	2.2	H-451	Perp	0.076	0.079
1	600	2.2	H-451	Para	0.083	0.080
5	1225-1350	9.9	H-327	Perp	0.137	0.082
5	1225-1350	9.9	H-327	Para	0.220	0.10
5	1350	3.6	H-451	Perp	0.207	0.09
5	1350	3.6	H-451	Para	0.195	0.10
7	875-920	5.1	H-327	Perp	0.079	0.063
7	875-920	5.1	H-327	Para	0.095	0.078
7	920	3.1	H-451	Perp	0.102	0.084
7	920	3.1	H-451	Para	0.115	0.094

[a] Perp = perpendicular, Para = parallel.

TABLE A-23
TENSILE TESTS ON H-327 GRAPHITE IRRADIATED IN OG-1 CAPSULE

Crucible No.	Hole No.	Irradiation Temperature (°C)	Fluence x 10^{-21} (n/cm^2) (E > 0.18 MeV)	Log Location and Orientation[a]	Specimen No.	Strain at Failure (%)	Ultimate Tensile Strength (psi)	Young's Modulus[b] (10^6 psi)	Secant Modulus[c] (10^6 psi)
-	-	-	0	E para	1	0.226	1874	1.61	0.83
				E para	2	0.248	2669	1.91	1.08
				E para	3	0.170	1956	2.16	1.15
				E para	4	0.132	1690	1.77	1.28
				E para	5	0.250	2648	1.87	1.06
				E para	6	0.203	2220	1.73	1.09
				E para	7	0.176	2281	2.49	1.30
				E para	8	0.224	2241	1.78	1.00
				E para	9	0.180	2159	1.85	1.20
				E para	10	0.185	2119	2.12	1.15
					Mean	0.199	2186	1.93	1.11
					Std dev	±0.035	±293	±0.25	±0.13
	-	-	0	C para	-	0.148[d]	1480 1340	1.54[d]	1.06[d]
	-	-	0	C perp	-	0.208[d]	950 890	0.58[d]	0.46[d]
2	16	700	2.9	E para	351	0.109	2933	3.93	2.69
	19			E para	352	0.115	3504	4.18	3.05
	22			E para	353	0.089	2709	3.77	3.04
	25			E para	354	0.118	3606	3.77	3.06
	32	640		E para	355	0.093	2995	4.38	3.22
	35			E para	356	0.114	3056	3.29	2.68
	39			E para	357	0.112	3422	3.85	3.06
	42			E para	358	0.124	3321	3.62	2.68
	45			E para	359	0.091	3035	4.23	3.34
	49			E para	360	0.104	2934	3.46	2.82
					Mean	0.107	3152	3.85	2.96
					Std dev	±0.012	±278	±0.33	±0.20
4	18	1100	3.7	E para	361	0.095	2485	3.32	2.62
	22	1100		E para	362	0.130	3198	3.18	2.46
	27	1050		E para	363	0.094	2445	3.22	2.60
	31			E para	364[e]	(0.057)	(1263)	(2.67)	(2.22)
	34			E para	365	0.131	3035	2.93	2.32
	37			E para	366	0.102	2832	3.14	2.78
	41			E para	367	0.118	2893	3.18	2.45
	44			E para	368	0.115	2872	3.61	2.50
					Mean	0.112	2822	3.23	2.53
					Std dev	±0.014	±254	±0.19	±0.14

TABLE A-23 (Continued)

Crucible No.	Hole No.	Irradiation Temperature (°C)	Fluence x 10^{-21} (n/cm^2) (E > 0.18 MeV)	Log Location and Orientation[a]	Specimen No.	Strain at Failure (%)	Ultimate Tensile Strength (psi)	Young's Modulus[b] (10^6 psi)	Secant Modulus[c] (10^6 psi)
6	16	1020	3.4	C perp	401	0.154	1080	1.18	0.86
	19			C perp	402	0.154	1120	0.96	0.73
	22			C perp PpP	403	0.097	856	1.22	0.88
	25			C perp	404	0.126	733	0.94	0.58
	32	960		C perp	405	0.162	1243	1.08	0.77
	35			C perp	406	0.111	978	1.33	0.88
	39			C perp	407	0.058	774	1.66	1.33
	42			C perp	408	0.110	1283	1.44	1.17
	45			C perp	409	0.062	754	1.30	1.22
	49			C perp	410	0.096	795	1.20	0.83
					Mean	0.110	962	1.23	0.93
					Std dev	±0.032	±198	±0.20	±0.23
8	18	900	2.6	C para	279	0.075	1996	3.12	2.66
	18			C para	280	0.099	2098	2.85	2.12
	21			C para	281	0.113	2648	3.38	2.34
	21			C para	282	0.084	2058	2.83	2.45
	24			C para	283	0.092	2017	2.67	2.19
	24			C para	284	0.108	2282	2.97	2.11
	30	860		C para	285	-	1732	3.12	-
	30			C para	286	0.082	1752	3.12	2.14
	33			C para	287	0.142	2159	2.59	1.52
	33			C para	288	0.106	2526	3.16	2.38
					Mean	0.100	2127	3.02	2.21
					Std dev	±0.019	±281	±0.27	±0.30
9	16	810	2.1	E para	369	0.143	3259	2.91	2.28
	19			E para	370	0.110	2730	3.10	2.48
	22			E para	371	0.099	2628	3.57	2.65
	25			E para	372	0.151	2995	2.55	1.98
	32	770		E para	373	0.107	2546	3.18	2.38
	35			E para	374	0.112	2832	3.26	2.53
	39			E para	375	0.118	3015	3.10	2.56
	42			E para	376	0.110	2445	3.04	2.22
	45			E para	377	0.129	2913	2.99	2.26
	49			E para	378	0.100	2506	3.34	2.51
					Mean	0.118	2787	3.10	2.39
					Std dev	±0.017	±249	±0.26	±0.19

[a] E = edge, C = center, para = parallel, perp = perpendicular.

[b] 100-1000 psi (parallel samples) or 100-600 psi (perpendicular samples) after preloading to 1000 psi (parallel samples) or 600 psi (perpendicular samples), unloading sample, and reloading.

[c] Ultimate tensile strength divided by fracture strain.

[d] Average values.

[e] Sample contained flaw; excluded from averages.

TABLE A-24
TENSILE TESTS ON H-451 GRAPHITE IRRADIATED IN OG-1 CAPSULE

Crucible No.	Hole No.	Irradiation Temperature (°C)	Fluence x 10^{-21} (n/cm^2) (E > 0.18 MeV)	Log Location and Orientation(a)	Specimen No.	Strain at Failure (%)	Ultimate Tensile Strength (psi)	Young's Modulus(b) (10^6 psi)	Secant Modulus(c) (10^6 psi)
-	-	-	0	C para	T-181	0.130	1446	1.22	1.11
				C para	182	0.230	1630	1.02	0.71
				C para	183	0.212	1650	1.15	0.78
				C para	184	0.169	1589	1.17	0.94
				C para	185	0.152	1548	1.20	1.02
				C para	186	0.211	1731	1.23	0.82
				C para	187	0.182	1243	0.95	0.68
				C para	188	0.187	1609	1.17	0.86
				C para	190	0.184	1630	1.17	0.89
					Mean	0.184	1564	1.14	0.87
					Std dev	±0.029	±135	±0.09	±0.13
-	-	-		C perp	T-219	0.210	1589	0.97	0.76
				C perp	220	0.215	1751	0.98	0.81
				C perp	221	0.252	1874	1.02	0.74
				C perp	222	0.223	1731	1.02	0.77
				C perp	223	0.210	1650	0.94	0.79
				C perp	224	0.267	2037	1.02	0.76
				C perp	225	0.172	1283	0.97	0.75
				C perp	226	0.181	1609	1.12	0.89
				C perp	227	0.241	1853	1.06	0.77
				C perp	228	0.147	1344	1.02	0.91
				C perp	1	0.227	1446	0.92	0.64
				C perp	2	0.242	1508	0.91	0.62
				C perp	3	0.342	2220	1.03	0.65
				C perp	5	0.219	1609	0.99	0.73
				C perp	6	0.214	1562	1.08	0.73
					Mean	0.224	1671	1.00	0.75
					Std dev	±0.043	±242	±0.05	±0.08
1	18	620	2.2	C para	T-101	0.142	2587	2.08	1.82
	18			C para	102	0.104	2384	2.31	2.29
	21			C para	103	0.122	2240	1.99	1.84
	21			C para	104	0.110	2343	2.29	2.13
	24			C para	105	0.138	2628	2.18	1.90
	24			C para	106	0.117	2383	2.32	2.04
	30	580		C para	107	0.126	2445	2.19	1.94
	30			C para	108	0.145	2852	2.30	1.97
	33			C para	109	0.130	2343	2.15	1.80
	33			C para	110	0.128	2648	2.30	2.07
					Mean	0.126	2485	2.22	1.98
					Std dev	±0.013	±177	±0.11	±0.15
3	16	950	3.4	C para	T-119	-	2200	2.12	-
	16			C para	120	0.144	2608	2.23	1.81
	19			C para	121	0.161	2608	1.93	1.62
	19			C para	122	0.142	1976	1.63	1.39
	22			C para	123	0.153	2485	2.04	1.62
	22			C para	124	0.154	2078	1.81	1.35
	25			C para	125	0.130	2811	2.39	2.16
	25			C para	126	0.149	2505	1.73	1.68
	32	910		C para	127	0.162	2587	2.04	1.60
	32			C para	128	0.126	2058	2.21	1.63
	35			C para	129	0.104	2037	2.44	1.96
	35			C para	130	0.152	2506	2.12	1.65
					Mean	0.143	2371	2.06	1.68
					Std dev	±0.017	±271	±0.24	±0.22

TABLE A-24 (Continued)

Crucible No.	Hole No.	Irradiation Temperature (°C)	Fluence x 10^{-21} (n/cm^2) (E > 0.18 MeV)	Log Location and Orientation[a]	Specimen No.	Strain at Failure (%)	Ultimate Tensile Strength (psi)	Young's Modulus[b] (10^6 psi)	Secant Modulus[c] (10^6 psi)
5	19	1370	3.6	C para	T-139	-	2384	-	-
	19	↓	↓	C para	140	0.166	2241	1.74	1.35
	23			C para	141	0.164	2058	1.83	1.25
	23			C para	142	0.172	2302	1.86	1.34
	28	1340		C para	143	0.170	2118	1.79	1.25
	28	↓		C para	144	0.188	2139	1.72	1.14
	32			C para	145	0.198	2383	1.69	1.20
	32			C para	146	0.163	2241	1.93	1.37
					Mean	0.174	2233	1.79	1.27
					Std dev	±0.012	±115	±0.08	±0.08
7	19	950	3.1	C perp	T-211	0.140	2058	1.88	1.47
	23	950		C perp	212	0.172	2628	1.85	1.53
	28	900		C perp	213	0.200	2770	1.60	1.39
	32	↓		C perp	214	0.168	2505	1.76	1.49
	35			C perp	215	0.185	2974	1.95	1.61
	39			C perp	216	0.162	2669	1.99	1.65
	43			C perp	217	0.176	2954	2.01	1.68
	46			C perp	218	0.179	2628	1.83	1.47
					Mean	0.172	2648	1.88	1.54
					Std dev	±0.016	±270	±0.13	±0.09
10	18	630	1.6	C para	T-163	0.126	2608	2.57	2.07
	18	↓	↓	C para	164	0.110	2648	2.55	2.41
	21			C para	165	0.103	2098	2.67	2.04
	21			C para	166	0.144	2872	2.51	1.99
	24			C para	167	0.132	1956	2.24	1.48
	24			C para	168	0.107	2384	2.81	2.23
	30	610		C para	169	0.098	2322	3.00	2.37
	30	↓		C para	170	0.128	2587	2.45	2.02
	33			C para	171	0.096	2221	2.74	2.31
	33			C para	172	0.114	2546	2.71	2.23
					Mean	0.116	2424	2.63	2.12
					Std dev	±0.015	±265	±0.20	±0.26

[a] C = center, E = edge; para = parallel, perp = perpendicular.

[b] 100-1000 psi, after preloading to 1000 psi, unloading sample, and reloading.

[c] Ultimate tensile strength divided by fracture strain.